AD NUMBER

AD912169

NEW LIMITATION CHANGE

TO

Approved for public release, distribution unlimited

FROM

Distribution authorized to U.S. Gov't. agencies only; Test and Evaluation; JUL 1973. Other requests shall be referred to Air Force Rocket Propulsion Laboratory, Attn: STINFO/DOZ, Edwards AFB, CA 93523.

AUTHORITY

afrpl ltr, 14 jan 1974

PREDICTION OF MINUTEMAN EXHAUST PLUME ELECTRICAL PROPERTIES

H.S. Pergament and R.R. Mikatarian

Technical Report AFRPL-TR-72-129

JULY 1973

AeroChem Research Laboratories, Inc.
Princeton, N.J. 08540

AIR FORCE ROCKET PROPULSION LABORATORY
DIRECTOR OF SCIENCE AND TECHNOLOGY
AIR FORCE SYSTEMS COMMAND
EDWARDS AIR FORCE BASE, CALIFORNIA

NOTICES

"When U.S. Government drawings, specifications, or other data are used for any purpose other than a definitely related government procurement operation, the Government thereby incurs no responsibility nor any obligation whatsoever, and the fact that the Government may have formulated, furnished, or in any way supplied the said drawings, specifications or other data, is not to be regarded by implication or otherwise, or in any manner licensing the holder or any other person or corporation, or conveying any rights or permission to manufacture use, or sell any patented invention that may in any way be related thereto."

AFRPL-TR-72-129

PREDICTION OF MINUTEMAN EXHAUST PLUME ELECTRICAL PROPERTIES

H.S. Pergament
R.R. Mikatarian

FOREWORD

This work was supported by the Air Force Weapons Laboratory, Kirtland Air Force Base, New Mexico, monitored by the Air Force Rocket Propulsion Laboratory under Contract No. F04611-71-C-0064 and performed during the period 6 December 1971 through 6 April 1972. The results were used to guide the design of equivalent plume conductivity circuits tested at the AFWL ARIES facility.

The authors gratefully acknowledge the helpful suggestions of Capt. William J. Rothschild, AFRPL and the support and encouragement of Capt. Peter A. Swan, AFWL, during the course of this program.

The contractor report number is AeroChem TP-281.

"This technical report has been reviewed and is approved."

Paul J. Daily, Lt. Col., USAF
Chief, Technology Division

ABSTRACT

Results of a comprehensive investigation of Minuteman exhaust plume electrical properties are presented. Electron density and electron-neutral collision frequency profiles are given for the Stage 1 plume at 100 kft and the Stage 2 plume at 118,200 and 300 kft. This work is motivated by the need to determine plume electrical conductivities, input data to an evaluation of EMP/exhaust plume interactions. The calculations are described in detail and include analyses of: (i) two-phase nozzle flow via the method of characteristics, (ii) nonequilibrium chemistry along nozzle and plume streamlines, (iii) inviscid plume properties via the method of characteristics, (iv) turbulent mixing / nonequilibrium chemistry along curved plume boundaries, and (v) nonequilibrium chemistry behind the Mach disc. The results include: gas and particle properties and chemical kinetic distributions of all neutral and charged species concentrations in the nozzle: inviscid boundaries, shock structure, Mach number contours and electron densities in the plume.

TABLE OF CONTENTS

LIST OF TABLES

LIST OF FIGURES

NOMENCLATURE

A^*	nozzle throat area
A_{ex}	nozzle exit area
C_p	specific heat at constant pressure
D	Mach disc diameter
d_N	nozzle exit diameter
k, k_1	constants--defined by Eq. (1)
M	Mach number
n	defined by $\mu \sim T^n$
n_e	electron density
Pr	Prandtl number
p	static pressure
r	radial distance from centerline
r_N	nozzle exit radius
T	temperature
W	mixture molecular weight
X_e -	electron mole fraction
x	axial distance from nozzle exit
Y	mass fraction

Greek Letters

γ	ratio of specific heats
μ	viscosity
ν_e	electron-neutral collision frequency

Subscripts

eq	equivalent nozzle
ex	nozzle exit plane
g	gas
∞	free stream
ℓ	liquid
s	solid

I. INTRODUCTION

Interaction of an electromagnetic pulse (EMP), following a nuclear explosion, with a missile in flight can induce skin currents which seriously affect the missile's electrical system. Because the exhaust plume is itself an electrical conductor currents induced in the plume can be transferred to the skin of the missile via its base. Thus an important problem is the extent of the electrical coupling between the missile body and exhaust plume. In order to estimate the magnitude of this problem the exhaust plume electrical conductivity must be known.

Minuteman EMP/plume interactions are under investigation at the Air Force Weapons Laboratory (AFWL). Their approach consists of: (i) design of an electrical circuit which (when connected to the missile) will "simulate" the induced skin currents* which result from plume/body electrical coupling, (ii) measurement of induced skin currents and (ii) interpretation of the results in terms of the Minuteman exhaust plume's influence on the skin currents induced by EMP throughout the flight trajectory.

AeroChem's contribution to this program has been to predict Minuteman exhaust plume electrical properties (electron density and electron-neutral collision frequency) for a limited number of first and second stage trajectory points; these predictions have been used (by AFWL) to calculate the plume/body electrical coupling. Although some predictions of Minuteman exhaust plume electrical properties have been reported[1] there has been no attempt, prior to the present effort, to apply the available systematic procedures (see, e.g. Refs. 2-5) for calculating plume electrical properties. It is the purpose of this report to present the results of our comprehensive investigation of Minuteman exhaust plume electron densities and collision frequencies--in which we utilize, wherever possible, state-of-the-art computational techniques for both nozzle and plume flows. A detailed study of the nozzle flow is essential for Minuteman because (i) the high particle loading (≈ 30% by weight) strongly influences the gas properties and composition at the nozzle exit plane and (ii) at the altitudes considered herein (100, 200, 300 kft) the only source of ionization (upstream of the plume shocks) is in the combustion chamber (i.e. there is no afterburning); thus electron densities within the plume are largely controlled by nozzle chemical kinetic processes.

The systematic calculation of Minuteman plume electrical properties involves a series of individual steps, starting with the following data (i) propellant composition and alkali metal impurity levels, (ii) combustion chamber

---

* This equivalent circuit is known as a plume "simulator".

pressure, (iii) nozzle design and (iv) flight trajectory. These steps include:

1. Thermochemical equilibrium calculation of combustion chamber properties.

2. Two-phase method of characteristics calculation of nozzle gas and particle flow properties.

3. Calculations of neutral and charged species concentrations along nozzle gas streamlines via a nonequilibrium chemistry program.

4. Plume method of characteristics calculations up to the first Mach disc to determine the plume boundary, inviscid flow properties and shock structure.

5. Neutral and charged species concentration calculations along plume streamlines via a nonequilibrium chemistry program.

6. Turbulent mixing/nonequilibrium chemistry calculations along curved plume boundaries to give flow properties and composition in the mixing regions.

7. Preliminary considerations of flow behind the first Mach disc to estimate plume electron densities.

Alternative approaches to these predictions are possible although few are as comprehensive as the procedure outlined above. These are mentioned throughout the following sections, together with our reasons for their rejection in favor of the present approach.

The pertinent results for (and the uncertainties in) each phase of the calculations are discussed below. These results will serve as a good starting point for more sophisticated models and will provide information for those interested in Minuteman nozzle and exhaust plume flows for other applications.

II. COMBUSTION CHAMBER/EQUILIBRIUM NOZZLE FLOW

Minuteman first and second stage propellant compositions and nozzle parameters pertinent to a one-dimensional equilibrium calculation of nozzle flow properties and composition are given in Table I. No measurements of alkali metal impurity levels in actual Minuteman propellants are available. However AeroChem measured[6] amounts of Na and K in samples of the Thiokol TPH-1011 propellant used in 2000-lb thrust motors. Assuming that the impurity content of a propellant is primarily dependent on the ingredients--rather than on the manner in which a particular rocket motor is manufactured--we can safely apply these measured values to the Minuteman Stage 1 propellant. Using similar reasoning, and noting that the dominant source of impurities is introduced via ammonium perchlorate,[7] we assume the impurity levels to be the same for the Stage 1 and Stage 2 propellants. The uncertainties in the results* due to this assumption are expected to be small.

Tables II and III give the one-dimensional equilibrium chamber and nozzle flow properties for Stages 1 and 2, respectively, computed via a standard thermochemical equilibrium code.[8] The following points should be noted:

(1) The quantities of combustibles, CO and H_2, in the exhaust products are very high (about 60 mole % for Stage 1 and about 50 mole % for Stage 2) at their one-dimensional nozzle exit pressures (see Table IV). There is therefore a large potential for exhaust plume afterburning.†

(2) Na and K contribute about equally to the total positive ion concentration in the combustion chamber. Even though the equilibrium decay of $[Na^+]$ is larger than the decay of $[K^+]$ in the nozzle expansion, both Na^+ and K^+ will be included in the nonequilibrium streamline calculations to determine their relative influence on electron-positive ion recombination.

(3) The Al-containing positive ions, Al^+ and $AlOH^+$ can be safely neglected in subsequent kinetic calculations because their concentrations are small compared to $[K^+]$; also $[AlO_2^-]$ can be neglected because it is small compared to $[Cl^-]$.

---

* Throughout this report the phrase "uncertainties in the results" refers to uncertainties in exhaust plume electron densities.

† which will occur at altitudes less than about 75 kft

(4) About 30% of the total mass of the mixture is in the form of Al_2O_3 liquid or solid particles. Thus differences between gas and particle temperatures and velocities at the nozzle exit plane are expected to be large.

Table IV gives the one-dimensional equilibrium (gas/particle and thermochemical) exit plane conditions for the area ratios given in Table I. These are useful reference values for assessing the influence of particle thermal and velocity lags on nozzle gas properties.

Input data to the two-phase method of characteristics nozzle program (see Section III) requires properties of the "gas only" at the temperature that exists for gas/particle equilibrium. Average specific heats and molecular weights of the gas are given in Table V.

III. NOZZLE FLOW

Some possible approaches to computing flow properties and composition in the Minuteman first and second stage nozzles (nozzle contours are shown in Figs. 1 and 2) and their limitations are listed in Appendix A. For the present study we chose to use an analysis in which (i) the two-phase two-dimensional nature of the flow is accounted for via a method of characteristics (MOC) solution and, (ii) the results of the MOC program are input to a non-equilibrium calculation of neutral and charged species concentrations along nozzle streamlines.

A. Gas and Particle Properties

The two-dimensional, two-phase, constant γ method of characteristics (MOC) program[9] used in this study is a proven tool for making nozzle performance calculations and is in wide-spread use. The analysis and computer code are discussed in detail in Ref. 9. The code requires input data on the gas properties (chamber conditions, average values of γ, specific heat, molecular weight, etc.), particle properties (particle mass fraction, and size distribution), and nozzle size and contour.

Specific input data for the present calculations are given in Table VI. The average gas properties are determined at the gas/particle equilibrium temperature (see Table V). The values of Pr, μ and n are reasonable[10] for calculations on Minuteman-type propellant combustion products; Y_p/Y_g is the mass fraction ratio in the combustion chamber. The particle size distribution is based primarily on a private communication[11] from Thiokol personnel who were involved in the experimental determination of particle sizes from

Minuteman first stage motors. These particle sizes are consistent with other measurements on large motors.[12] We assumed the particle size distribution for Stage 2 to be identical to that for Stage 1. (We will demonstrate later that reasonable uncertainties in the particle size distribution do not seriously influence the gas properties.)

The first step in the calculation procedure is to establish an initial data line ($M \geq 1$) for the MOC solution. For a gas/particle flow this line is downstream of the throat (see Figs. 1 and 2). Flow properties in the transonic region are obtained from a one-dimensional sink flow solution[9]--assuming a conical inlet section which joins smoothly to the throat radius of curvature. The two-phase MOC solution starts at the end of the transonic region and marches downstream in the "usual" manner.[13]

Figures 3-8 show the calculated distributions of pressure, gas temperature and gas velocity along the wall and centerline. The relative values of wall and centerline properties are typical[14] for bell-shaped nozzles. Just downstream of the throat the flow along the wall expands more rapidly than the flow along the centerline which has not yet been influenced by the expansion waves emanating from the wall. However, far downstream the pressure on the centerline drops below the wall pressure as the flow along the centerline still experiences the influence of the rapid expansion occurring further upstream along the wall. Shocks which may form in the nozzle cannot be handled by the MOC program. Instead, as noted in the Stage 1 results, the effect of a strong isentropic compression is experienced (axial distance from throat ≈ 17 in.) by all fluid properties. In the Stage 2 nozzle the compression (at ≈ 37 in. from the throat) is weak and only the gas velocity (Fig. 8) is significantly affected.

Particle velocities, temperatures and mass flow rates for each size particle (2, 4, 6, and 8 μ) are shown in Figs. 9-14; limiting particle streamlines (LPS)* are shown in Figs. 1 and 2. Particles are seen (Figs. 11 and 12) to remain at their melting temperature (2318 K) for a considerable portion of the nozzle flow. It is also interesting to note that the 2 μ particles on the centerline are sufficiently small to respond to the Stage 1 nozzle compression--as evidenced by the decrease in velocity (Fig. 9) and increase in temperature (Fig. 11) near the point where the compression wave intersects the axis. Particle mass flow rates (per unit area), which are needed input data to the calculation of heterogeneous electron/positive ion recombination rates, are presented in Figs. 13 and 14.

---

* LPS is defined as the bounding particle streamline for a given particle size, i.e. all particles of the given size are contained between the centerline and the LPS.

In order to determine the influence of uncertainties in the particle size distribution on the gas properties, additional (Stage 2) nozzle calculations were made assuming uniform particle diameters of 3μ and 8μ. This range of particle diameters appears to be reasonable[12] for rocket motors approximately equal in size to the Minuteman motors. The results of these parametric calculations, together with results using the standard (2, 4, 6, 8μ) particle size distribution are shown in Figs. 15-17--where it can be noted that even serious errors in particle size distributions (within the 3 - 8μ range) do not significantly influence the gas properties.* This is a very important conclusion since there is usually a large uncertainty in the actual size distribution generated by highly aluminized solid propellant systems.

Nozzle exit plane gas and particle properties (input to the exhaust plume MOC program and the turbulent mixing/nonequilibrium chemistry plume program) are given in Figs. 18-21. Radial distributions of gas properties (Figs. 18 and 20) are as expected. Properties are seen to be nearly constant from the centerline up to $r/r_N \approx 0.6$, and then vary rapidly up to the nozzle lip. Of particular importance are the large differences between actual and one-dimensional equilibrium exit plane properties. Use of the one-dimensional properties in plume calculations could therefore result in serious errors. Exit plane distribution of particle properties appears to be consistent with the gas properties. It is interesting to note that, for Stage 1, (Fig. 19a) both 6μ and 8μ particles remain at their melting temperature across the entire exit plane. Also note that there is little difference between gas and particle flow angles (Figs. 19b and 21b).

Figure 22 shows that uncertainties in particle size distributions (over the 3μ and 8μ range) do not have a serious effect on Stage 2 exit plane properties.

The above results are then used as follows:

(1) Gas pressure, temperature and velocity distributions along the wall and centerline are input data to the calculation of nonequilibrium neutral and charged species concentrations in the nozzle.

(2) Nozzle exit plane gas properties are input data to the exhaust plume MOC and turbulent mixing/nonequilibrium chemistry programs.

(3) Particle properties are used to calculate heterogeneous electron/ion recombination rates. (There was, unfortunately, insufficient time to perform these calculations for the present study. Errors in exhaust plume electron densities introduced by neglecting heterogeneous recombination are discussed in Section III.B. All necessary data for future calculations are given in this report.)

---

* The key parameter is therefore the particle mass fraction (Table V).

B. Neutral and Charged Species Concentrations

A new computer code had to be written to make nonequilibrium calculations of neutral and charged species concentrations along streamlines in a two-phase gas/particle flow. This code takes input data from the nozzle MOC calculations and integrates the species continuity equations along streamlines. An implicit numerical integration procedure was used similar to that incorporated into the JANNAF ODK program.[15]*

Figures 3-8 give the input gas properties for the Stage 1 and Stage 2 nozzle wall and centerline nonequilibrium calculations. Initial conditions were specified at the beginning of the transonic flow region--as determined from the two-phase MOC program; these are given in Table VII. The initial mole fraction of Na^+, K^+, Cl^-, and e^- were adjusted slightly (in proportion to their absolute values) to maintain charge balance because Al^+, $AlOH^+$ and AlO_2^- were neglected.

The reaction mechanism and rate coefficients for the nozzle streamline calculations are given in Table VIII. The rate coefficients are those recommended by Jensen and Kurzius[16] and recently updated by Jensen and Jones;[17] they are considered to be the best available values. The wide range of the error bounds for many reactions (particularly those directly affecting charged species concentrations) must be accounted for in assessing the accuracy of results (this point will be discussed later).

Figures 23-30 give species mole fraction distributions along the wall and centerline for the Stage 1 and Stage 2 nozzles as computed by the new nonequilibrium streamline code. The following points should be noted:

(1) The major neutral species mole fractions remain approximately constant (Figs. 23 and 27).

(2) H and Cl mole fractions freeze rapidly, while the other free radicals (O, OH) show a continuous decay (Figs. 24, 25, 28 and 29).

(3) NaCl and KCl mole fractions remain approximately constant while Na and K mole fractions freeze rapidly (Figs. 25 and 29).

(4) Electron mole fractions decay rapidly to their minimum values (Figs. 26 and 30). The subsequent increase in $[e^-]$ occurs because the three-body recombination rates (Reactions 17 and 18) become small compared to the reverse of Reaction 22, i.e. $H + Cl^- \rightarrow HCl + e^-$, which dominates over the forward reaction at low temperatures.

---

* The ODK program does not allow gas temperature and velocity distributions as input data. It was therefore not possible to use it for this problem.

This increase in $[e^-]$ has important implications with regard to the plume calculations (Section IV.B). Note that $[Na^+]$ recombines much faster than $[K^+]$, and Na-containing species can safely be neglected in subsequent kinetic calculations of this type.*

The differences between wall and centerline values reflect the differences in pressure/temperature histories. Only [O], $[O_2]$ and [H] are seen to have significantly large radial variations at the exit plane.

The influence, on electron mole fractions, of varying the rate coefficients for Reactions (19) and (22) (Table VIII) is shown in Fig. 31. We chose to vary these particular rate coefficients because: (i) previous studies[18,19] showed plume electron densities to be quite sensitive to the rate of Reaction (19)--and using $k_{19}/10$ in afterburning plume calculations gave better comparisons with attenuation data than using k_{19} and (ii) $[e^-]$ is known to be sensitive to the rate of Reaction (22)--which has a large lower bound.† The results of this parametric study (Fig. 31) show that varying k_{19} and k_{22} by factors of 10 and 100 respectively (which are within the error bounds cited in Table VIII), has relatively little effect on $[e^-]$ at the nozzle exit plane. If heterogeneous electron-positive ion recombination rates were included the exit plane values of $[e^-]$ would decrease by perhaps a factor of 2--making the values given in Figs. 26 and 30 conservatively large.

IV. INVISCID PLUME PROPERTIES AND SHOCK STRUCTURE

The method of characteristics (MOC) is the standard technique for computing inviscid underexpanded rocket plume properties. When coupled with the Rankine-Hugoniot equations, which describe property variations across shocks, it is an extremely useful method for determining inviscid plume boundaries, internal shock structure and flow properties--up to the first Mach disc.‡ The computer code used to make these calculations[20] was developed at Lockheed, and has been demonstrated[21] to give predictions of plume boundaries and shock structures which are in good agreement with experimental observations.

---

* However the influence of Na on the initial positive ion concentrations will have to be accounted for.

† The recommended rate coefficient for Reaction (22) shown in Table VIII is larger, by two orders of magnitude than the value originally recommended by Jensen and Kurzius.[16]

‡ Calculations downstream of the first Mach disc are discussed in Section VII.

In the present calculations we assume that the particles have a negligible influence on gas properties in the p[illegible]ne. This appears to be a reasonable assumption since the gas expands very rapidly downstream of the exit plane, resulting in decreased particle drag and gas/particle heat transfer rates. The errors introduced in the calculations of plume electrical properties by imposing this assumption are negligible.

A. Location of First Mach Disc

The position of the first Mach disc in underexpanded free jets has been studied experimentally by several investigators.[22-27] Lewis and Carlson[22] developed a semi-empirical relationship for the axial position of the Mach disc based upon measurements on jets from a 15° half angle conical nozzle into still air. They showed that

$$x/d_N = k\, M_{ex}\, \gamma_{ex}^{k_1} \left(\frac{p_{ex}}{p_\infty}\right)^{k_1} \tag{1}$$

where the empirical constants, k_1 and k_2 were found to be 0.69 and 0.5, respectively.

Additional studies[23-26] have confirmed the form of Eq. (1) and extended the correlation to account for the effect of a supersonic free stream; thus for $M_\infty > 1$,

$$x/d_N = k\, M_{ex}\, \gamma_{ex}^{k_1} \left(\frac{p_{ex}}{p_\infty}\right)^{k_1} M_\infty^{-k_1/2} \tag{2}$$

Equation (2) correlates data over a wide range of pressure ratios, jet exit Mach numbers and free stream Mach numbers and can therefore be used to predict first Mach disc locations in rocket plumes with a relatively high confidence level.*

The influence of solid particles on the position of the Mach disc has also been experimentally studied by Lewis and Carlson.[22] They measured x/d_N as a function of particle mass fraction and found the following correction factor (to Eq. (2)),

---

* The influence of nozzle exit flow angle on first Mach disc locations has not yet been experimentally determined. Equation (2) covers the range of flow angles from 0 to 15 deg, which is the range of interest for the Stage 1 and Stage 2 nozzles.

$$f(Y_p) = \left[1 + 0.197\ M_{ex}^{1.45}\ Y_p^{0.65}\right]^{-1} \tag{3}$$

Therefore, for gas-particle flows with a supersonic free stream the position of the Mach disc can be located from

$$x/d_N = \frac{0.69\ M_{ex}\ Y_{ex}^{0.5}}{f(Y_p)} \left(\frac{p_{ex}}{p_\infty}\right)^{0.5} M_\infty^{-0.25} \tag{4}$$

Experimental data on the Mach disc diameter are given by Crist, et al,[27] and D'Attorre and Harshbarger,[24] but these data have not been reduced to empirical relationships. It has however been found that the diameter has the same pressure ratio dependence as the axial location, i.e.

$$D/d_N \propto (p_{ex}/p_\infty)^{0.5} \tag{5}$$

Because of the lack of more definitive data, we determined D by using the MOC solution up to the value of x/d_N determined from Eq. (4). The Mach disc diameter was then taken to be the intercepting shock diameter at the axial location of the disc.

B. Equivalent Single Nozzle Approximation

Minuteman first stage consists of a four-nozzle assembly (see Fig. 32). Thus the interaction of four exhaust plumes should, in principle, be taken into account in calculating first stage electrical properties. However techniques for making interacting plume flow field calculations have not yet been developed. We therefore utilized an equivalent single nozzle approximation in which the four nozzles shown in Fig. 32 were replaced by a single nozzle, with the same total mass flow rate as the four nozzles (i.e. $(r_N)_{eq} = 2\ r_N$). At values of x/r_N large compared to the plume intersection distance, this assumption should be reasonably good. However the assumption breaks down in the vicinity of the missile base and a detailed analysis of the intersecting plume flow field would be needed for an accurate description of the electrical properties in this region.

C. Results

Figure 33 shows the plume boundary, intercepting shock, Mach disc and constant Mach number contours* for Stage 1 at 100 kft (free stream Mach number = 5.15) as computed from the Lockheed MOC program[20] (using the input data given in Table IX). Note the rapid expansion in the region contained by the shock and the plume centerline--so that $M > 8$ before the first Mach disc. Also observe that the Mach numbers are relatively constant in the region between the shock and the boundary. Figure 34 shows the influence of free stream Mach number on the size of the plume and position of the Mach disc.

The results for Stage 2 at 118 kft, 200 kft and 300 kft are shown in Figs. 35-37, respectively. At 118 kft the ratio of nozzle exit pressure to the pressure behind the external shock (not shown in Fig. 35) is only about 2--too low for a Mach disc to form. Instead we predict that the diamond pattern (i.e. a negligibly small Mach disc) typical of plumes with exit to free stream pressure ratios slightly greater than unity will form. Also shown in Fig. 35 are the locations of the streamlines along which kinetic calculations were made (see Section V). The Stage 2, 300 kft results (Fig. 37) show that the boundary and shock approach each other with increasing altitude and the Mach disc moves far downstream and is located at $x/r_N = 770$.

V. NONEQUILIBRIUM CHEMISTRY - PLUME STREAMLINES

The nonequilibrium chemistry calculations along plume streamlines were made with the same computer code used to determine neutral and charged species concentrations in the Stage 1 and Stage 2 nozzles. Input data to the code were pressure, temperature and velocity distributions along individual streamlines, as defined by the MOC calculations, and the species mole fractions at the nozzle exit plane, given in Figs. 23-30. The streamlines† were followed from the exit plane to the shock--then downstream of the shock to the plume boundary.‡ Calculations were made along a sufficient number of streamlines to describe electron densities throughout the inviscid plume; some of

---

* All plume properties e.g. pressure, temperature, etc., can be computed from the standard isentropic flow relationships using the values of γ, stagnation pressure and stagnation temperature listed in Table IX.

† Only streamlines that intersect the shock upstream of the triple point were considered.

‡ The flow behind the (relatively weak) intercepting shock is essentially frozen.

these results are presented in Figs. 38-40. Figure 38 shows the electron density (and electron mole fraction) variation along the centerline of the Stage 1 plume--up to the Mach disc. It is interesting to note that X_{e^-} increases--because the reaction $H + Cl \rightarrow HCl + e^-$ is still significantly fast at temperatures slightly less than the nozzle exit plane temperature. However X_{e^-} rapidly approaches a "frozen" value, after which n_e decreases in proportion to the gas density. Figure 39 shows the influence of the value of k_{22} used in the kinetic calculations on X_{e^-} in the Stage 2 plume. Using k_{22} recommended by Jensen and Jones[17] results in an order of magnitude increase in X_{e^-} before the first shock intersection with the plume axis (see Fig. 35).

This increase in X_{e^-} was unexpected--since it has been generally thought that X_{e^-} decreases in inviscid plumes due to the three-body recombination reactions (17) and (18) (Table VIII). However the thermodynamics of Reaction (22) favors the backward reaction as temperature decreases. Thus X_{e^-} is controlled by a two-body reaction which produces electrons rather than a three-body reaction which depletes electrons. This situation occurs even if $k_{22}/100$ (which is within the error bounds recommended by Jensen and Jones) is used in the calculations (as seen in Figs. 39 and 40).

Whether X_{e^-} actually increases in an inviscid plume has not been checked out experimentally. It is, of course, possible that the mechanism listed in Table VIII is not complete, and that some competing two-body recombination reactions have been omitted. Jensen[28] has suggested that the formation of hydrated ions (e.g. $K \cdot H_2O^+$) in the chamber and the subsequent recombination reaction, $K \cdot H_2O^+ + e^- \rightarrow$ Products might influence X_{e^-} in the nozzle and plume since the recombination rate for this two-body reaction is faster than the three-body recombination reactions (17) and (18). However there was insufficient time in this short study to explore the above (and other) possible additions to the reaction mechanism of Table VIII. We therefore chose (as a compromise) $k_{22}/100$ for the "standard" electron density calculations reported in Figs. 46, 48, 50, and 52 , and estimate these results to be within about a factor of 3 of the actual values.

The results shown in Fig. 40 for $k_{22}/100$ give n_e distribution in the inviscid plume (up to the intercepting shock and Mach disc) for the Stage 2 altitudes under investigation.

VI. MIXING/NONEQUILIBRIUM CHEMISTRY ALONG CURVED PLUME BOUNDARIES

The discussion to this point has demonstrated how electron densities in the inviscid plume have been computed. The next step is to couple these results with a calculation of the properties in the mixing region. An analysis which completely couples the mixing/nonequilibrium chemistry equations (along the curved plume boundary) to the method of characteristics solution is beyond the scope of the present study.* For the present calculations we have utilized an approximate method in which the computed pressure distribution along the inviscid plume boundary (which takes into account the external plume shock caused by the expanded plume boundary) is input to the mixing/nonequilibrium chemistry program.[29] We then determine the position of the dividing streamline† from the program and assume that the plume properties computed along the dividing streamline are the same as those along the inviscid plume boundary. The radial property distributions and width of the mixing region are then taken directly from the computer output. This type of solution is reasonable only until the computed mixing region intersects the plume axis. Downstream of this region the radial property distribution must be estimated. Further downstream however, the effects of the curved boundary become small, the plume pressure becomes nearly constant and equal to the ambient pressure and the axisymmetric mixing/nonequilibrium chemistry program should give reasonably accurate plume electron densities.

Input data to the mixing/nonequilibrium chemistry calculations include the species mole fractions at the nozzle exit‡ given in Figs. 23-30 and the pressure, temperature and velocity data given in Table X. Figure 41 shows the plume boundary pressures computed from the MOC program, while Fig. 42 shows the relative position of the dividing streamlines and plume boundaries.§

---

* Such an analysis and computer code will be developed under a subsequent AFRPL contract. In our initial work on this problem however we have formulated the appropriate equations and have considered various numerical solutions.

† The dividing streamline is the streamline which starts at the nozzle lip.

‡ We assume that the species mole fractions remain frozen at their exit plane values during the Prandtl-Meyer expansion from the nozzle lip pressure to initial boundary pressure.

§ No results are shown for Stage 2, 300 kft since mixing has little influence on electron densities at this altitude.

For Stage 1 (100 kft) and Stage 2 (118 kft) the new superposition technique described above appears to be reasonable; however for Stage 2 (200 kft) the plume boundary location is much different from the dividing streamline location, resulting in a greater inaccuracy in predicted electron densities. Temperature and electron mole fraction distributions along the dividing streamlines are given in Fig. 43.

The mixing region was assumed to be turbulent for all calculations. The eddy viscosity model used was that of Donaldson and Gray,[30] modified by Tufts and Smoot[31] to account for non-zero free stream velocities.

VII. FLOW PROPERTIES BEHIND FIRST MACH DISC

There has been no published work to date which gives a good computational scheme for determining flow properties and composition behind the first Mach disc (within the second shock cell). We have made a limited attempt to develop such a computational procedure by investigating the mixing that occurs along the slip line, between the fluid passing through the Mach disc(normal shock) and the fluid passing through the oblique shock. (Thus each fluid has a different total pressure.) There was insufficient time however to make complete calculations with the AeroChem Mixing/Nonequilibrium Chemistry program.* Therefore electron densities along the centerline behind the Mach disc were determined from the streamline kinetic program.

These calculations were made for the Stage 1, 100 kft plume. The initial pressure, temperature and velocity were computed from normal shock relations; initial species mole fractions were assumed to be equal to their values upstream of the Mach disc (see Table XI). Pressure, temperature and velocity distributions along the centerline (up to the start of the second shock cell--at $x/r_N \approx 50$) were estimated by reference to other MOC calculations.† These estimates are given in Fig. 44. Also shown are initial calculations made with the mixing/nonequilibrium chemistry program. Note the relatively large changes in velocity and temperature due to mixing, indicating the importance of viscous effects in this region.

---

* This will be pursued in a future contract with AFRPL.

† with lower nozzle exit to ambient pressure ratios, which gave results behind the first oblique shock intersection with the axis, and up to the second shock intersection.

Figure 45 shows the very large predicted centerline electron mole fractions and electron densities downstream of the Mach disc. We expect that the effects of mixing along the slip line will be to lower peak electron densities and increase the electron decay rates.

VIII. ELECTRON DENSITY AND COLLISION FREQUENCY PROFILES

Complete electron density and collision frequency profiles, obtained from the analyses described in Sections IV-VII, are given in Figs. 46-53. For the purpose of establishing error bounds on the plume electrical conductivity (a function of n_e and ν_e) we assume that the collision frequencies have been accurately computed (via the collision cross sections cited in Ref. 32) and all errors are "lumped" into the error bounds placed on n_e.

Stage 1 n_e profiles (Fig. 46) are estimated to be correct to within a factor of 3, up to the position of the first Mach disc ($x/r_N = 27$). Profiles downstream of this point, within the second shock cell are based on the centerline n_e profiles (shown in Fig. 45), which have been arbitrarily reduced by about an order of magnitude to account for mixing across the slip line (Section VI). Values of n_e between $x/r_N = 27$ and $x/r_N = 50$ are estimated to be correct to within a factor of 10.

The Stage 2, 118 kft plume has a negligibly small Mach disc (Fig. 35). Thus, conditions downstream of the shock intersection with the plume centerline can be determined via the method of characteristics. We therefore expect the Stage 2 (118 kft) values of n_e (Figs. 48a and 48b) to be accurate to within a factor of 3 for $x/r_N \leq 20$, and within a factor of about 6 for $x/r_N > 20$. The dashed curves on Figs. 48a and 48b, i.e. "slow mixing" were determined using the original Donaldson/Gray eddy viscosity formulation.[30] These results imply negligibly small mixing rates for $x/r_N < \approx 30$.* Use of the Tufts/Smoot correction[31] gives more realistic turbulent mixing rates; the resulting n_e profiles are the solid curves in Figs. 48a and 48b. These curves should be used for future electrical conductivity calculations.

Stage 2, 200 kft profiles (Figs. 50 and 51) have been computed up to the approximate position of the first Mach disc. The dashed curves give the results for "slow mixing".* Thus, we observe that at $x/r_N = 60$ the inner mixing boundary is located at $r/r_N \approx 12$, still far from the plume centerline. These n_e profiles are expected to be accurate to within a factor of 3, up to $x/r_N = 74$. Calculations downstream of $x/r_N = 74$ must include an analysis of flow behind the Mach disc, which was not made in the present study. We would, however, expect increases in n_e similar to those observed in the Stage 1 plume (Fig. 46).

---

* Thus, in this region the "slow mixing" profiles are identical to the inviscid profiles.

The influence of mixing on the n_e and ν_e profiles for Stage 2 (300 kft) is neglibibly small. Thus, the profiles given in Figs. 52 and 53 are those determined from the inviscid plume calculations only. Values of n_e are expected to be accurate to within a factor of 3.

IX. SUMMARY AND RECOMMENDATIONS

The electron density and collision frequency profiles presented herein have been determined from the most comprehensive study made to date of Minuteman exhaust plume electrical properties. Estimated error bounds on computed electron densities range from a factor of 3 to 10, depending on plume location and flight conditions. Collision frequencies are assumed to be essentially correct.

In the process of computing plume electrical properties we have shown that:

(1) Gas property distributions at the nozzle exit plane depend strongly on the weight percent of particles in the flow--but are weakly dependent on the precise particle size distribution (within the range of 2-8 μ particle diameters).

(2) Variation of the important rate coefficients for the charged species reactions within their ranges of uncertainty do not have a significant influence on nozzle exit plane electron densities.

(3) Inviscid plume electron densities are very sensitive to the rate coefficient for $H + Cl^- \rightarrow HCl + e^-$, which produces electrons at relatively low temperatures.

(4) Electron production behind the first Mach disc, and within the second shock cell, is significantly high for Stage 1 (at 100 kft) and must be accounted for in determining electron density profiles.

We recommend that future calculations on Minuteman exhaust plumes include: (i) the influence of heterogeneous electron/positive ion recombination on plume electron densities, (ii) the use of coupled method of characteristics/turbulent mixing/nonequilibrium chemistry analysis for those flight conditions where the mixing region is significantly large compared to the plume boundary radius and (iii) implementation of the technique initiated herein to determine flow properties and composition behind the first Mach disc via an analysis of mixing/nonequilibrium chemistry along the slip line.

REFERENCES

1. Pergament, H.S. and Lam, S.H., AeroChem contribution to "Flame Plasma Effects Study" (U), Third Interim Report, prepared jointly with RCA, Defense Electronics Products Division; AeroChem TN-54, RADC-TDR-64-512, DDC AD 357 197, December 1964. (SECRET)

2. Pergament, H.S. and Calcote, H.F., "A Mathematical Model for Predicting RF Interference Effects in Rocket Exhaust Plumes," Proceedings of the Third Symposium on the Plasma Sheath - Plasma Electromagnetics of Hypersonic Flight, Vol. II (Air Force Cambridge Research Laboratories, Hanscom Field, Bedford, Mass., May 1967), pp. 309-354.

3. Pergament H.S. and Calcote, H.F., "Thermal and Chemi-Ionization Processes in Afterburning Rocket Exhausts," Eleventh Symposium (International) on Combustion (The Combustion Institute, Pittsburgh, 1967), pp. 597-611.

4. Smoot, L.D., Simonsen, J.M. and Hedman, P.O., "Development and Evaluation of a Flight Attenuation Model," Naval Weapons Center, TP 5048, November 1971.

5. Pergament, H.S., "The Role of Eddy Viscosity Models in Predicting Afterburning Rocket Exhaust Plume Properties and Radar Attenuation," Fifth Plume-Signal Interference Conference (U), CPIA Publ. No. 186 (Applied Physics Lab., Johns Hopkins Univ., Silver Spring, 1969), pp. 417-437. (CONFIDENTIAL)

6. Pergament, H.S., Birnbaum, S. and Mikatarian, R.R., "Radar Reflectivity of Turbulent Rocket Exhaust Plumes" (U), AeroChem TP-167, Annual Report, AFRPL-TR-67-251, DDC AD 388 832, December 1967. (CONFIDENTIAL)

7. Smoot, L.D., "Mechanisms That Cause Radar Attenuation" (U), Lockheed Propulsion Company, Final Report, LPC-756-F, 15 January 1967. (CONFIDENTIAL)

8. Gordon, S. and Zeleznik, F.J., "A General IBM 704 or 7090 Computer Program for Computation of Chemical Equilibrium Compositions, Rocket Performance and Chapman-Jouguet Detonations, NASA TN D-1737, October 1963.

9. Nickerson, G.R. and Kliegel, J.R., "Axisymmetric Two-Phase Perfect Gas Performance Program," TRW Systems Report No. 02874-6006-R000, Vol. I and II, April 1967.

10 Hoffman, J., Purdue University, January 1972 (private communication); see also Air Force Aero Propulsion Laboratory, TR-71-52, Vol. I and II.

11. Lund, R., Thiokol Chemical Corporation, January 1972 (private communication).

12. Delaney, L.J., "Particle Characteristics in Two Phase Plumes," Proceedings of the Rocket Plume Phenomena Specialists Meeting, Vol. I (Aerospace Corporation, San Bernardino, October 1968) pp. 209-232.

13. Ferri, A., Elements of Aerodynamics of Supersonic Flows (MacMillan Co., New York, 1949).

14. Pergament, H.S. and Mikatarian, R.R., "Calculation of Nonequilibrium Nozzle and Exhaust Plume Properties for Saturn Launch Vehicles," AeroChem TP-160, Final Report, August 1967.

15. Frey, H.M., Kliegel, J.R., Nickerson, G.R., and Tyson, T.J., "ICRPG One-Dimensional Kinetic Reference Program," July 1968.

16. Jensen, D.E. and Kurzius, S.C., "Rate Constants for Calculations on Nozzle and Rocket Exhaust Flow Fields," AeroChem TP-149, NASA CR-90528, March 1967.

17. Jensen, D.E. and Jones, G.A., "Gas-Phase Reaction Rate Coefficients for Rocketry Applications," RPE Technical Report No. 71/9, October 1971.

18. Pergament, H.S. and Jensen, D.E., "Influence of Chemical Kinetic and Turbulent Transport Coefficients on Afterburning Rocket Plumes," J. Spacecraft Rockets 8, 643-649 (1971).

19. Pergament, H.S., "Interpretation of Simulated Rocket Exhaust Plume Radar Attenuation Data" (U), JANNAF 6th Plume Technology Meeting, CPIA Publ. No. 209 (Applied Physics Lab., Johns Hopkins Univ., Silver Spring, 1971) pp. 489-514. (CONFIDENTIAL)

20. Smith, S.D. and Ratliff, A.W., "Rocket Exhaust Plume Computer Program Improvement," Vol. I - Final Report, Lockheed Missiles and Space Co. HREC-7761-1, LMSC-HREC D162220-I, June 1971.

21. Ratliff, A.W., "Comparisons of Experimental Supersonic Flow Fields with Results Obtained by Using a Method of Characteristics Solution," Lockheed Missiles and Space Co., LMSC/0082-9, LMSC/HREC, A782592, April 1966.

22. Lewis, Jr., C.H. and Carlson, D.J., "Normal Shock Location in Underexpanded Gas and Gas-Particle Jets," AIAA J. 2, 776-777 (1964).

23. D'Attorre, L. and Harshbarger, F.C., "Parameters Affecting the Normal Shock Location in Underexpanded Gas Jets," AIAA J. 3, 530-531 (1965).

24. D'Attorre, L. and Harshbarger, F.C., "Further Experimental and Theoretical Studies of Underexpanded Jets Near the Mach Disc," General Dynamics/Astronautics GDA-DBE-64-041, July 1964.

25. D'Attorre, L. and Harshbarger, F., "Experimental Studies of Underexpanded Jets Near the Mach Disc," General Dynamics/Astronautics GDA-DBE-64-008, February 1964.

26. D'Attorre, L. and Harshbarger, F., "The Behavior of the Mach Disc Up to Moderate Pressure Ratios," General Dynamics/Astronautics GDA-DBE-64-042, July 1964.

27. Crist, S., Sherman, P.M. and Glass, D.R., "Study of the Highly Underexpanded Sonic Jet," AIAA J. 4, 68-71 (1966).

28. Jensen, D.E., Rocket Propulsion Establishment, March 1972 (private communication).

29. Mikatarian, R.R. and Pergament, H.S., "AeroChem Axisymmetric Mixing with Nonequilibrium Chemistry Computer Program," AeroChem TP-200, AFRPL-TR-69-167, DDC AD 856 017, June 1969.

30. Donaldson, C. duP. and Gray, K.E., "Theoretical and Experimental Investigation of the Compressible Free Mixing of Two Dissimilar Gases," AIAA J. 4, 2017-2025 (1966).

31. Tufts, L.W. and Smoot, L.P., "A Turbulent Mixing Coefficient Correlation for Coaxial Jets with and without Secondary Flows," J. Spacecraft Rockets 8, 1183-1190 (1971).

32. Molmud, P., "The Electrical Conductivity of Weakly Ionized Gases," ARS Preprint 2586-62; presented at ARS Ions in Flames and Rocket Exhausts Conference, Palm Springs, 10-12 October 1962.

TABLE I

MINUTEMAN PROPELLANT COMPOSITIONS AND NOZZLE PARAMETERS (U)

	Stage 1 (Thiokol TPH-1011)	Stage 2 (Aerojet ANB-3066)
Composition, wt. %		
Ammonium Perchlorate	70	73
Aluminum	16	15
Binder	14 (PBD/acrylic acid acrylinitrile)	15 (PBCT)
Elements, gram-atoms		
C	0.929	0.865
H	3.68	3.88
O	2.47	2.50
N	0.627	0.625
Al	0.593	0.556
Cl	0.600	0.621
Impurities, ppm		
Na	180	180
K	50	50
Heat of Formation (Propellant), kcal/mole	-43.6	-43.8
Chamber Pressure, psia	741	445
Throat Diameter, in.	7.22	9.6
Exit Diameter, in.	22.9	48
A_{ex}/A^*	10	25
r_N, in.	---	48
$(r_N)_{eq.}$, in.	45.6	---

TABLE II

ONE DIMENSIONAL EQUILIBRIUM NOZZLE FLOW PROPERTIES

Minuteman Stage 1

Pressure, psia	741	429 (throat)	300	200	100	50	10	5	1
Temperature, K	3410	3210	3080	2940	2690	2450	2080	1870	1430
Enthalpy, kcal/100 g	-43.6	-56.5	-64.5	-73.0	-86.6	-98.9	-124.2	-133.6	-151.7
Specific Heat, cal/100 g	43.9	43.7	43.6	43.5	43.2	42.8	41.6	40.9	39.1
Moles gas/100 g	3.57	3.54	3.53	3.51	3.49	3.47	3.46	3.46	3.45
Composition, moles/100 g									
CO	8.95(-1)	8.95(-1)	8.94(-1)	8.93(-1)	8.90(-1)	8.85(-1)	8.72(-1)	8.62(-1)	8.17(-1)
CO_2	5.90(-2)	5.98(-2)	6.06(-2)	6.19(-2)	6.51(-2)	6.99(-2)	8.19(-2)	9.32(-2)	1.38(-1)
HCl	5.02(-1)	5.26(-1)	5.40(-1)	5.54(-1)	5.72(-1)	5.84(-1)	5.92(-1)	5.94(-1)	5.95(-1)
H	1.29(-1)	1.02(-1)	8.52(-2)	6.72(-2)	4.06(-2)	2.11(-2)	6.67(-3)	2.07(-3)	5.21(-5)
H_2	1.02(0)	1.03(0)	1.04(0)	1.05(0)	1.06(0)	1.07(0)	1.09(0)	1.10(0)	1.15(0)
OH	2.98(-2)	2.03(-2)	1.52(-2)	1.05(-2)	5.00(-3)	1.95(-3)	3.50(-4)	6.93(-5)	4.46(-7)
H_2O	5.31(-1)	5.26(-1)	5.22(-1)	5.18(-1)	5.13(-1)	5.07(-1)	4.95(-1)	4.84(-1)	4.40(-1)
N_2	3.14(-1)	3.15(-1)	3.15(-1)	3.16(-1)	3.16(-1)	3.16(-1)	3.16(-1)	3.16(-1)	3.16(-1)
Al_2O_3(c)	2.76(-1)	2.83(-1)	2.87(-1)	2.91(-1)	2.94(-1)	2.96(-1)	2.96(-1)	2.96(-1)	2.96(-1)
K	4.26(-6)	3.50(-6)	3.11(-6)	2.57(-6)	1.71(-6)	9.86(-7)	3.64(-7)	1.30(-7)	4.42(-9)
KCl	9.69(-5)	1.06(-4)	1.07(-4)	1.11(-4)	1.18(-4)	1.24(-4)	1.27(-4)	1.28(-4)	1.28(-4)
Na	7.03(-5)	5.97(-5)	5.22(-5)	4.38(-5)	2.99(-5)	1.79(-5)	7.44(-6)	2.84(-6)	1.33(-7)
NaCl	6.62(-4)	6.89(-4)	7.02(-4)	7.19(-4)	7.42(-4)	7.60(-4)	7.75(-4)	7.80(-4)	7.83(-4)
Cl	4.24(-2)	3.52(-2)	3.01(-2)	2.44(-2)	1.53(-2)	8.22(-3)	2.70(-3)	8.58(-4)	2.32(-5)
Al^+	3.02(-6)	8.50(-7)	3.28(-7)	9.62(-8)	7.86(-9)	3.42(-10)	6.18(-13)	2.14(-15)	6.03(-23)
$AlOH^+$	2.75(-6)	7.49(-7)	2.87(-7)	8.53(-8)	7.50(-9)	3.81(-10)	8.25(-13)	4.36(-15)	5.30(-22)
K^+	2.52(-5)	2.14(-5)	1.77(-5)	1.40(-5)	8.39(-6)	4.22(-6)	1.17(-6)	3.20(-7)	5.24(-9)
Na^+	2.76(-5)	1.93(-5)	1.47(-5)	1.01(-5)	4.70(-6)	1.75(-6)	2.81(-7)	5.05(-8)	2.38(-10)
Cl^-	5.60(-5)	4.11(-5)	3.22(-5)	2.40(-5)	1.30(-5)	5.94(-6)	1.45(-6)	3.70(-7)	5.48(-9)
e^-	1.04(-6)	6.22(-7)	4.21(-7)	2.61(-7)	9.74(-8)	2.80(-8)	3.36(-9)	3.90(-10)	5.11(-13)
AlO_2^-	1.22(-6)	4.78(-7)	2.36(-7)	9.83(-8)	1.66(-8)	1.81(-9)	2.06(-11)	2.53(-13)	7.32(-19)

TABLE III

ONE DIMENSIONAL EQUILIBRIUM NOZZLE FLOW PROPERTIES

Minuteman-Stage 2

Pressure, psia	445	259 (throat)	200	100	50	10	5	1
Temperature, K	3410	3230	3140	2910	2680	2310	2100	1630
Enthalpy, kcal/100 g	-43.8	-56.5	-62.3	-76.9	-90.3	-117	-128	-148
Specific Heat, cal/100 g-°K	44.0	43.8	43.7	43.5	43.2	42.2	41.6	39.9
Moles gas/100 g	3.57	3.54	3.52	3.48	3.46	3.43	3.42	3.41
Composition, moles/100 g								
CO	7.85(-1)	7.82(-1)	7.81(-1)	7.77(-1)	7.72(-1)	7.60(-1)	7.50(-1)	7.11(-1)
CO_2	7.86(-2)	8.11(-2)	8.24(-2)	8.65(-2)	9.16(-2)	1.04(-1)	1.13(-1)	1.53(-1)
HCl	5.19(-1)	5.41(-1)	5.51(-1)	5.73(-1)	5.92(-1)	6.08(-1)	6.15(-1)	6.20(-1)
H	1.54(-1)	1.27(-1)	1.14(-1)	8.05(-2)	5.12(-2)	2.19(-2)	9.43(-3)	5.02(-4)
H_2	8.69(-1)	8.76(-1)	8.79(-1)	8.88(-1)	8.98(-1)	9.14(-1)	9.27(-1)	9.68(-1)
OH	5.44(-2)	3.98(-2)	3.36(-2)	1.98(-2)	1.01(-2)	2.71(-3)	8.24(-4)	1.41(-5)
H_2O	6.88(-1)	6.93(-1)	6.95(-1)	6.99(-1)	7.00(-1)	6.93(-1)	6.84(-1)	6.46(-1)
N_2	3.10(-1)	3.11(-1)	3.11(-1)	3.12(-1)	3.12(-1)	3.12(-1)	3.12(-1)	3.12(-1)
Al_2O_3(c)	2.60(-1)	2.67(-1)	2.69(-1)	2.73(-1)	2.76(-1)	2.77(-1)	2.78(-1)	2.78(-1)
K	4.57(-6)	3.94(-6)	3.73(-6)	2.89(-6)	2.03(-6)	1.03(-6)	4.88(-7)	3.54(-8)
KCl	9.00(-5)	1.00(-4)	9.94(-5)	1.07(-4)	1.14(-4)	1.23(-4)	1.26(-4)	1.28(-4)
Na	7.88(-5)	6.94(-5)	6.44(-5)	5.04(-5)	3.61(-5)	1.95(-5)	9.95(-6)	9.12(-7)
NaCl	6.42(-4)	6.68(-4)	6.78(-4)	7.08(-4)	7.33(-4)	7.58(-4)	7.71(-4)	7.83(-4)
Cl	6.17(-2)	5.30(-2)	4.85(-2)	3.59(-2)	2.37(-2)	1.06(-2)	4.66(-3)	2.58(-4)
Al^+	3.20(-6)	9.97(-7)	5.41(-7)	8.08(-8)	7.80(-9)	6.71(-11)	9.58(-13)	6.68(-19)
$AlOH^+$	3.16(-6)	9.55(-7)	5.15(-7)	7.75(-8)	7.96(-9)	7.07(-11)	1.30(-12)	2.72(-18)
K^+	3.16(-5)	2.79(-5)	2.48(-5)	1.78(-5)	1.13(-5)	4.54(-6)	1.81(-6)	6.80(-8)
Na^+	3.62(-5)	2.64(-5)	2.24(-5)	1.29(-5)	6.38(-6)	1.56(-6)	4.43(-7)	5.92(-9)
Cl^-	7.00(-5)	5.42(-5)	4.67(-5)	3.03(-5)	1.75(-5)	6.06(-6)	2.24(-6)	7.39(-8)
e^-	1.50(-6)	9.83(-7)	7.77(-7)	3.87(-7)	1.61(-7)	3.31(-8)	6.92(-9)	3.22(-11)
AlO_2^-	2.19(-6)	9.82(-7)	6.34(-7)	1.72(-7)	3.42(-8)	1.37(-9)	6.07(-11)	1.64(-15)

TABLE IV

ONE DIMENSIONAL EQUILIBRIUM NOZZLE EXIT CONDITIONS

	Stage 1	Stage 2
Pressure, psia	11	2.1
Temperature, K	2100	1800
Velocity, ft/sec	8500	9300
Mach Number[a]	2.86	3.40

[a] $\gamma = 1.19$, $\bar{W} = 28$ for equilibrium gas/particle mixture

TABLE V

AVERAGE "GAS ONLY" SPECIFIC HEAT AND MOLECULAR WEIGHT IN NOZZLE

	Stage 1		Stage 2	
	Chamber	1-D Exit	Chamber	1-D Exit
Temperature, K	3410	2100	3410	1800
Y_g	0.718	0.698	0.734	0.716
Y_s	0.282	0.302	0.266	0.284
C_p, cal/g- K	0.439	0.417	0.440	0.410
C_{p_s}, cal/g- K	0.339	0.338	0.339	0.336
C_{p_g}, cal/g- K	0.478	0.452	0.477	0.438
W_g	20	20	20.6	21.0
γ_g	1.26	1.28	1.26	1.28

TABLE VI

INPUT DATA FOR 2-PHASE MOC NOZZLE CALCULATIONS

	Stage 1	Stage 2
Chamber Pressure, psia	741	445
Chamber Temperature, K	3410	3410
Gas Properties (assumed constant)		
γ_g	1.27	1.27
W_g	20	20.8
C_{p_g}, cal/mole- K	9.35	9.50
Pr	0.78	0.78
μ,[a] lbm/ft-sec	6.0×10^{-5}	6.0×10^{-5}
n, ($\mu \sim T^n$)	0.67	0.67
Particle Properties (Al_2O_3)		
γ_p/γ_g	0.393	0.363
Diameter (μ)/weight % of total		
	2/10	2/10
	4/40	4/40
	6/40	6/40
	8/10	8/10
Solidification Temperature, K	2320	2320
Density, lbm/ft^3	250	250
Specific Heat (T = 2320 K)		
C_{p_ℓ}, cal/mole- K	34.6	34.6
C_{p_s}, cal/mole- K	33.0	33.0
Enthalpy (T = 2320 K)		
h_ℓ, kcal/mole	87.8	87.8
h_s, kcal/mole	61.8	61.8
Nozzle Properties		
Inlet Half Angle, deg	40	40
Throat Radius of Curvature, in.	7.99	9.64

[a] at combustion chamber temperature

TABLE VII

INITIAL CONDITIONS FOR NONEQUILIBRIUM NOZZLE STREAMLINE CALCULATIONS

	Stage 1	Stage 2
Axial Distance from Throat, in.	-8.0[a] (C.L.)	-8.4
	-7.0 (wall)	-5.9
Pressure, psia	710	400
Temperature, K	3400	3400
Velocity, fps	900	1070
Composition, mole fraction		
CO	2.57(-1)	2.20(-1)
CO_2	1.69(-2)	2.22(-2)
HCl	1.45(-1)	1.46(-1)
H	3.50(-2)	4.20(-2)
H_2	2.93(-1)	2.44(-1)
OH	8.20(-2)	1.42(-2)
H_2O	1.52(-1)	1.93(-1)
N_2	9.06(-2)	8.70(-2)
O	6.30(-4)	1.50(-3)
O_2	1.30(-4)	4.50(-3)
K	1.22(-6)	1.21(-6)
KCl	2.78(-5)	2.74(-5)
Na	2.00(-5)	2.15(-5)
NaCl	1.90(-4)	1.92(-4)
Cl	1.20(-2)	1.65(-2)
Na^+	8.50(-6)	9.70(-6)
K^+	7.80(-6)	8.70(-6)
Cl^-	1.60(-5)	1.80(-5)
e^-	2.90(-7)	4.00(-7)

[a] negative distances are measured upstream of throat

TABLE VIII

REACTION MECHANISM AND RATE COEFFICIENTS[a]

FOR NONEQUILIBRIUM NOZZLE AND PLUME CALCULATIONS

$$k = AT^{-N} \exp B/RT$$

	Reaction	A[b]	N	B	Error Bound[c] Upper	Error Bound[c] Lower
1.	$O + O + M \rightarrow O_2 + M$	1(-29)	1	0	30	30
2.	$O + H + M \rightarrow OH + M$	1(-29)	1	0	30	30
3.	$H + H + M \rightarrow H_2 + M$	5(-29)	1	0	30	30
4.	$H + OH + M \rightarrow H_2O + M$	2(-28)	1	0	10	10
5.	$CO + O + M \rightarrow CO_2 + M$	1(-29)	1	-2,500	3	30
6.	$OH + OH \rightarrow H_2O + O$	1.0(-11)	0	-780	5	5
7.	$OH + H_2 \rightarrow H_2O + H$	3.6(-11)	0	-5,200	3	3
8.	$O + H_2 \rightarrow OH + H$	2.9(-11)	0	-9,460	3	3
9.	$H + O_2 \rightarrow OH + O$	3.7(-10)	0	-16,800	3	3
10.	$CO + OH \rightarrow CO_2 + H$	9(-13)	0	-1,080	5	5
11.	$H + Cl + M \rightarrow HCl + M$	4(-26)	2	0	100	100
12.	$Cl + H_2 \rightarrow HCl + H$	4(-11)	0	-4,400	10	10
13.	$H_2O + Cl \rightarrow HCl + OH$	5(-11)	0	-19,000	30	30
14.	$OH + Cl \rightarrow HCl + O$	3(-11)	0	-5,000	30	30
15.	$K + HCl \rightarrow KCl + H$	6(-10)	0	-5,000	10	30
16.	$Na + HCl \rightarrow NaCl + H$	5(-10)	0	-8,000	10	30
17.	$K^+ + e^- + M \rightarrow K + M$	2(-22)	1.5	0	5	5
18.	$Na^+ + e^- + M \rightarrow Na + M$	1.5(-20)	2	0	5	5
19.	$K^+ + Cl^- \rightarrow K + Cl$	1(-8)	0.5	0	10	100
20.	$Na^+ + Cl^- \rightarrow Na + Cl$	3(-8)	0.5	0	10	10
21.	$Cl + e^- + M \rightarrow Cl^- + M$	3(-30)	0	0	30	30
22.[d]	$HCl + e^- \rightarrow H + Cl^-$	1(-8)	0	-20,000	30	100

[a] Taken from Refs. 16 and 17, which fully discuss the sources of all rate coefficient data.

[b] cm-molecule-sec units

[c] Estimated values (taken from Refs. 16 and 17, which give precise definitions of error bounds). A is multiplied by the upper bound to give the maximum value of of k; A is divided by the lower bound to give the minimum value of k.

[d] Lower bound for k_{22} used in "standard" plume streamline and mixing/chemistry calculations (see Section V.).

TABLE IX

INPUT DATA
FOR EXHAUST PLUME
METHODS OF CHARACTERISTICS PROGRAM (U)

	Stage 1	Stage 2
Altitude, kft	100	118, 200, 300
Free Stream Mach Number	5.15	5.8, 6.1, 8.9
Stagnation Pressure, psia	180	87
Stagnation Temperature, K	3440	3380
Specific Heat Ratio	1.28	1.28
Molecular Weight	20	21
Mach Number[a, b]		
Centerline	2.50	3.22
Nozzle Lip	2.80	3.22
Exit Plane Flow Angle		
Nozzle Lip, deg	12.7	16

[a] Initial data line is nozzle exit plane. Mach number and flow angle distributions are give in Fig. 18 (Stage 1).

[b] Conical source flow in the nozzle was assumed to establish the initial data line for Stage 2.

TABLE X

INPUT DATA FOR MIXING/NONEQUILIBRIUM CHEMISTRY CALCULATIONS[a]

	Stage 1	Stage 2	
Altitude, kft	100	118	200
Jet Velocity,[b] fps	10000	9300	10150
Jet Temperature,[b] K	1200	1170	735
Initial Boundary Pressure, atm	0.114	0.0453	0.0052
Free Stream Velocity, fps	4850	5300	3850
Free Stream Temperature, K	430	430	1400

[a] Pressure distributions are given in Fig. 41.

[b] Jet velocity and temperature refer to rocket exhaust conditions after a Prandtl Meyer expansion to initial boundary pressure.

TABLE XI

INITIAL CONDITIONS FOR NONEQUILIBRIUM CHEMISTRY CALCULATIONS DOWNSTREAM OF MACH DISC

	Stage 1, 100 kft
Temperature, K	3330 (1060 K-free stream)[a]
Pressure, psia	0.24
Velocity, fps	1500 (9890 fps-free stream)[a]
Composition, Mole Fraction	
CO	2.35(-1)
CO_2	3.68(-2)
HCl	1.58(-1)
H	1.89(-3)
H_2	2.82(-1)
OH	1.00(-4)
H_2O	2.16(-1)
N_2	9.10(-2)
O	4.95(-7)
O_2	2.00(-7)
K	1.28(-7)
KCl	3.55(-5)
Na	2.56(-6)
NaCl	2.20(-4)
Cl	8.40(-4)
Na^+	1.87(-7)
K^+	1.28(-6)
Cl^-	1.46(-6)
e^-	4.34(-9)

[a] Refers to free stream temperature and velocity input to mixing/chemistry program. Species mole fractions in free stream were assumed equal to initial species mole fractions immediately downstream of Mach disc.

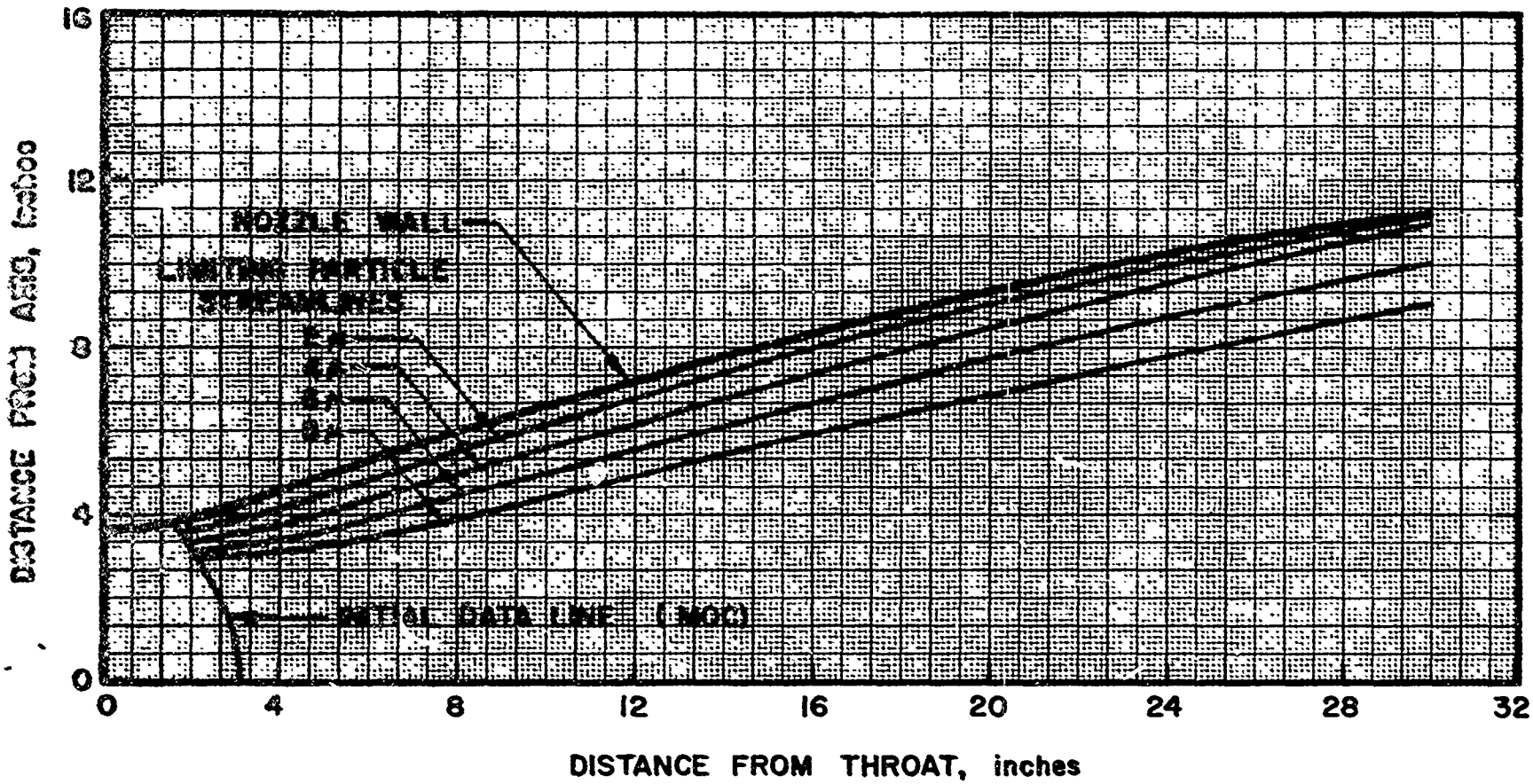

FIG. 1 STAGE 1 NOZZLE CONTOUR AND LIMITING PARTICLE STREAMLINES

Initial data line is for Method of Characteristics (MOC) calculation

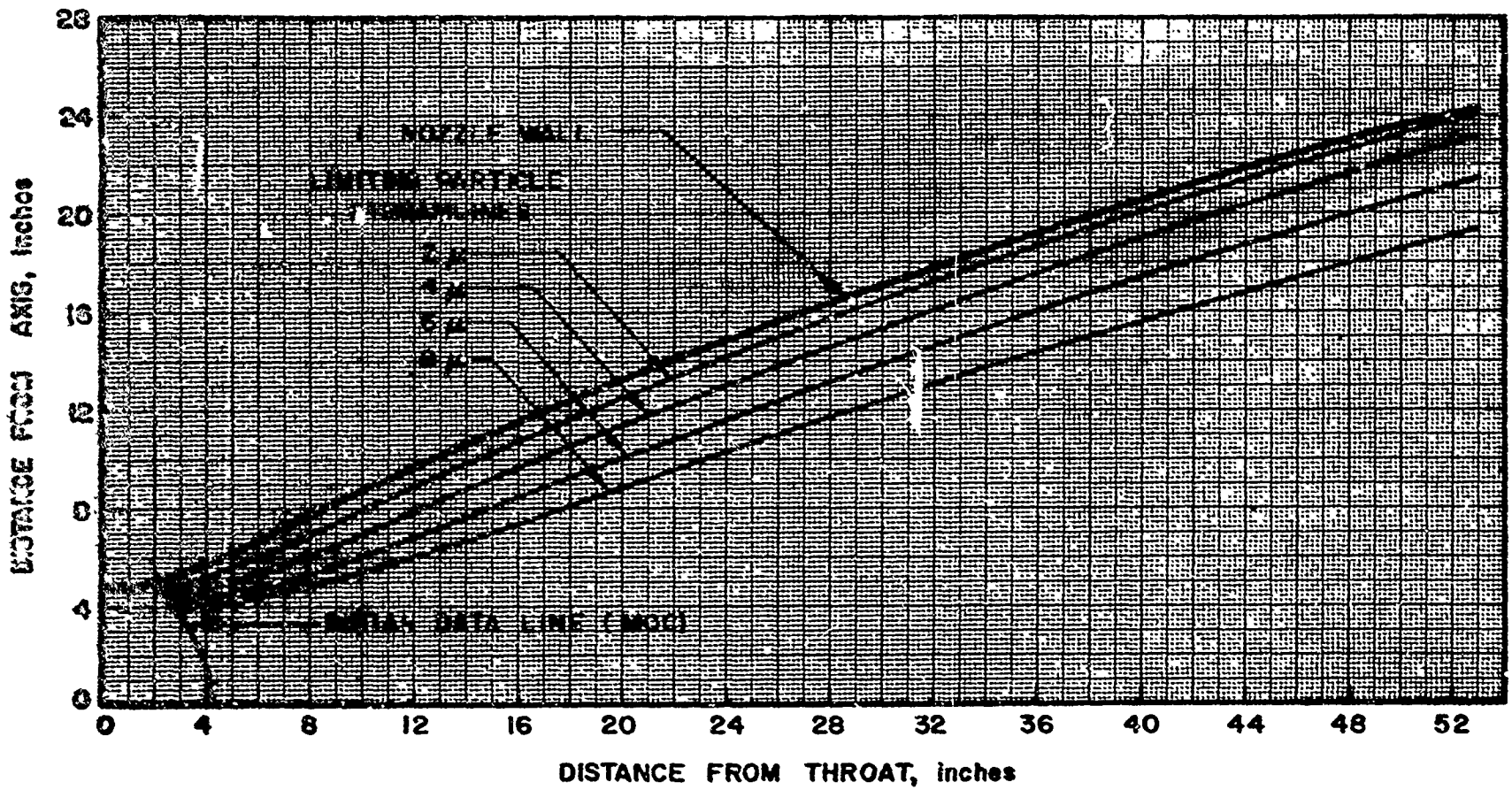

FIG. 2 STAGE 2 NOZZLE CONTOUR AND LIMITING PARTICLE STREAMLINES

Initial data line is for Method of Characteristics (MOC) calculation

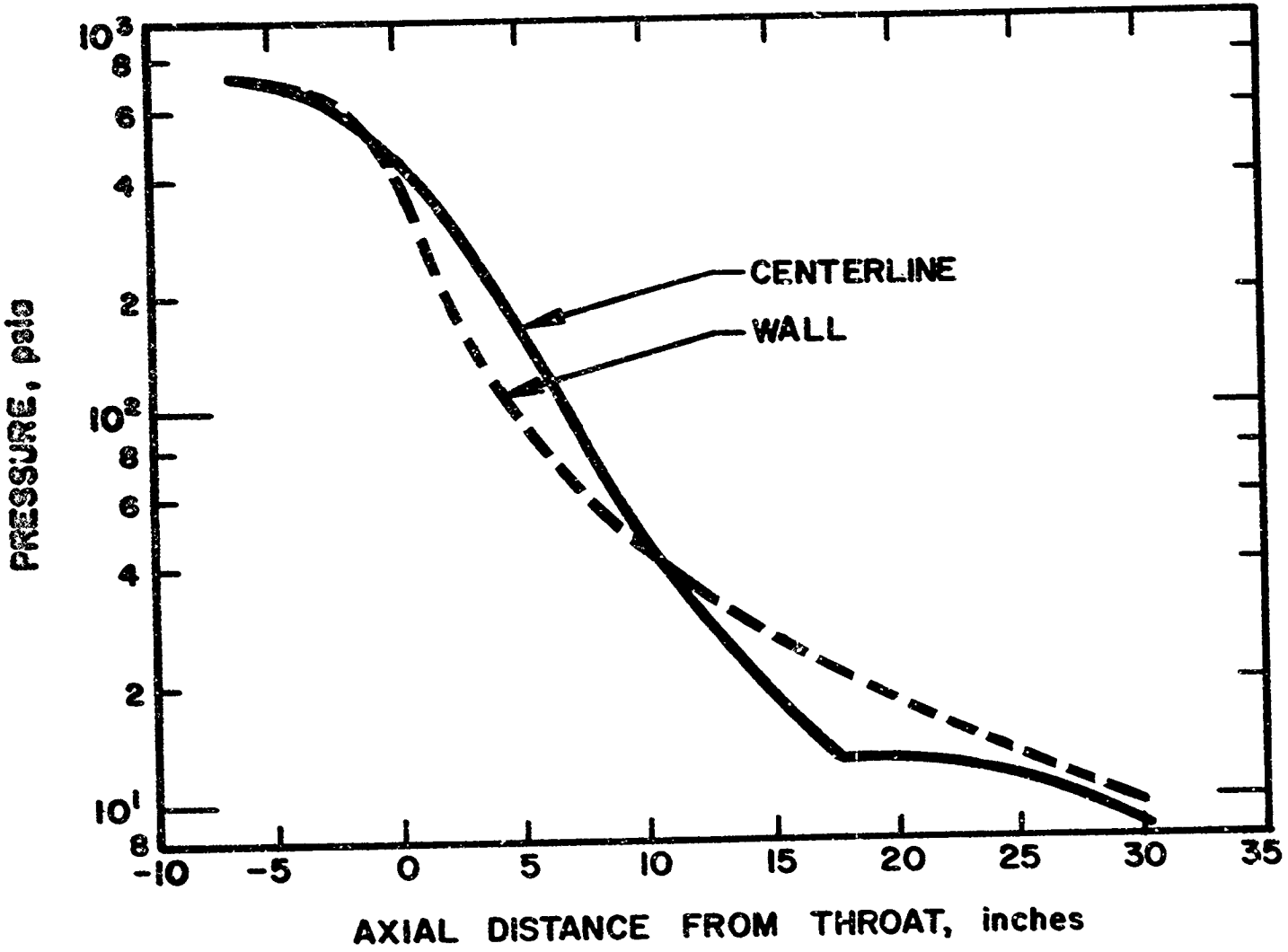

FIG. 3 PRESSURE DISTRIBUTIONS IN STAGE 1 NOZZLE

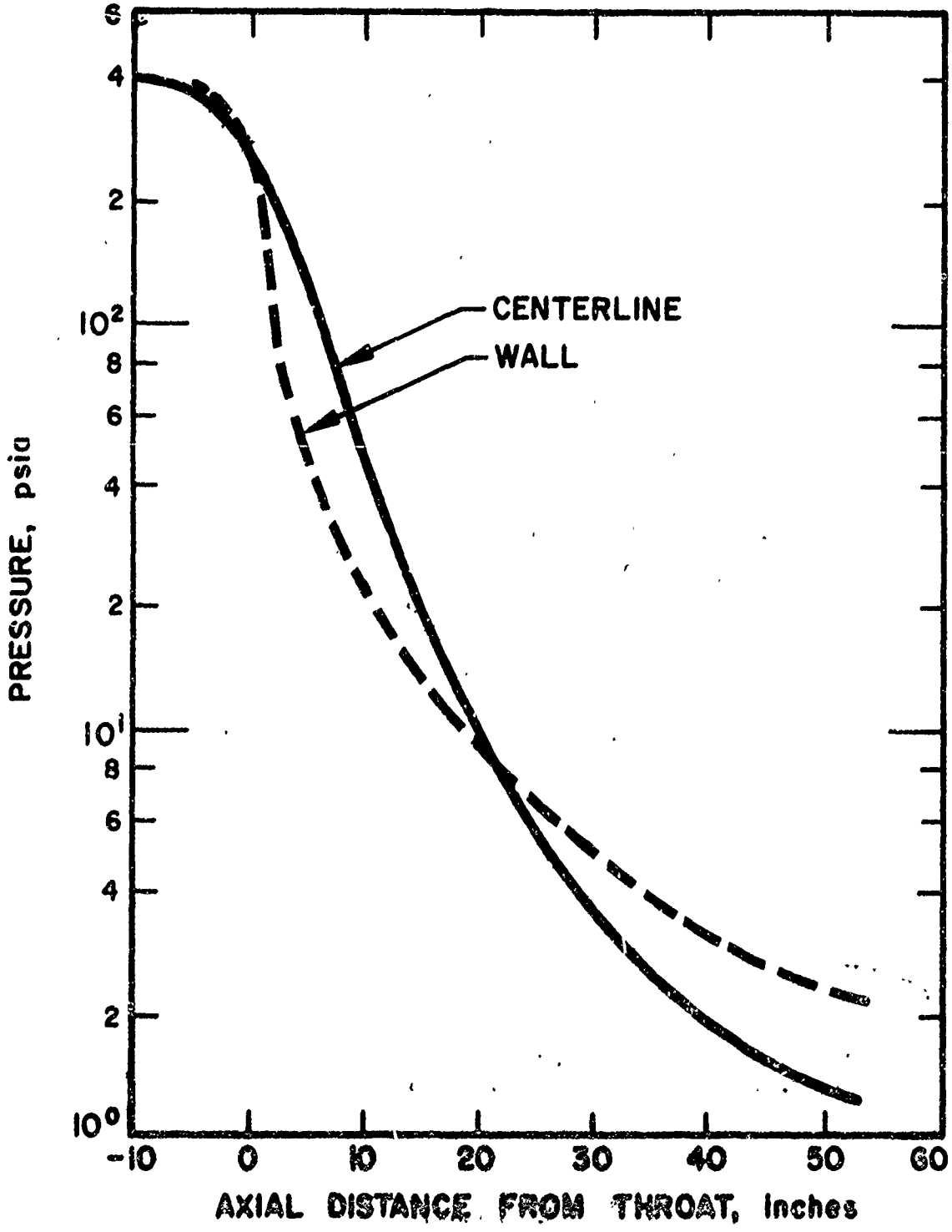

FIG 4 PRESSURE DISTRIBUTIONS IN STAGE 2 NOZZLE

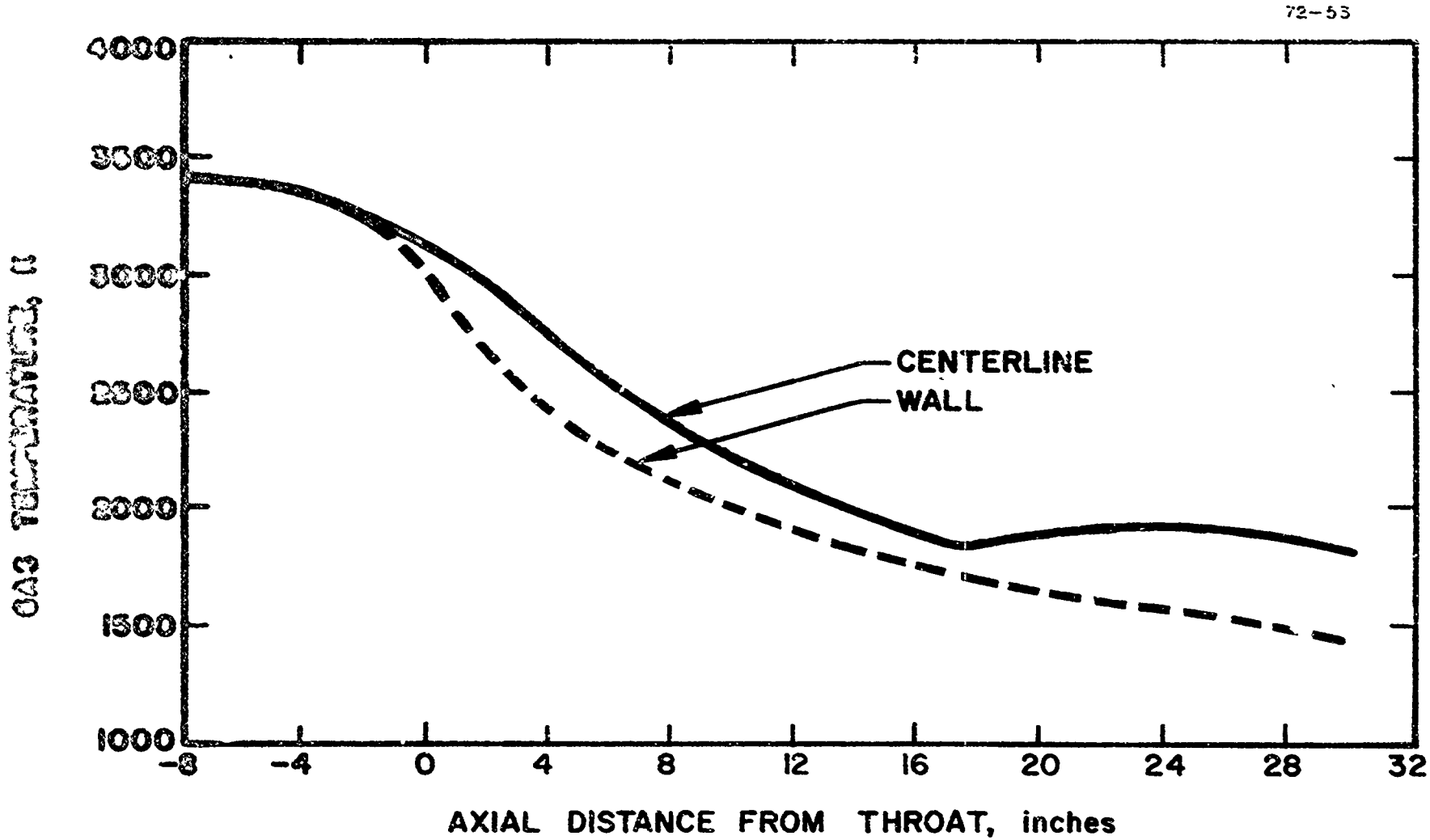

FIG. 5 GAS TEMPERATURE DISTRIBUTIONS IN STAGE 1 NOZZLE

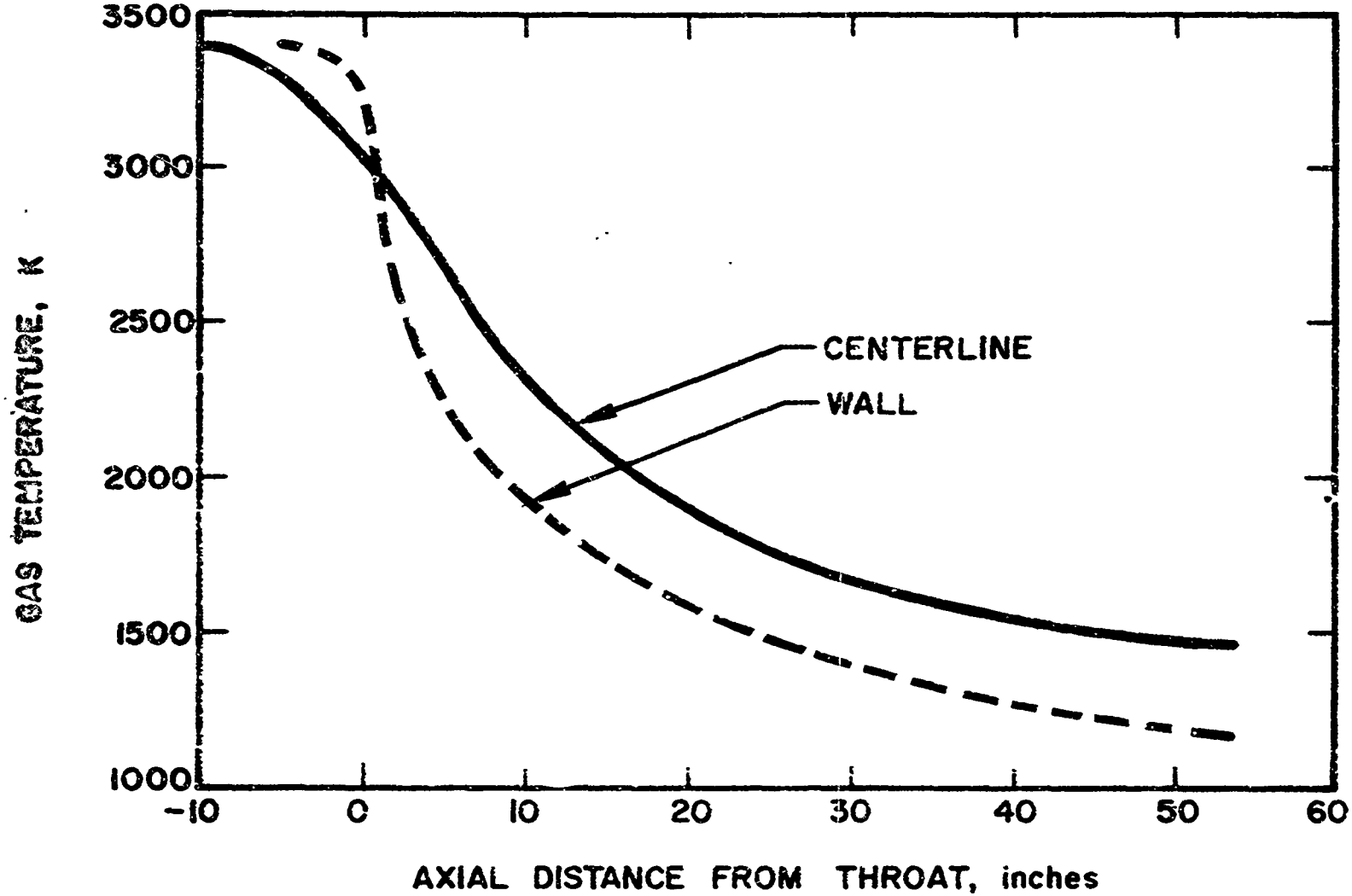

FIG. 6 GAS TEMPERATURE DISTRIBUTIONS IN STAGE 2 NOZZLE

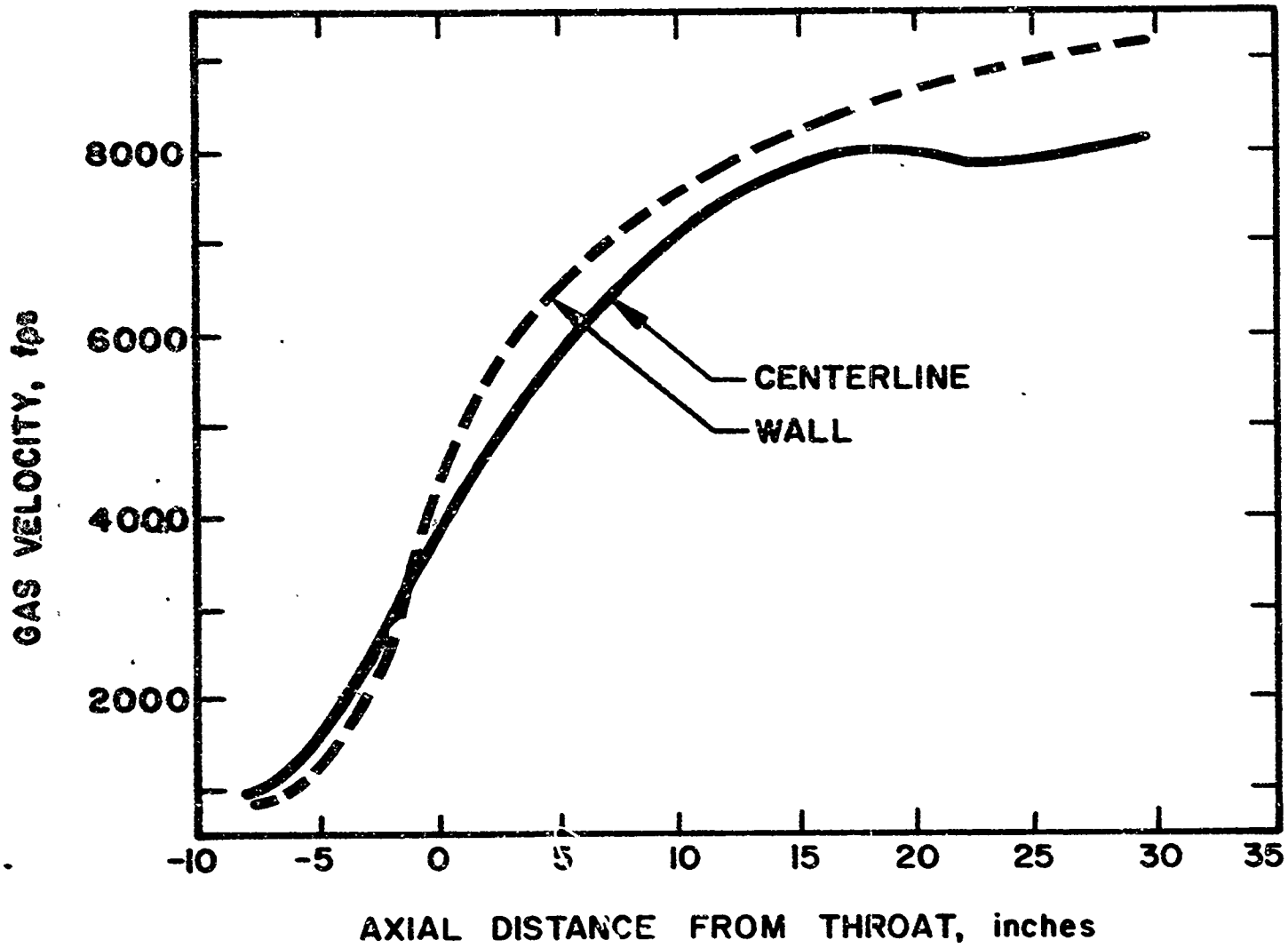

FIG. 7 GAS VELOCITY DISTRIBUTIONS IN STAGE 1 NOZZLE

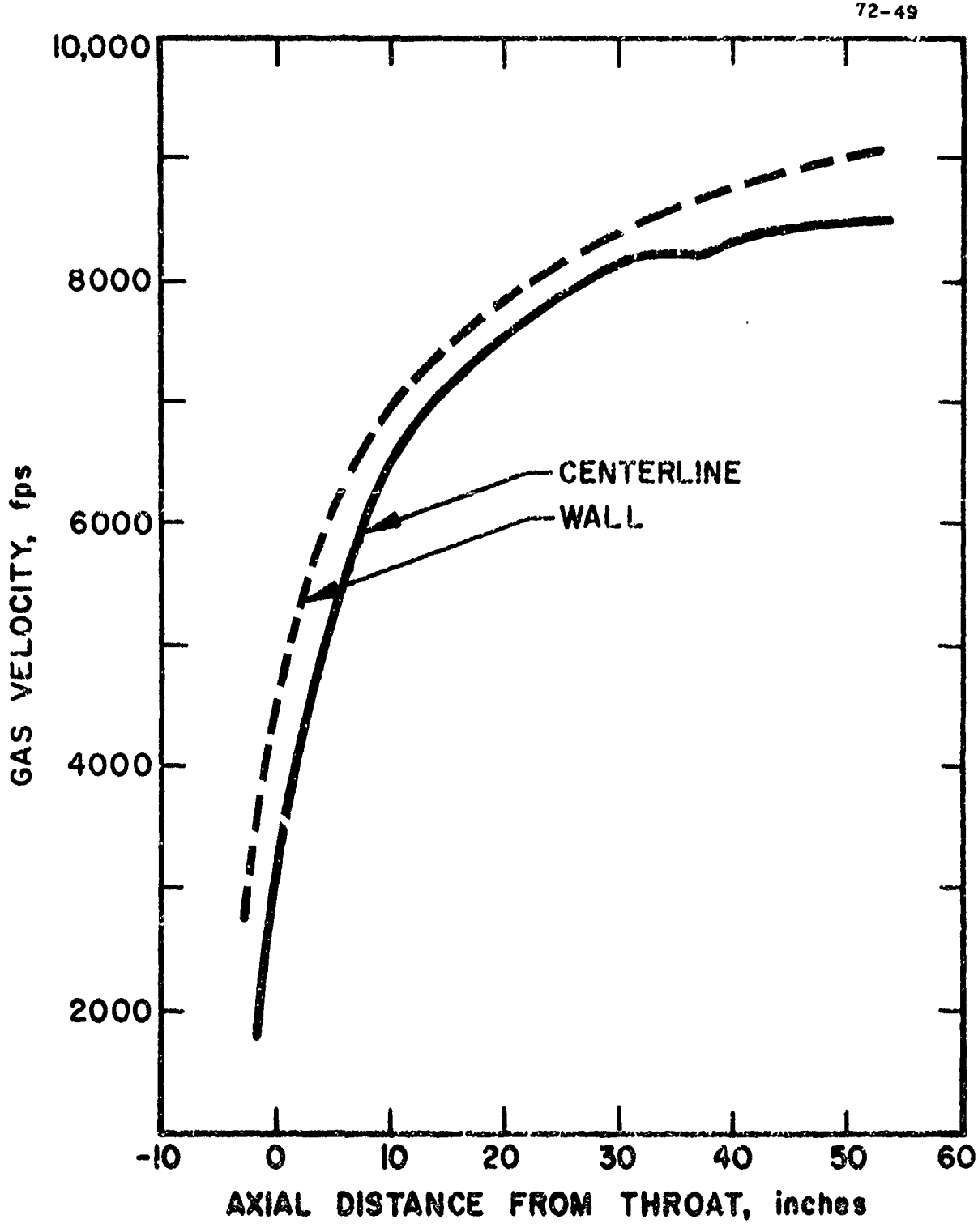

FIG. 8 GAS VELOCITY DISTRIBUTIONS IN STAGE 2 NOZZLE

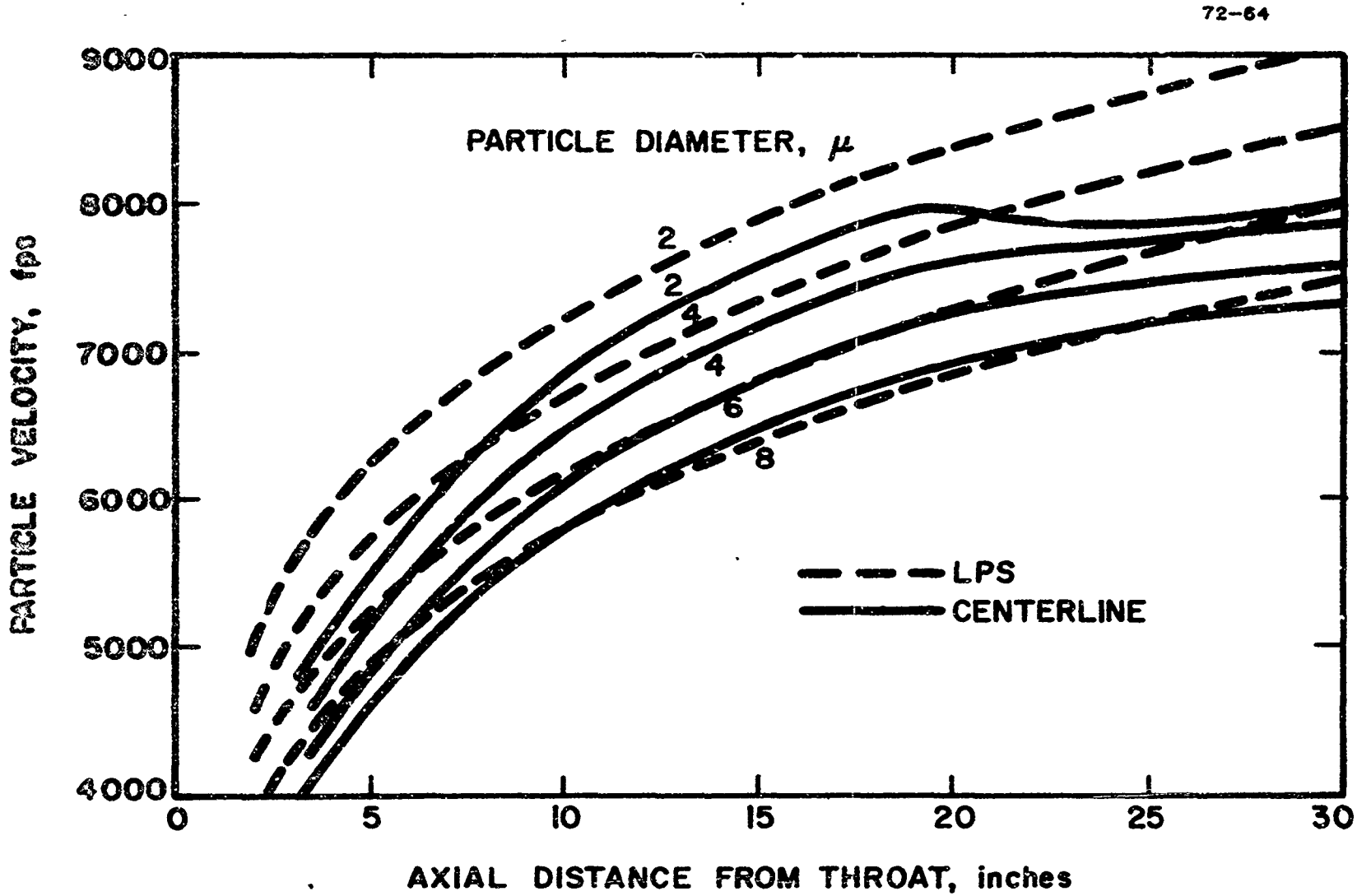

FIG. 9 PARTICLE VELOCITY DISTRIBUTIONS IN STAGE 1 NOZZLE

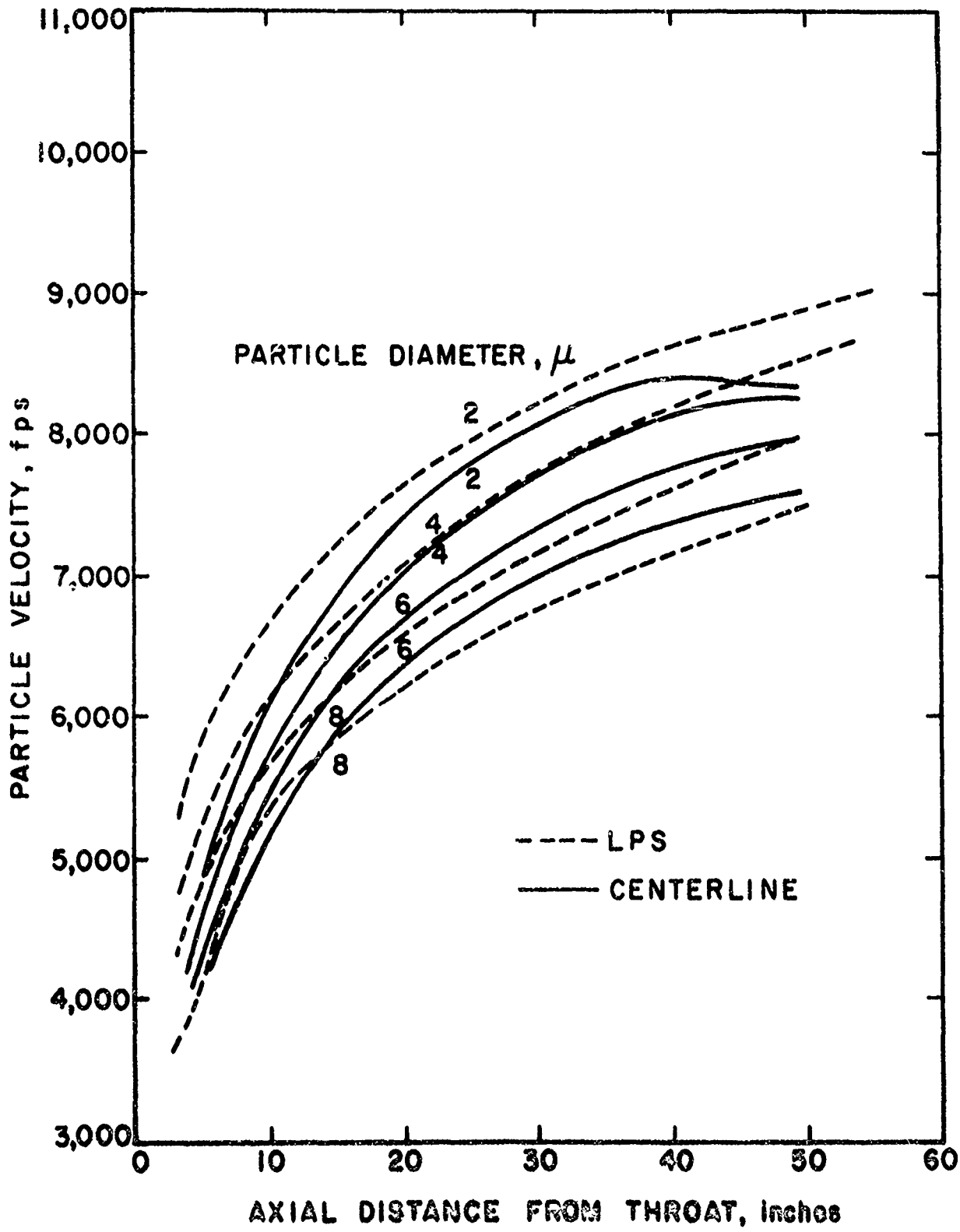

FIG. 10 PARTICLE VELOCITY DISTRIBUTIONS IN STAGE 2 NOZZLE

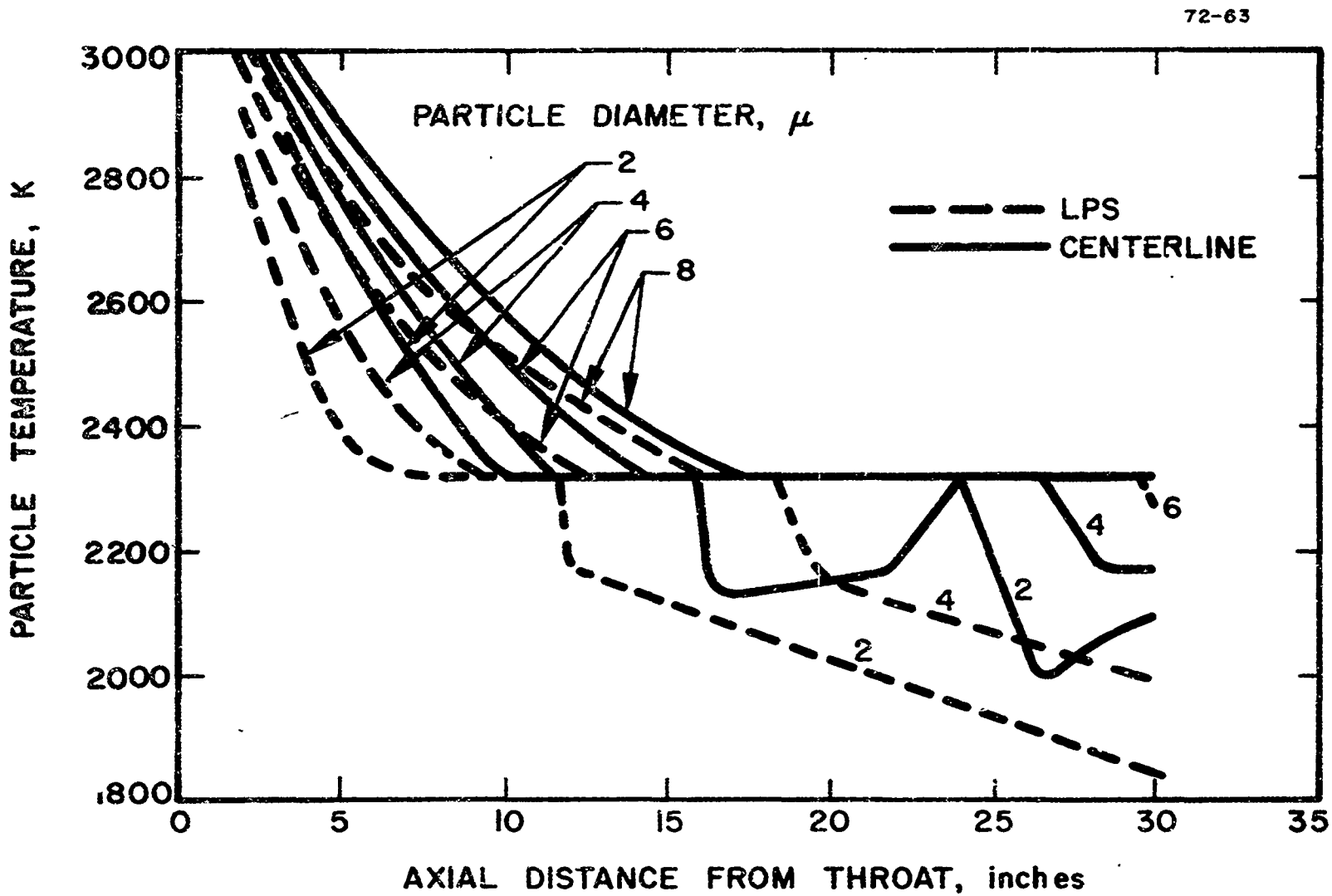

FIG. 11 PARTICLE TEMPERATURE DISTRIBUTIONS IN STAGE 1 NOZZLE

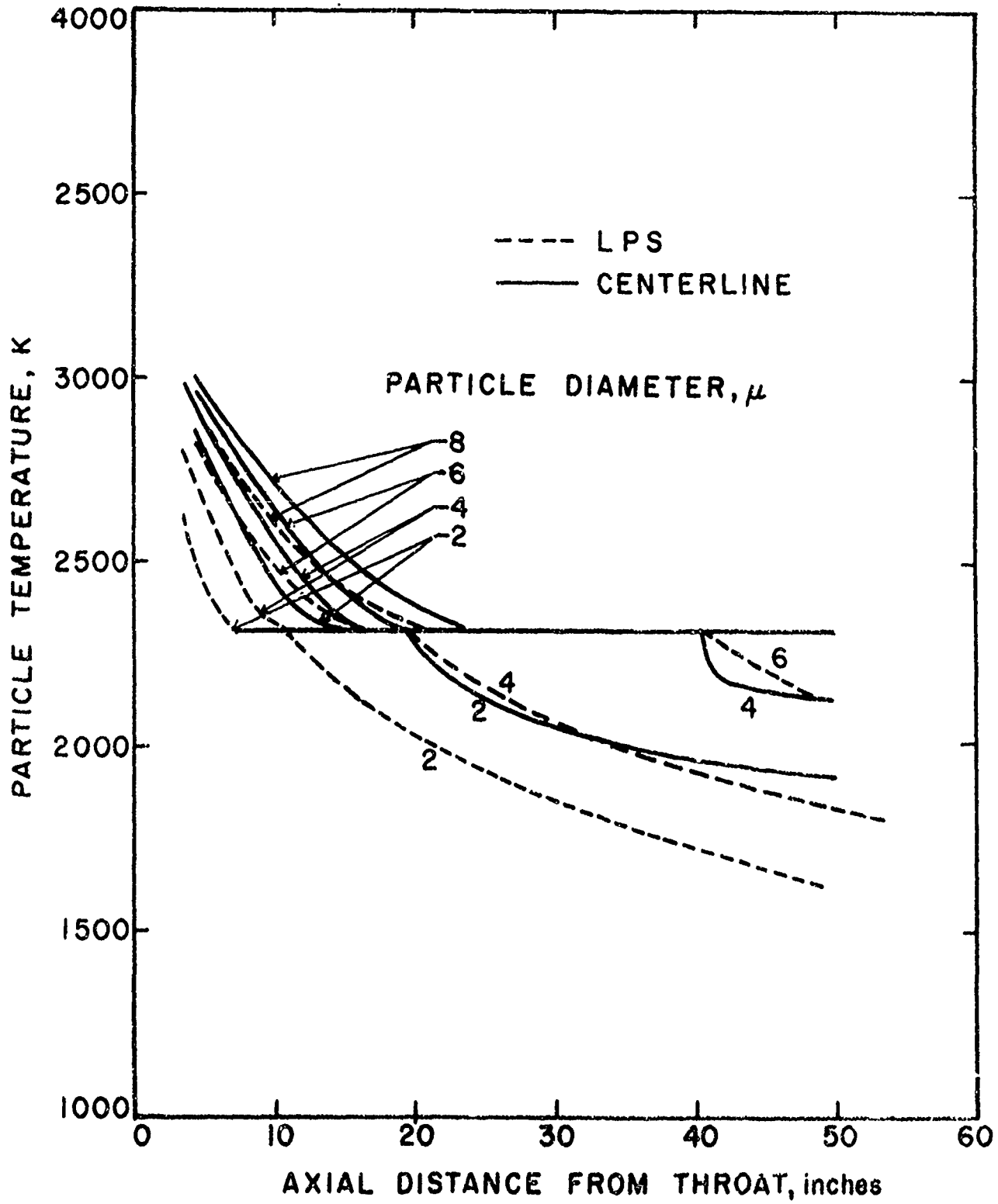

FIG. 12 PARTICLE TEMPERATURE DISTRIBUTIONS IN STAGE 2 NOZZLE

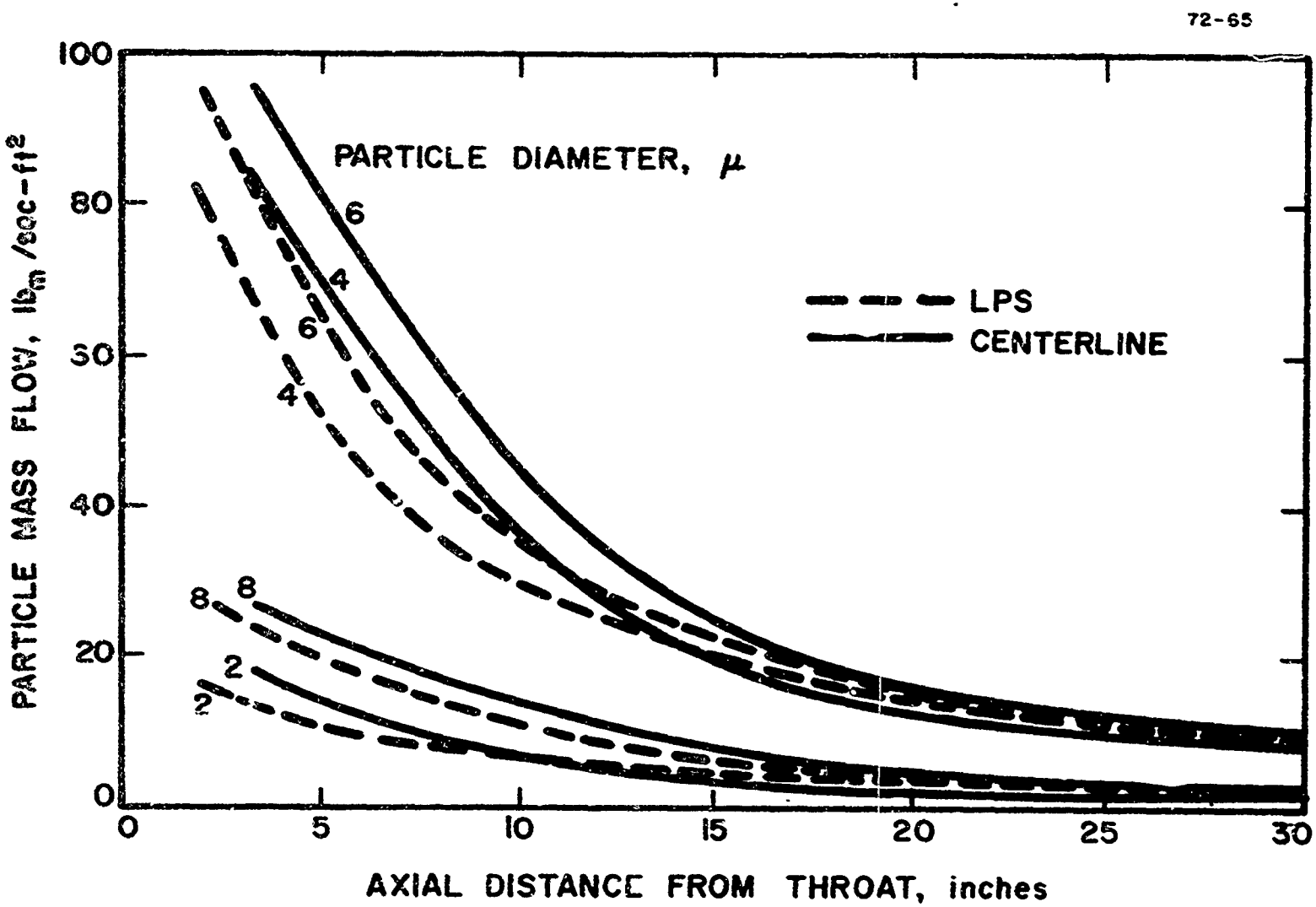

FIG. 13 PARTICLE MASS FLOW RATES IN STAGE 1 NOZZLE

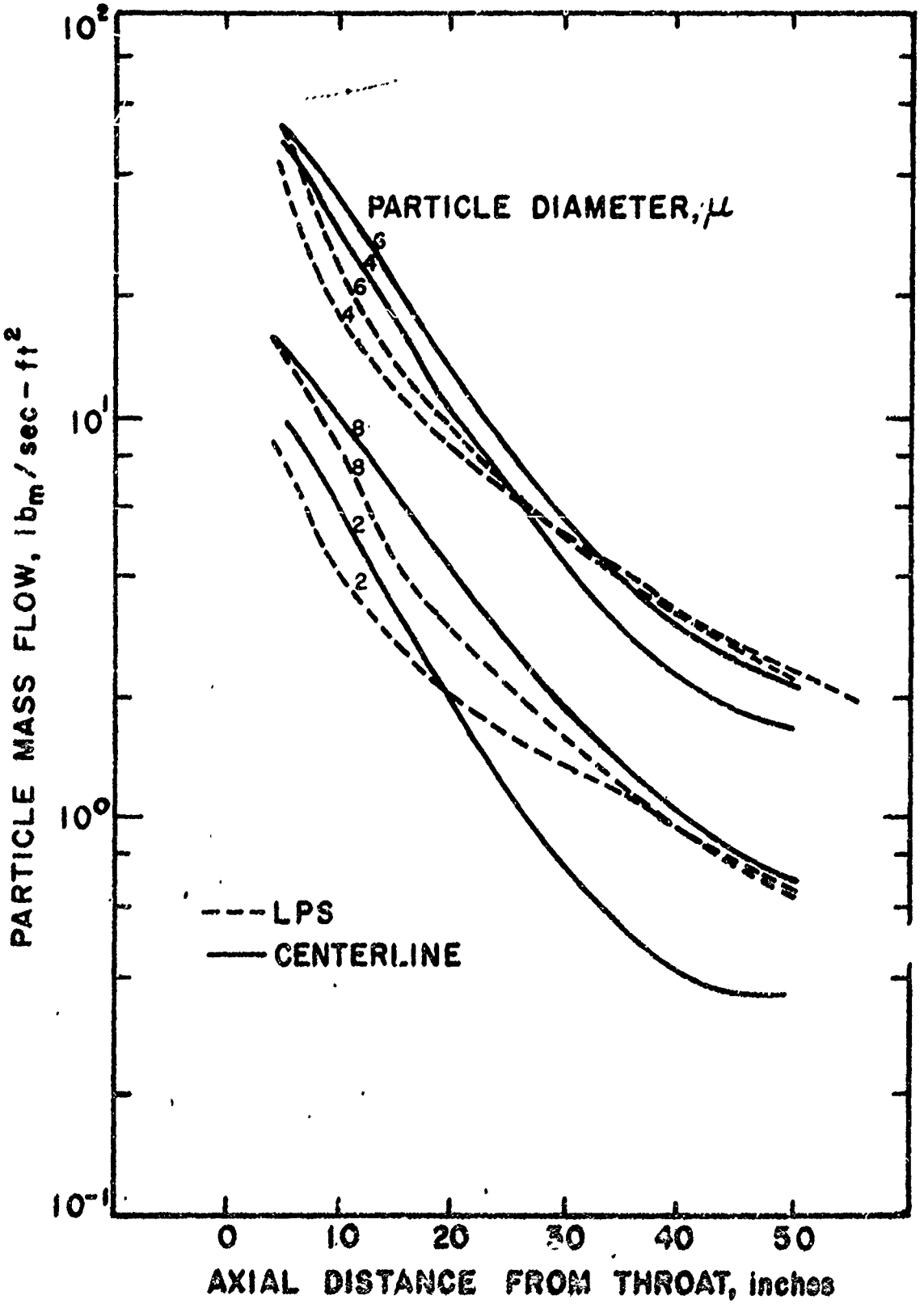

FIG. 14 PARTICLE MASS FLOW RATES IN STAGE 2 NOZZLE

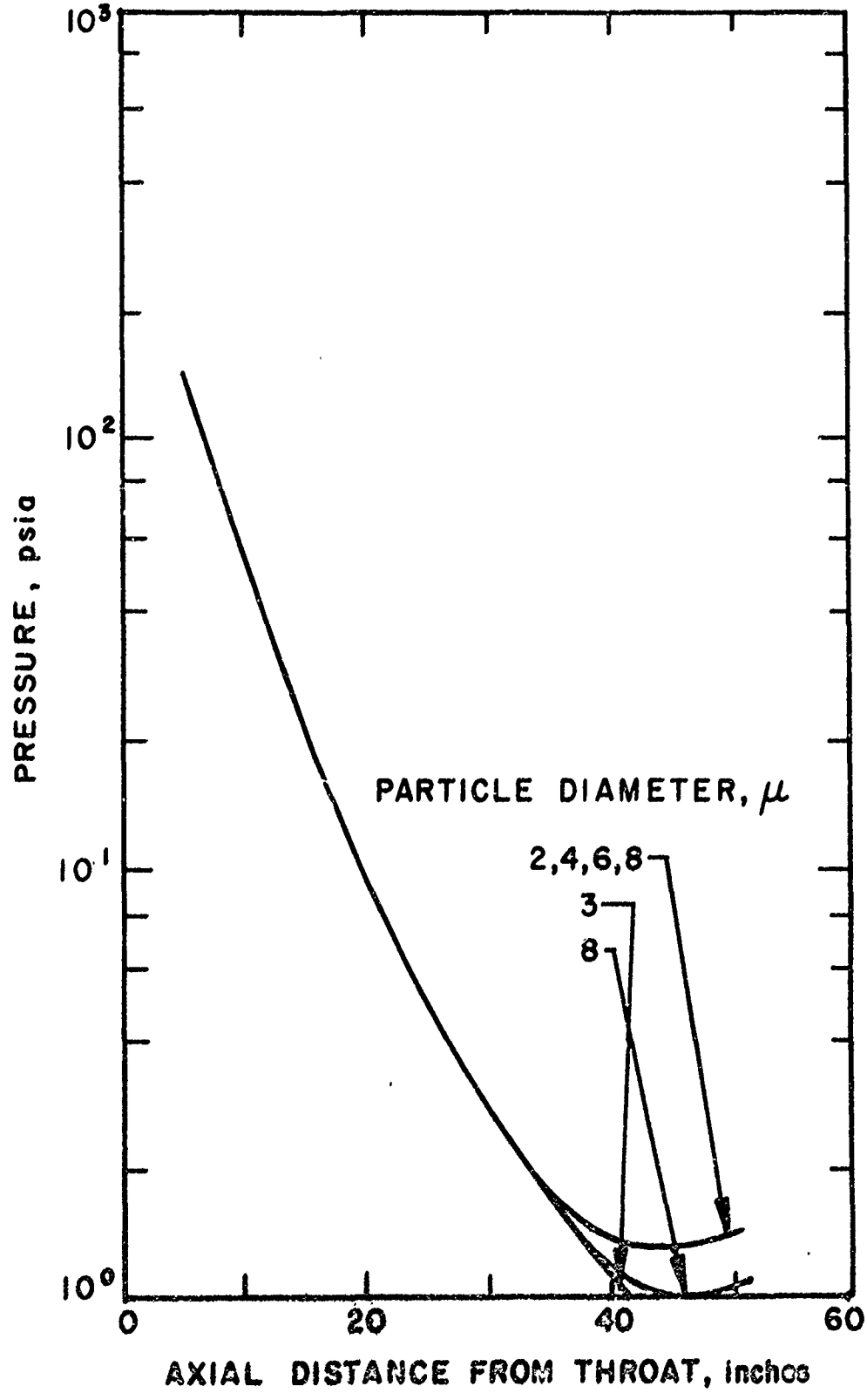

FIG. 15 INFLUENCE OF PARTICLE SIZE ON CENTERLINE PRESSURES IN STAGE 2 NOZZLE

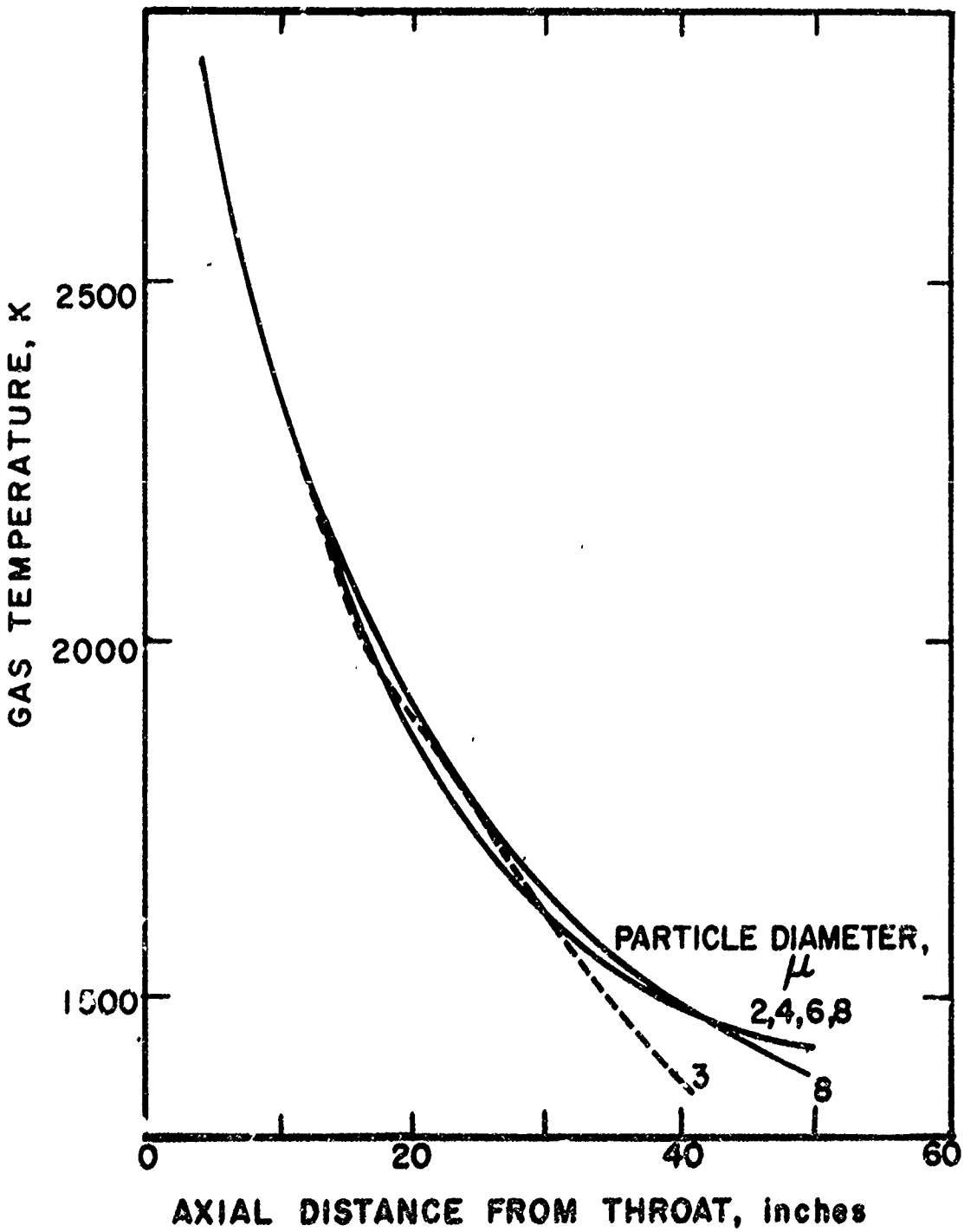

FIG. 16 INFLUENCE OF PARTICLE SIZE ON CENTERLINE GAS TEMPERATURES IN STAGE 2 NOZZLE

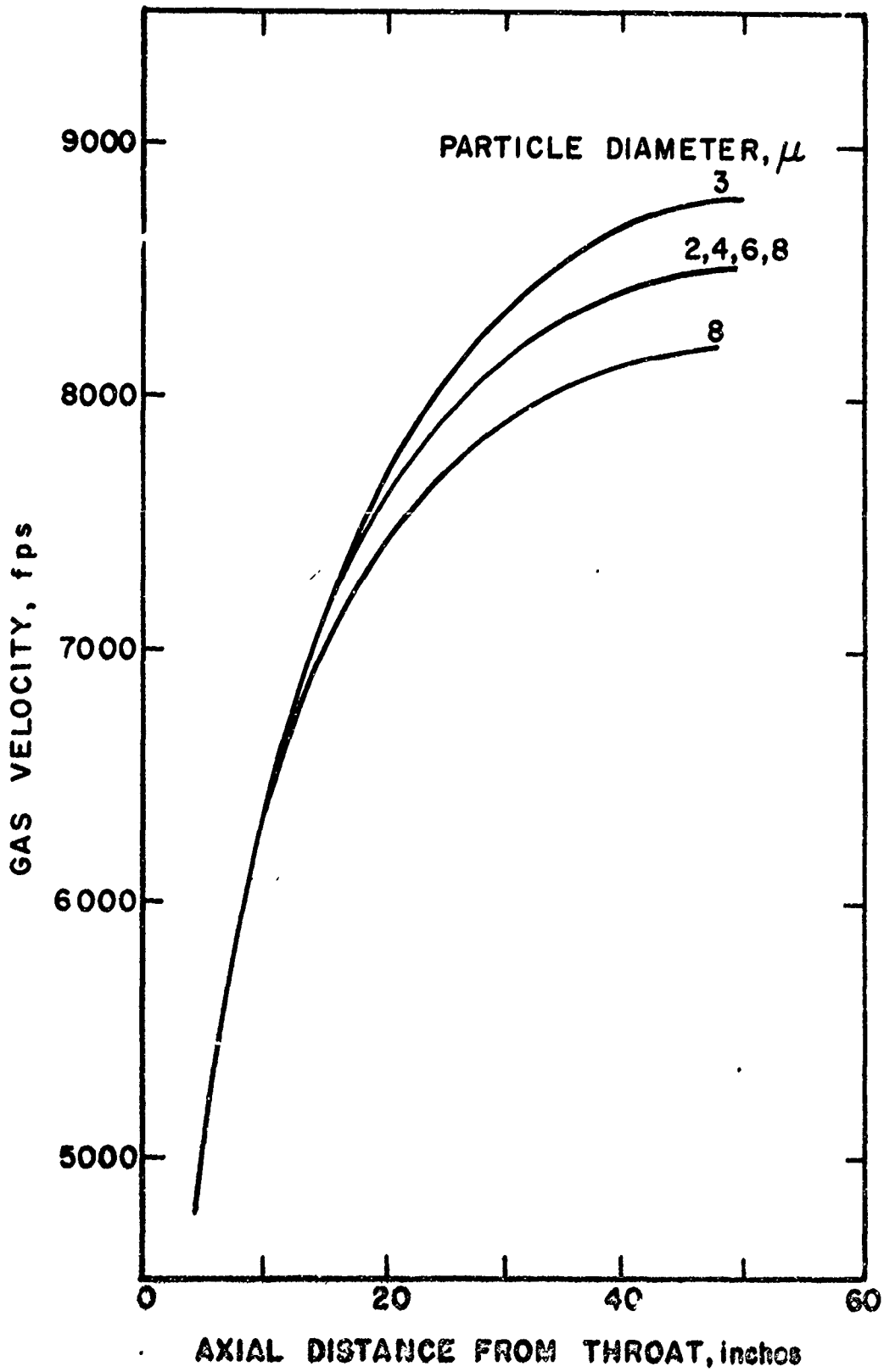

FIG. 17 INFLUENCE OF PARTICLE SIZE ON CENTERLINE GAS VELOCITIES IN STAGE 2 NOZZLE

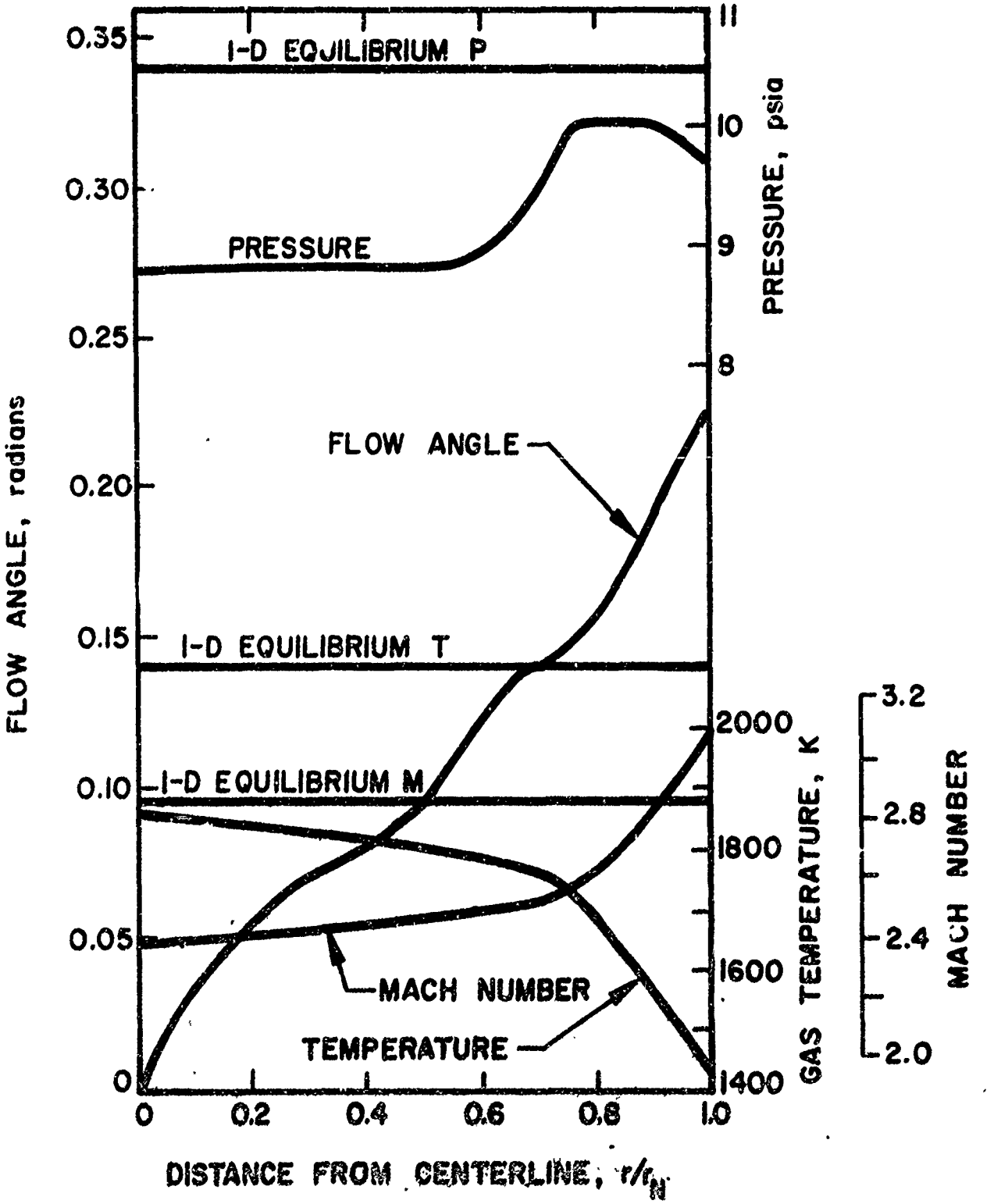

FIG. 18 STAGE 1 NOZZLE EXIT PLANE GAS PROPERTIES

Flow angle ≡ angle between velocity vector and plume axis
1-D Equilibrium P, T, M from Table IV

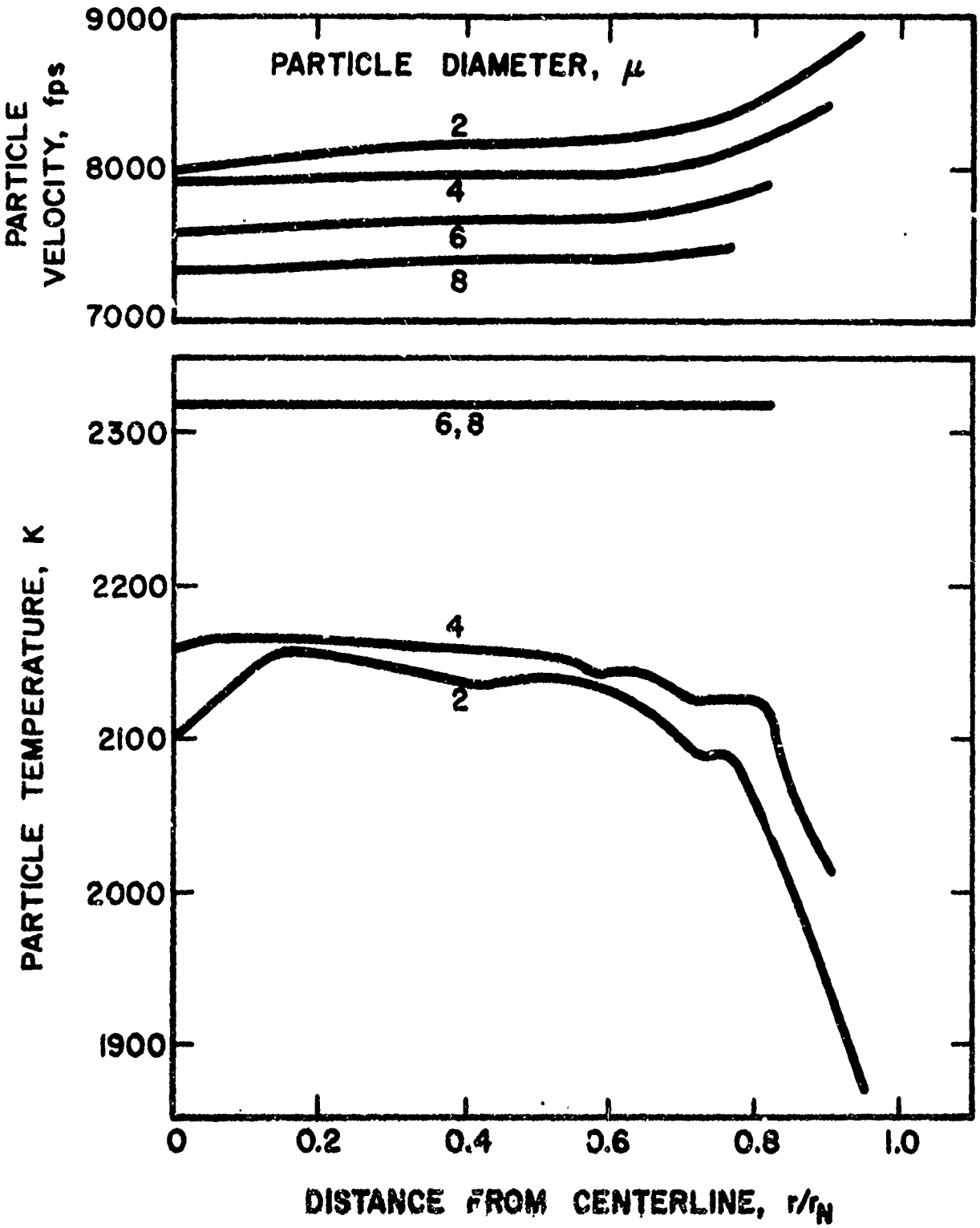

FIG. 19a STAGE 1 NOZZLE EXIT PLANE PARTICLE PROPERTIES

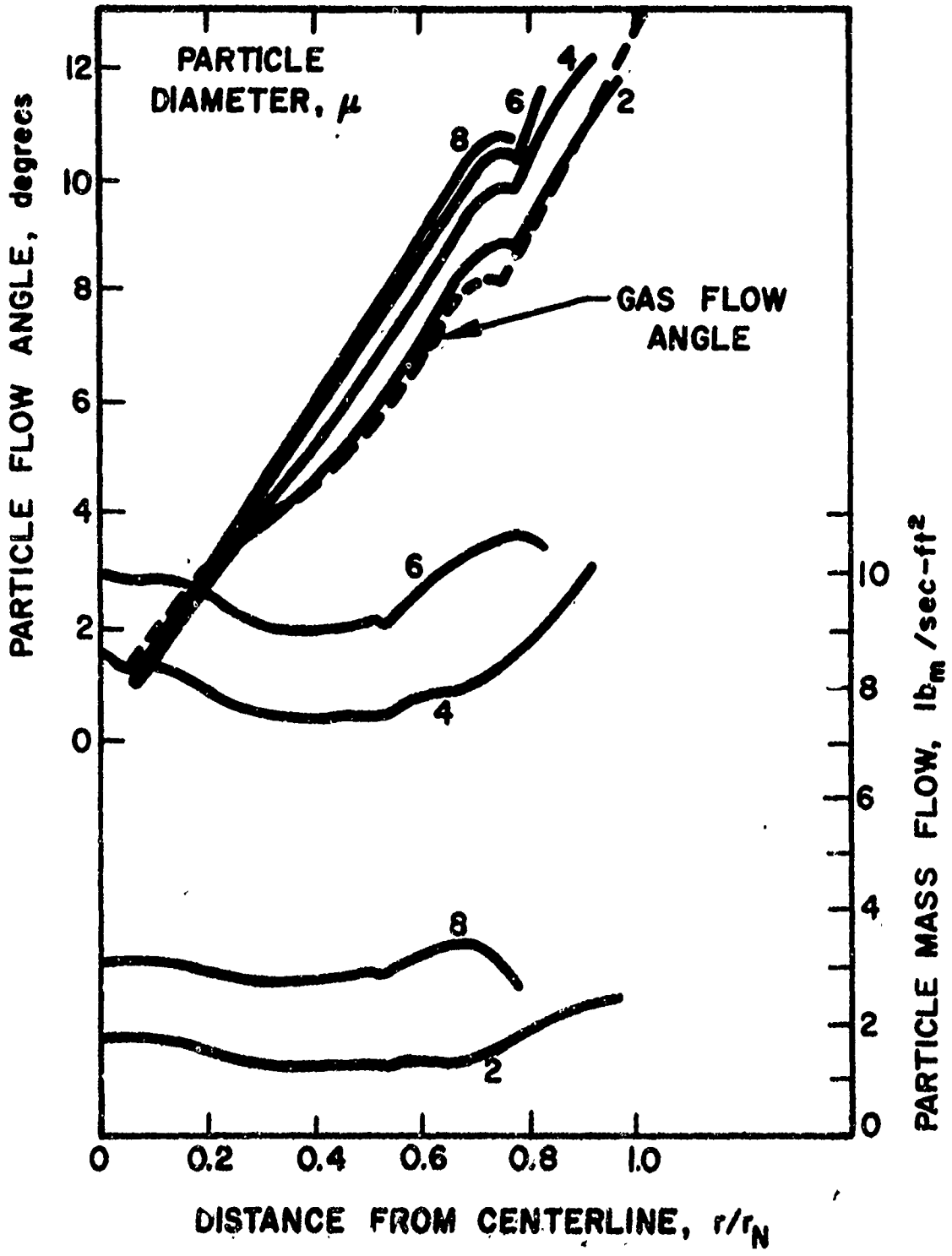

FIG. 19b STAGE 1 NOZZLE EXIT PLANE PARTICLE PROPERTIES

Flow angle ≡ angle between velocity vector and plume axis

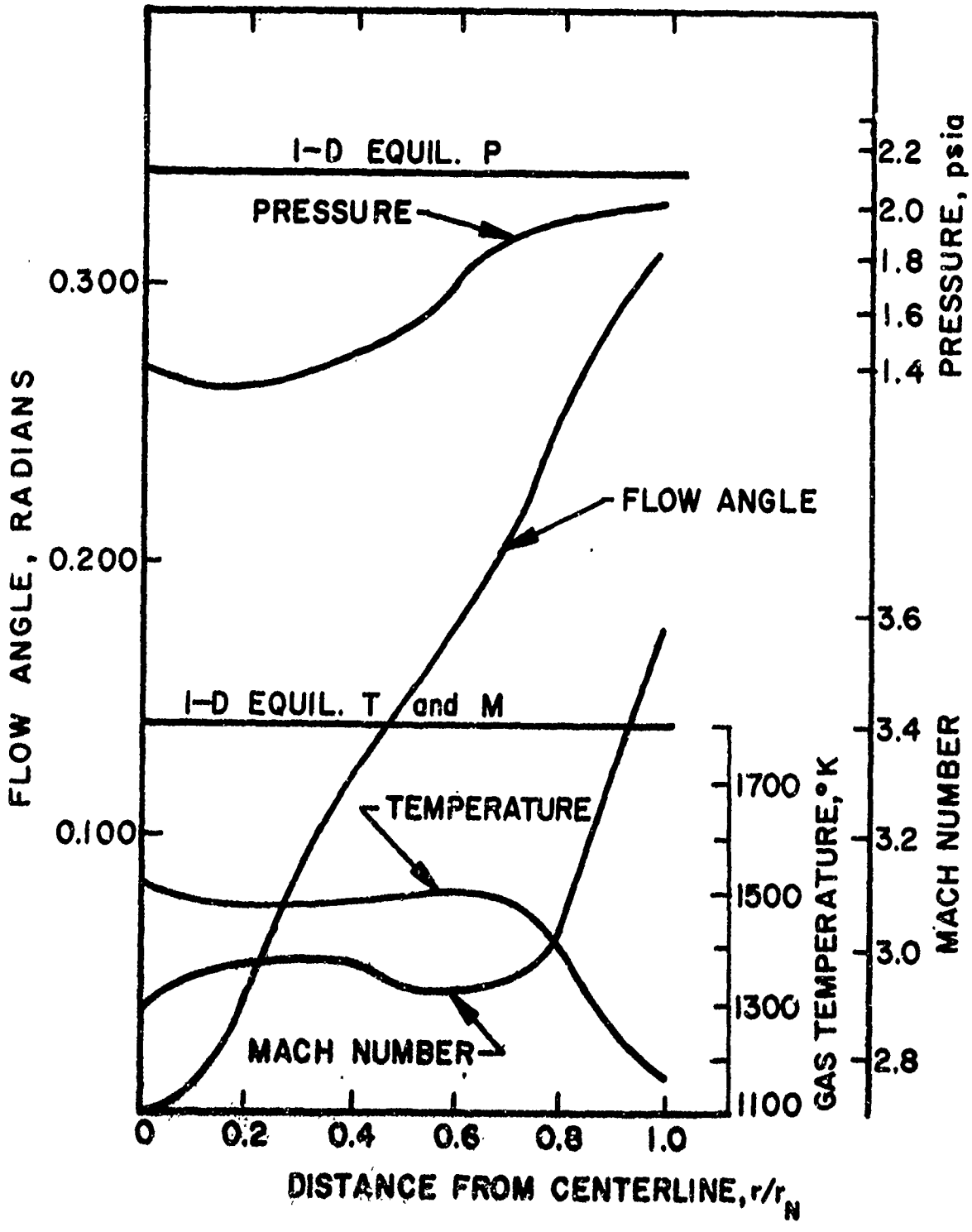

FIG. 20 STAGE 2 NOZZLE EXIT PLANE GAS PROPERTIES

Flow angle ≡ angle between velocity vector and plume axis
1-D Equilibrium P, T, M from Table IV

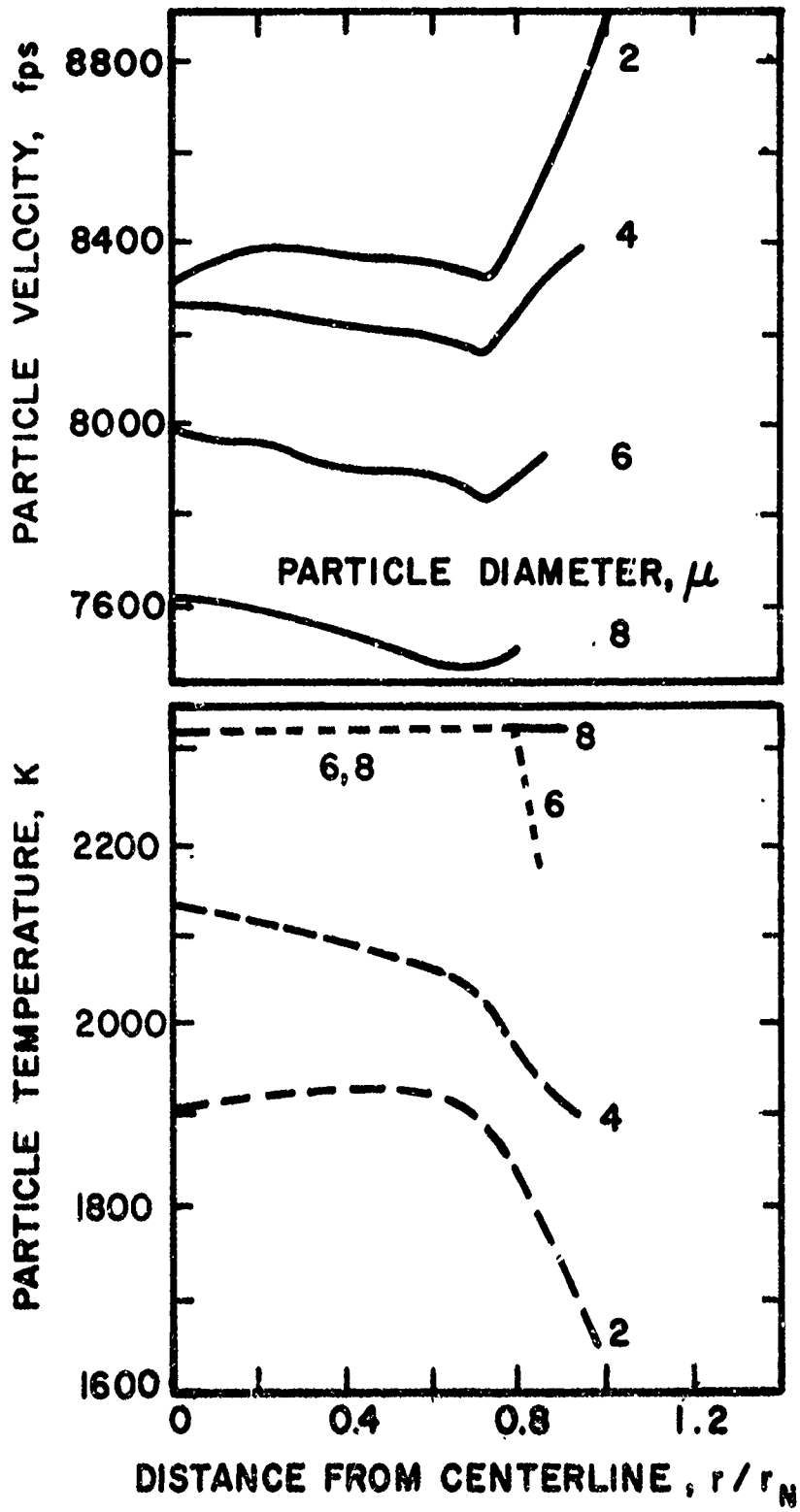

FIG. 21a STAGE 2 NOZZLE EXIT PLANE PARTICLE PROPERTIES

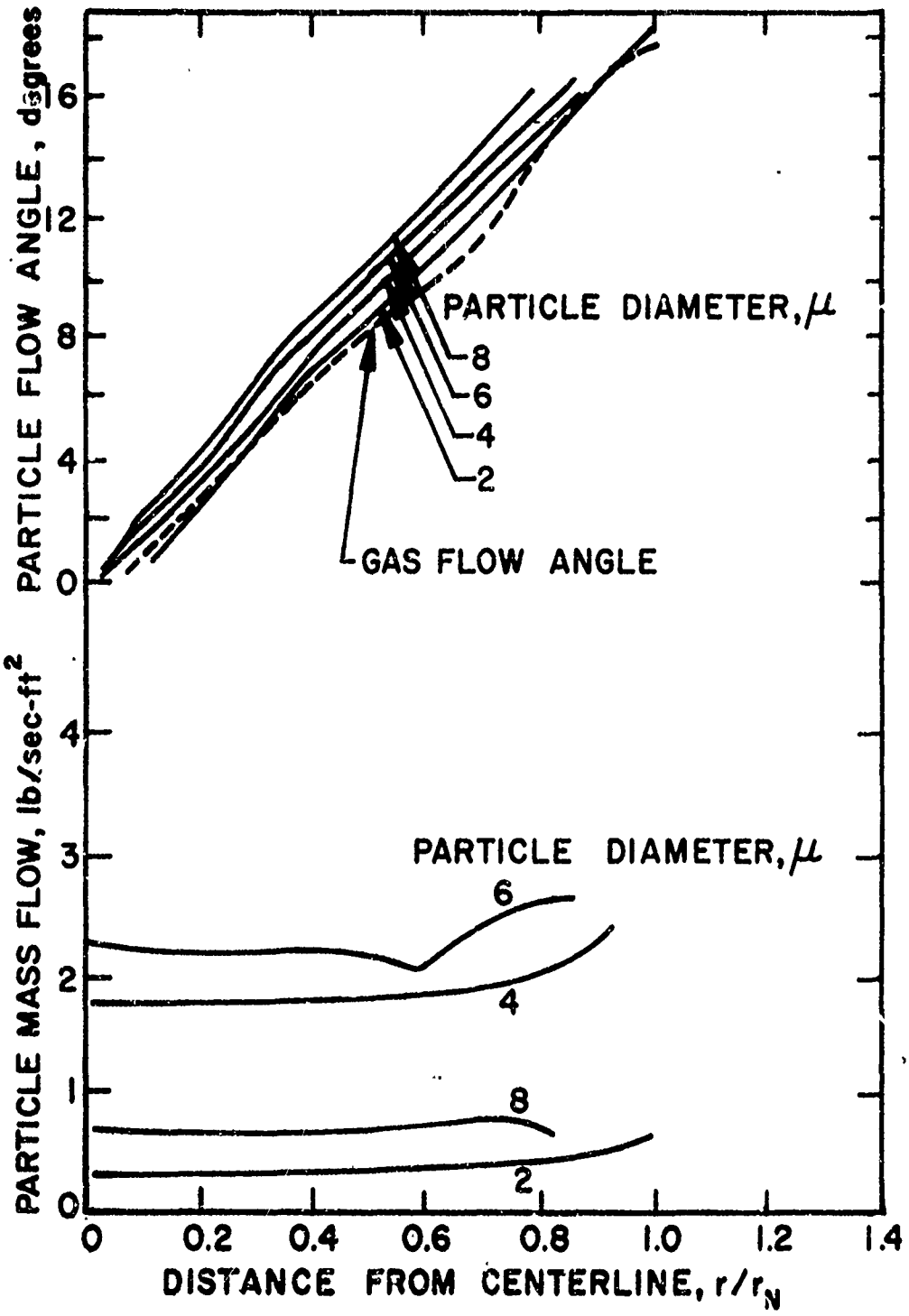

FIG. 21b STAGE 2 NOZZLE EXIT PLANE PARTICLE PROPERTIES

Flow angle ≡ angle between velocity vector and plume axis

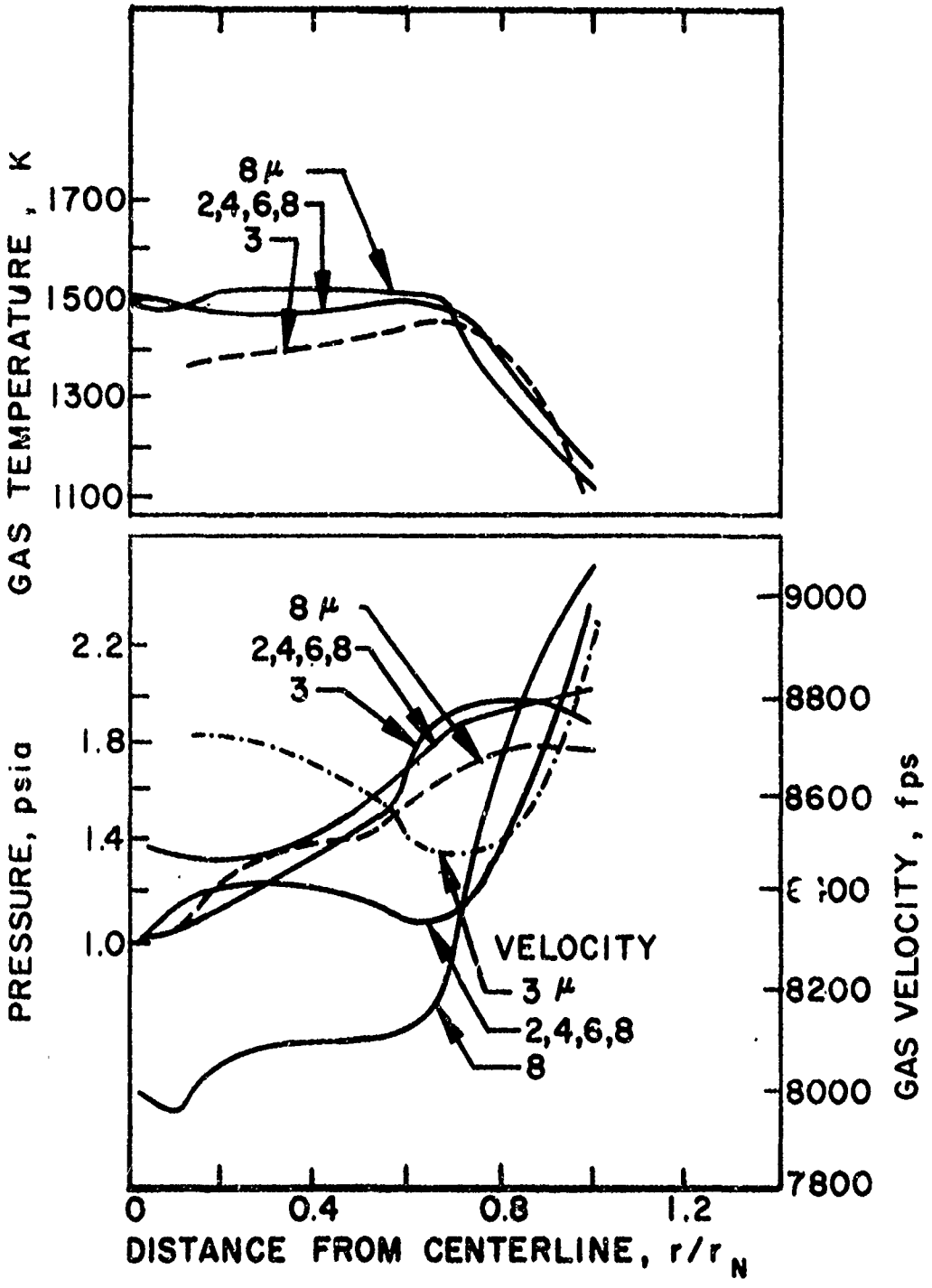

FIG. 22 INFLUENCE OF PARTICLE SIZE ON STAGE 2 NOZZLE EXIT PLANE GAS PROPERTIES

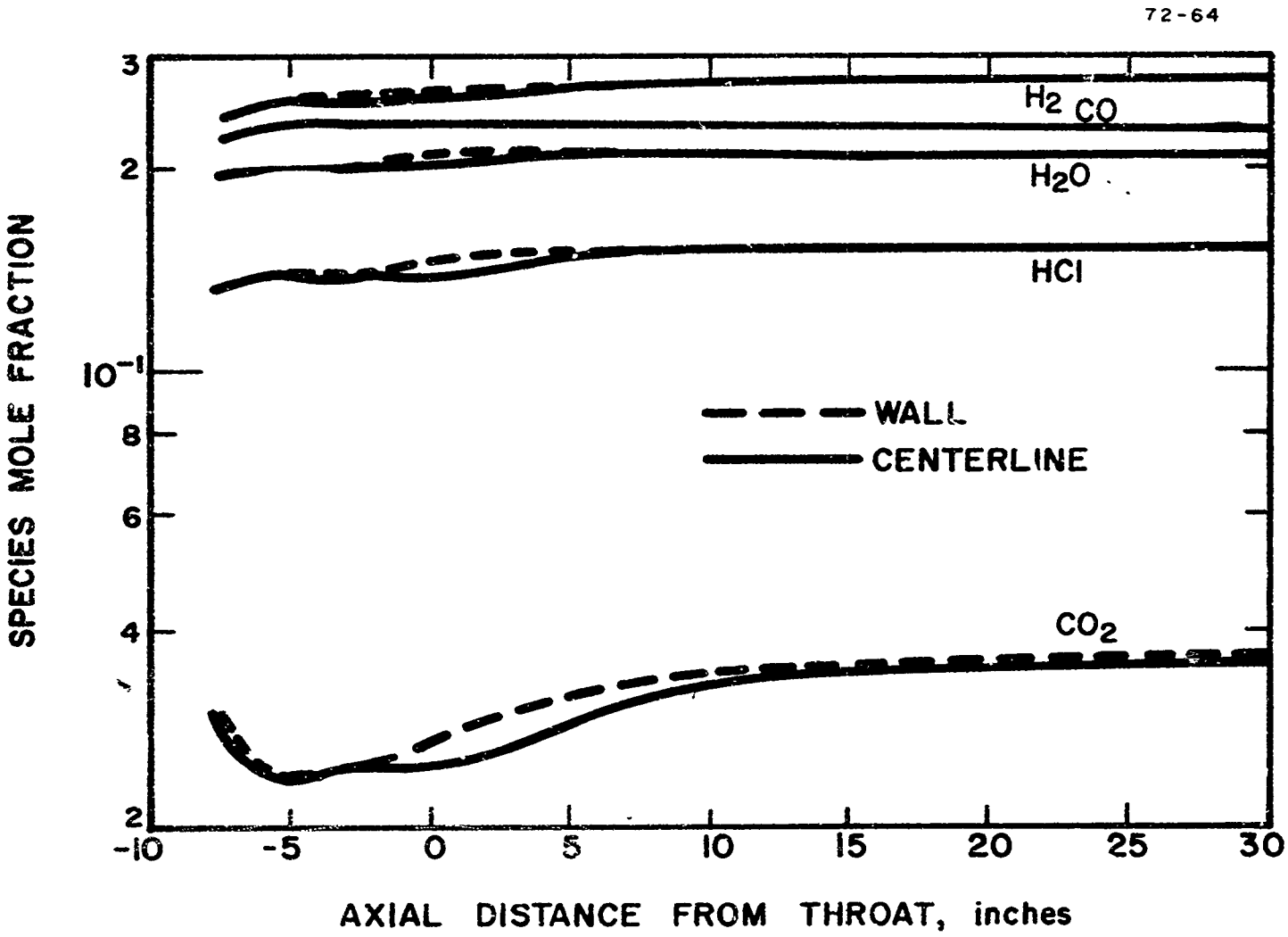

FIG. 23 H_2, CO, H_2O, HCl, CO_2 MOLE FRACTION DISTRIBUTIONS IN STAGE 1 NOZZLE

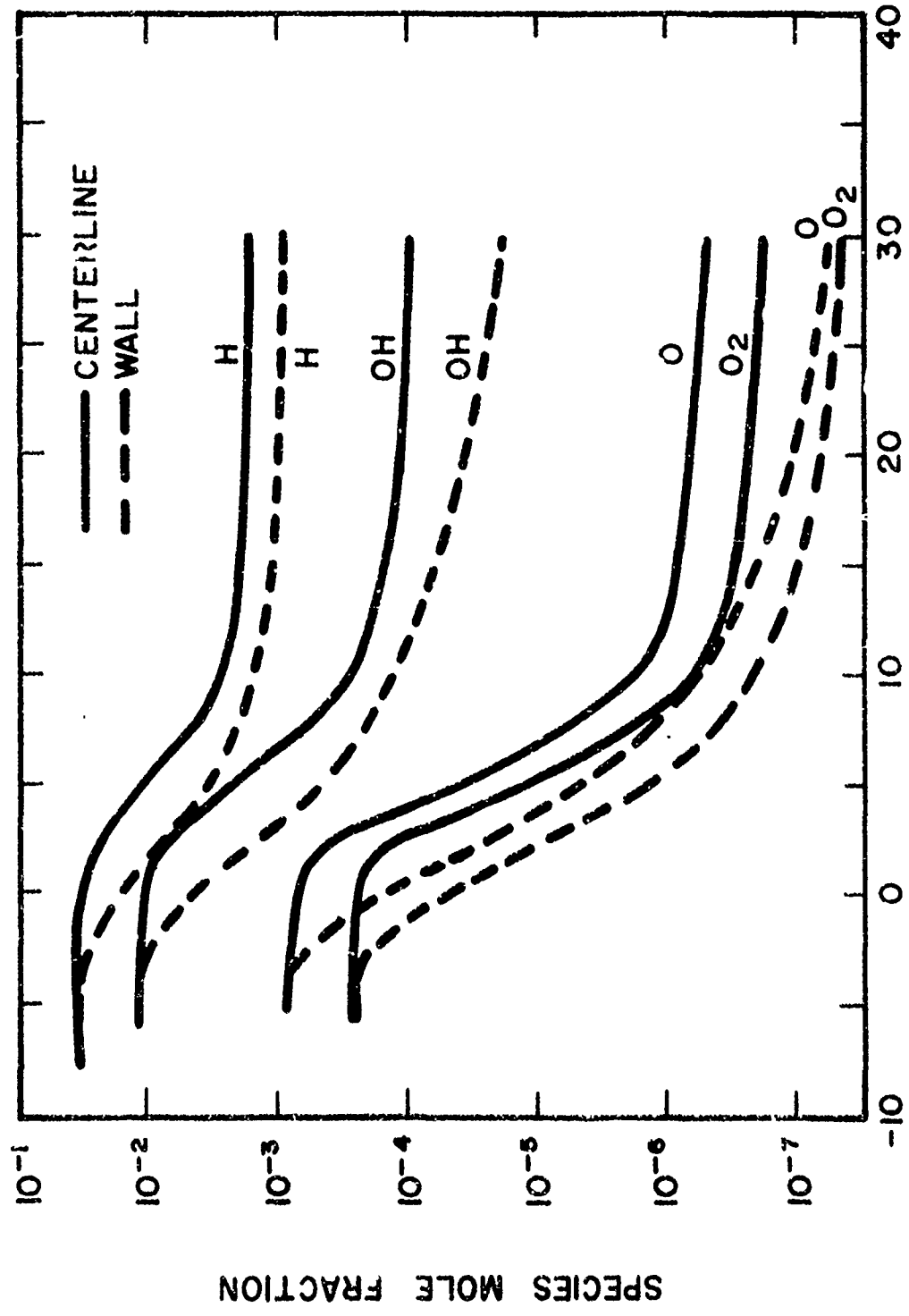

FIG. 24 H, OH, O, O_2 MOLE FRACTION DISTRIBUTIONS IN STAGE 1 NOZZLE

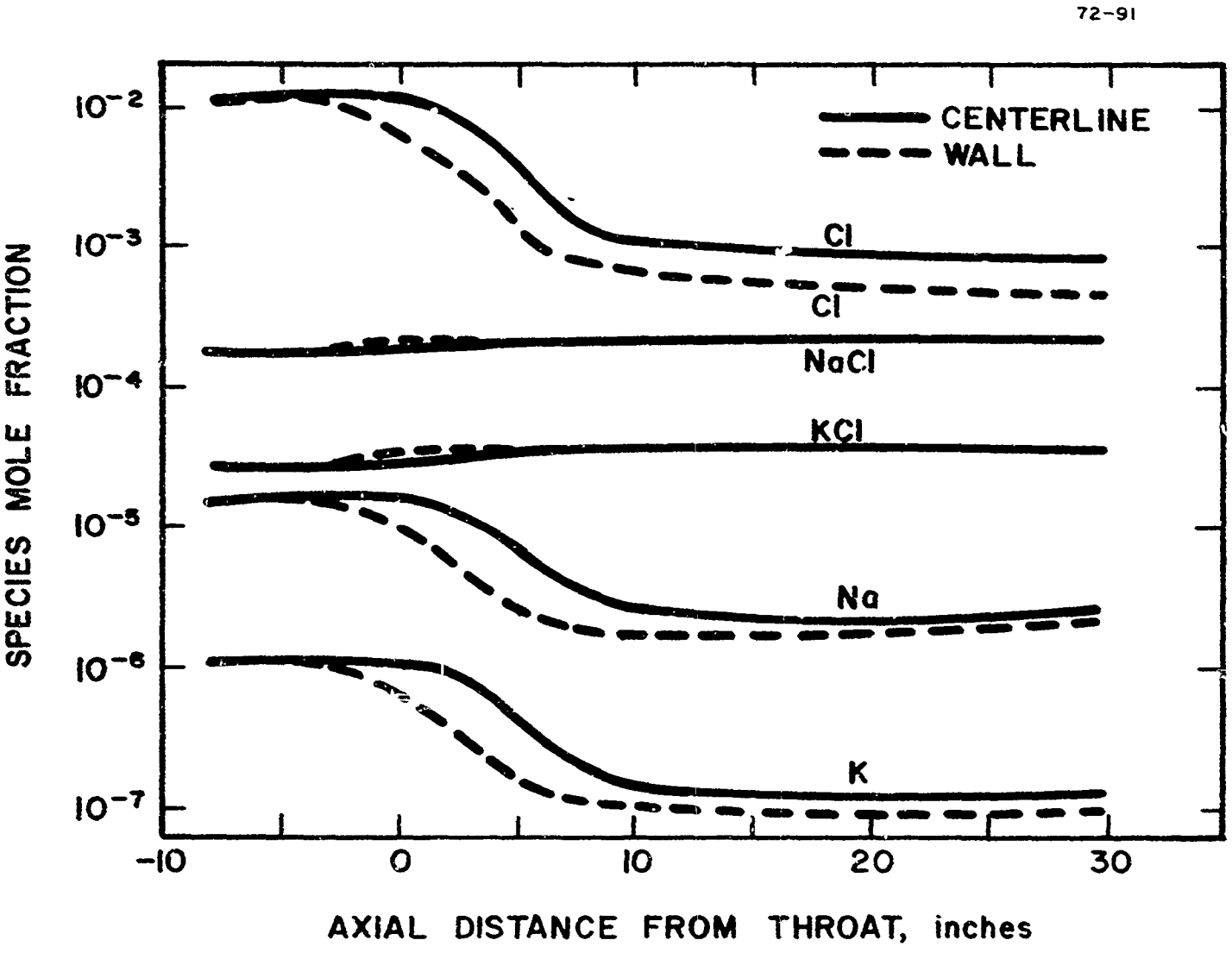

FIG. 25 Cl, NaCl, KCl, Na, K MOLE FRACTION DISTRIBUTIONS IN STAGE I NOZZLE

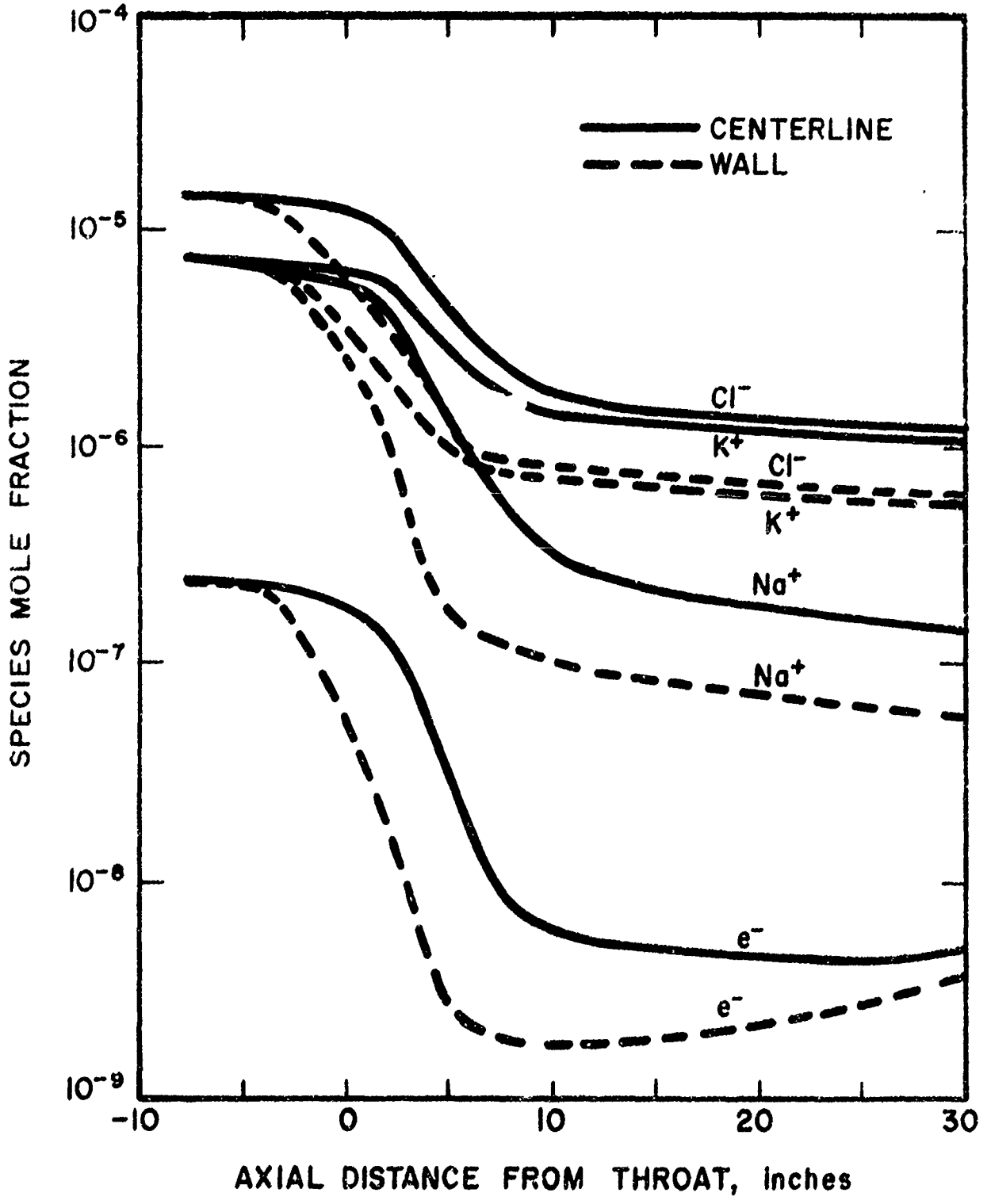

FIG. 26 Cl^-, K^+, Na^+, e^- MOLE FRACTION DISTRIBUTIONS IN STAGE 1 NOZZLE

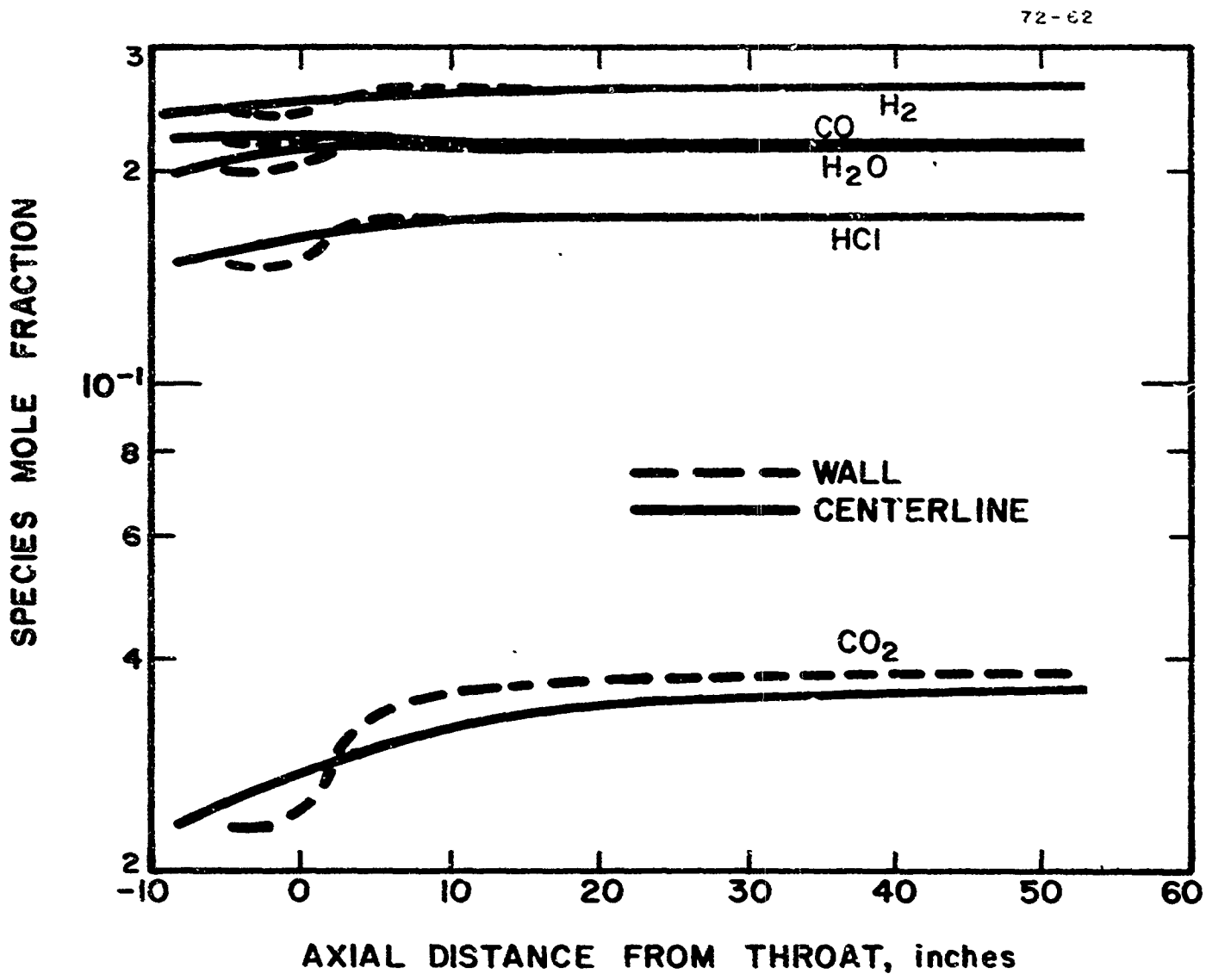

FIG. 27 H_2, CO, H_2O, HCl, CO_2 MOLE FRACTION DISTRIBUTIONS IN STAGE 2 NOZZLE

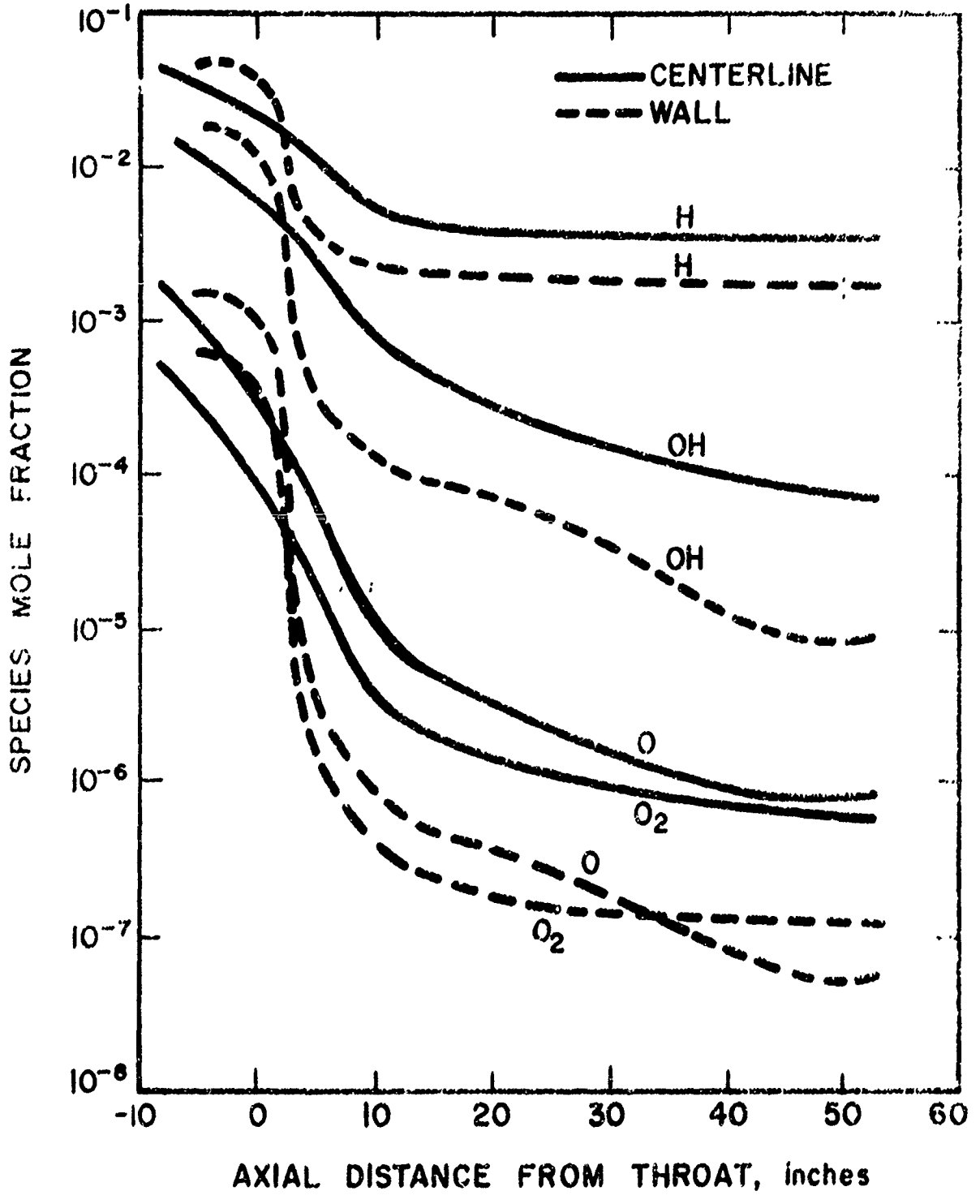

FIG. 28 H, OH, O, O_2 MOLE FRACTION DISTRIBUTIONS IN STAGE 2 NOZZLE

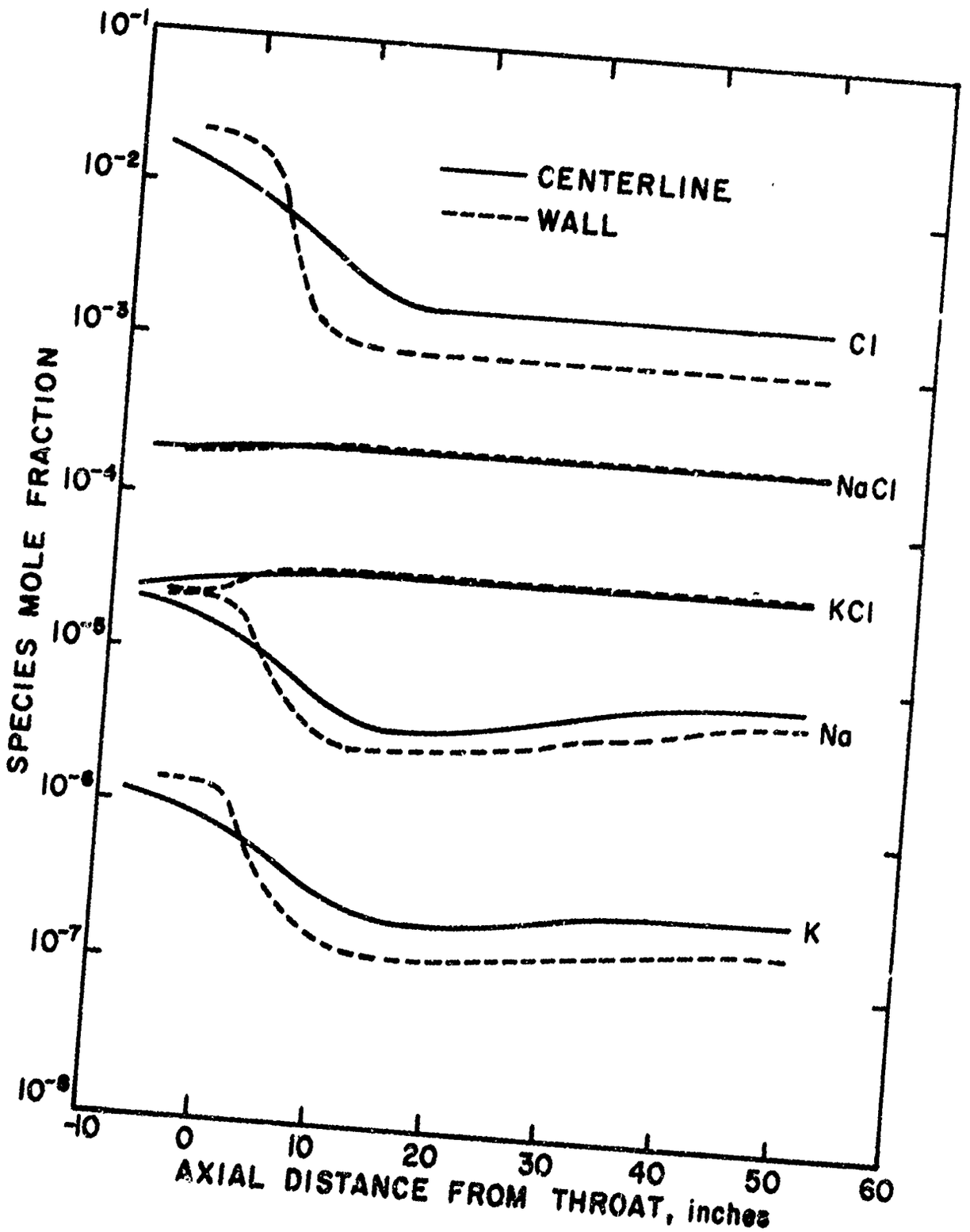

FIG. 29 Cl, NaCl, KCl, Na, K MOLE FRACTION DISTRIBUTIONS IN STAGE 2 NOZZLE

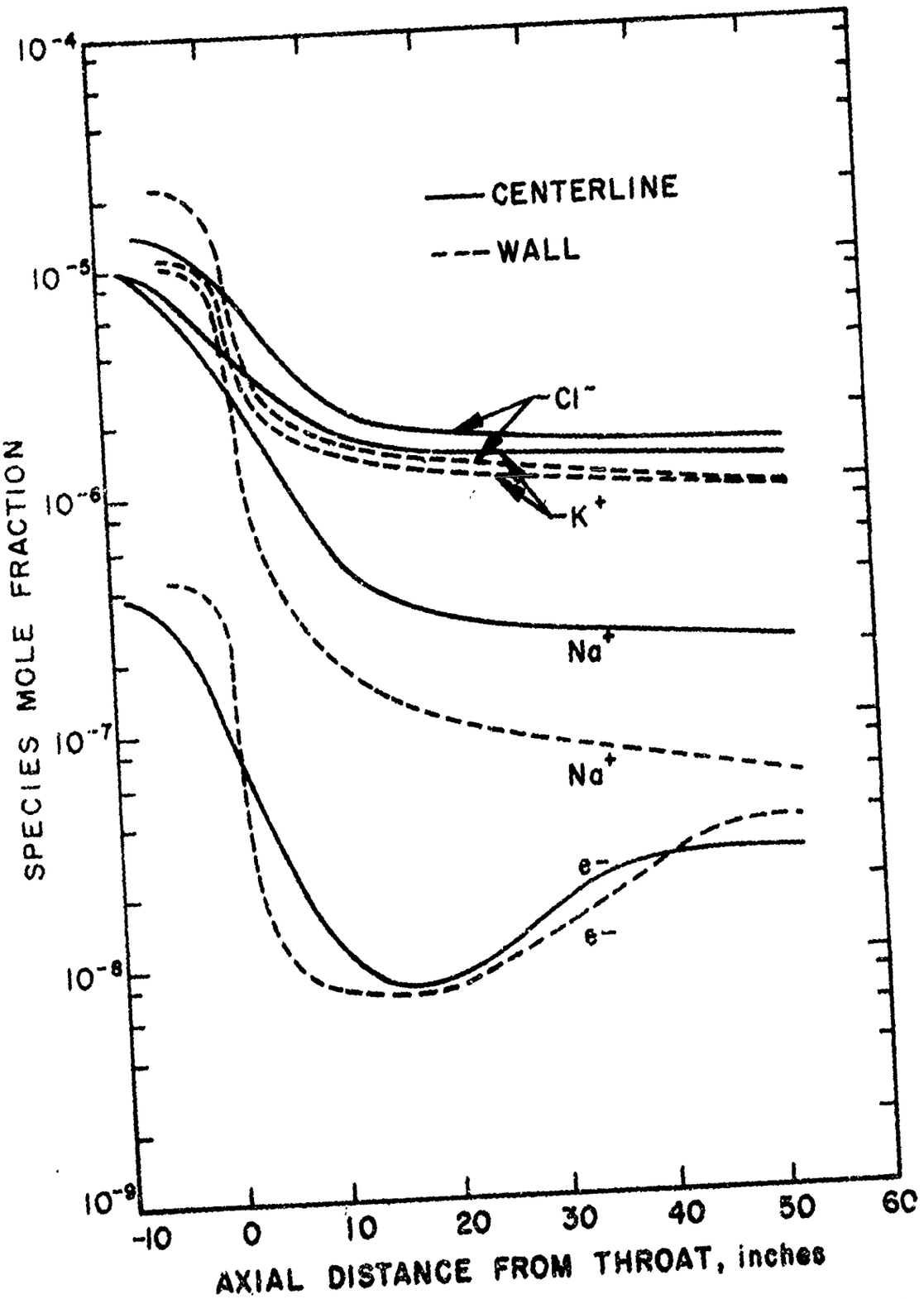

FIG. 30 Cl^-, K^+, Na^+, e^- MOLE FRACTION DISTRIBUTIONS IN STAGE 2 NOZZLE

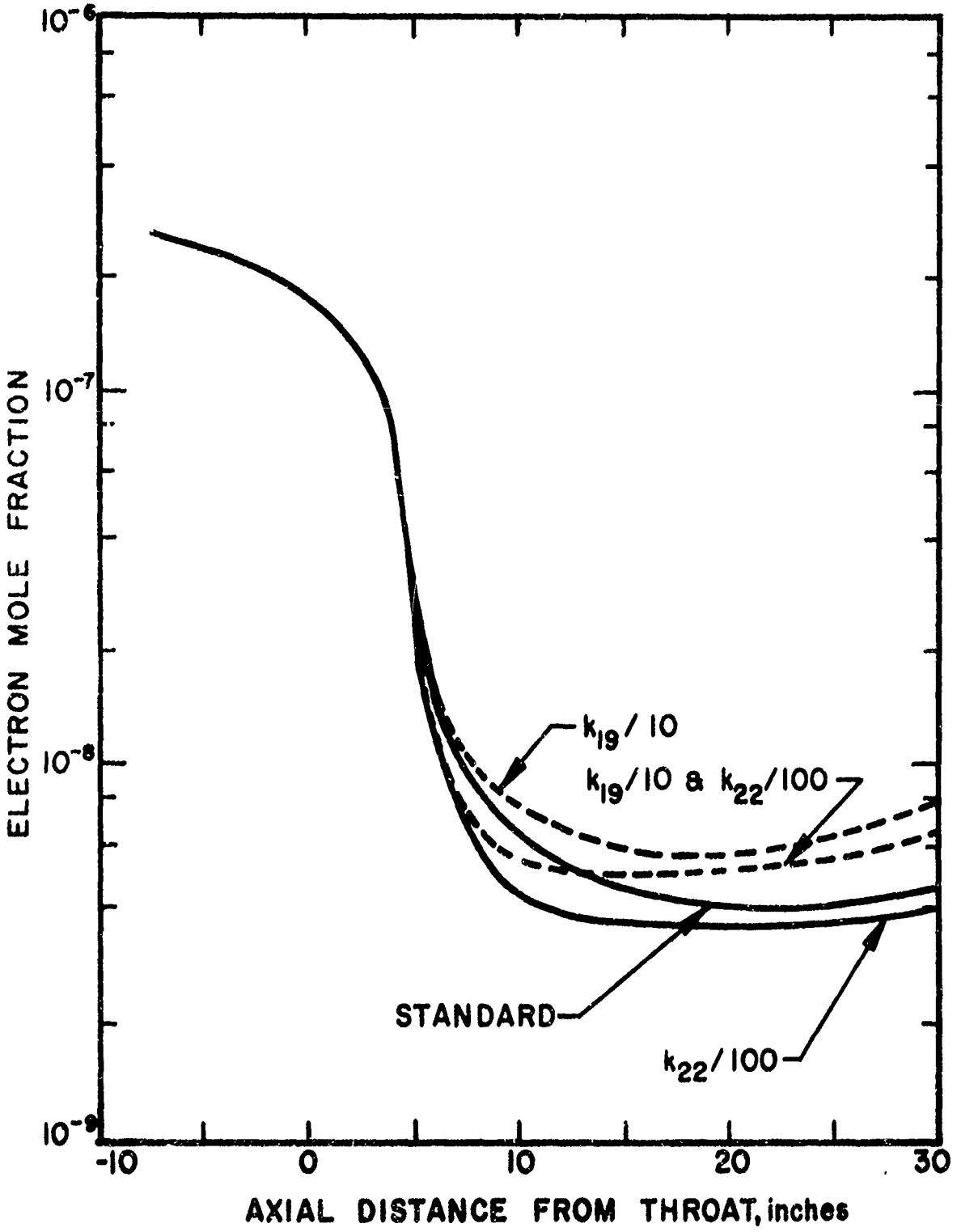

FIG. 31 INFLUENCE OF RATE COEFFICIENTS ON CENTERLINE ELECTRON MOLE FRACTIONS IN STAGE 1 NOZZLE

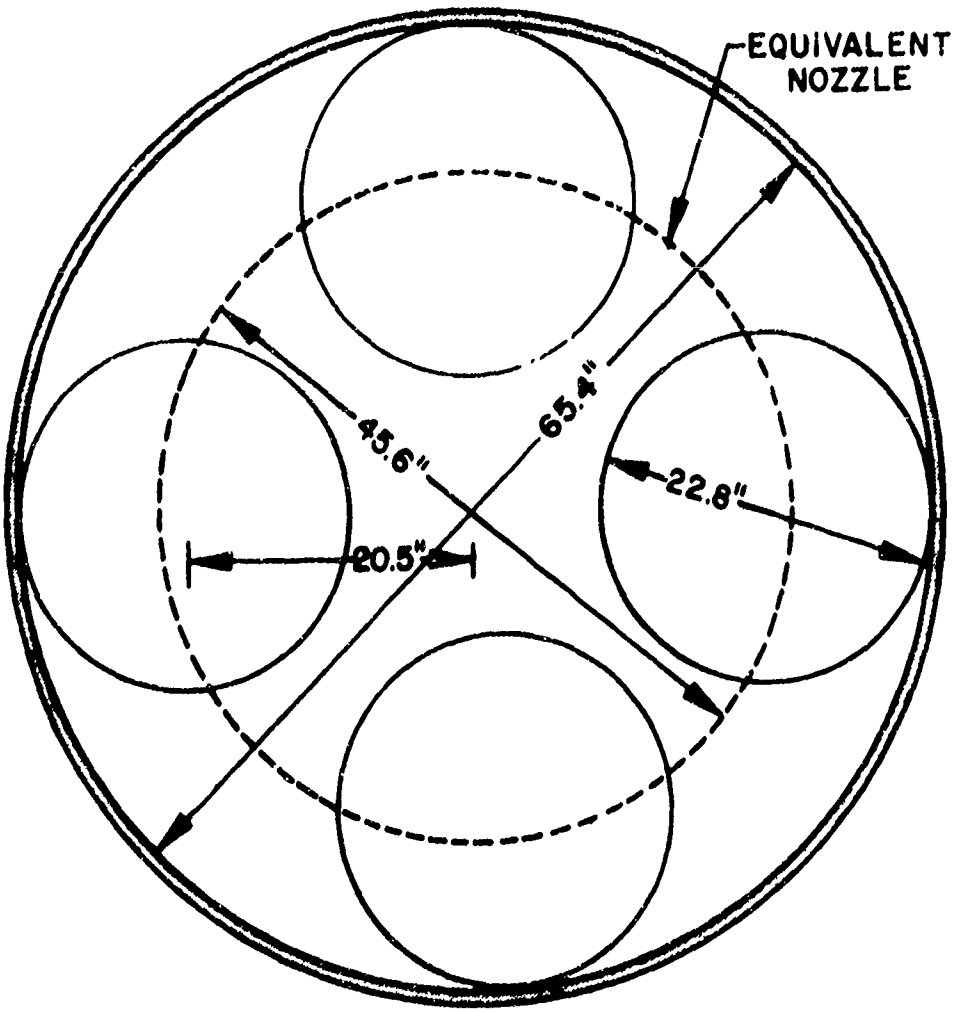

FIG. 32 MULTIPLE NOZZLE CONFIGURATION ON STAGE 1

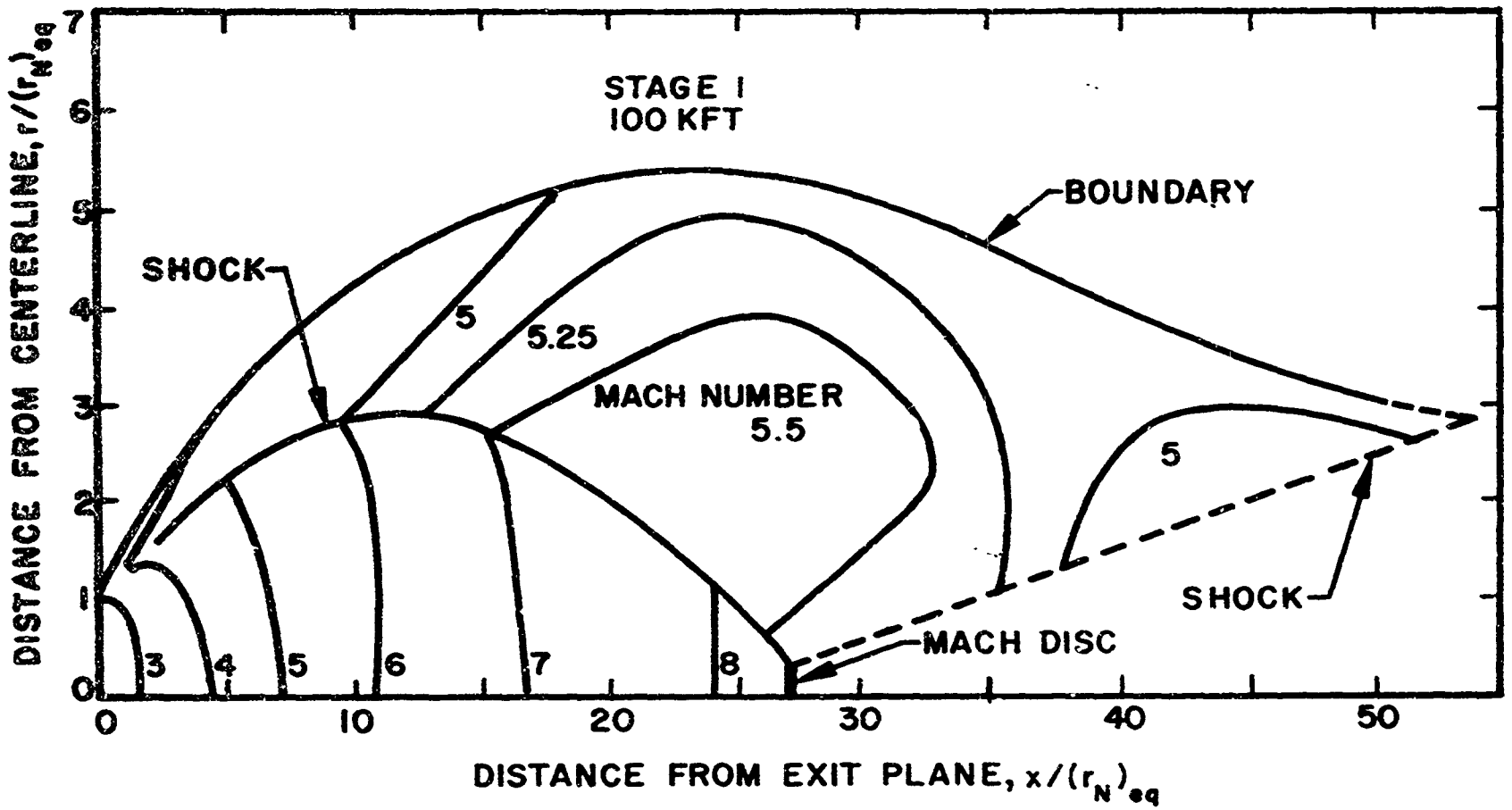

FIG. 33 PLUME BOUNDARIES, SHOCK STRUCTURE
AND CONSTANT MACH NUMBER CONTOURS
FOR STAGE I PLUME (100 kft)

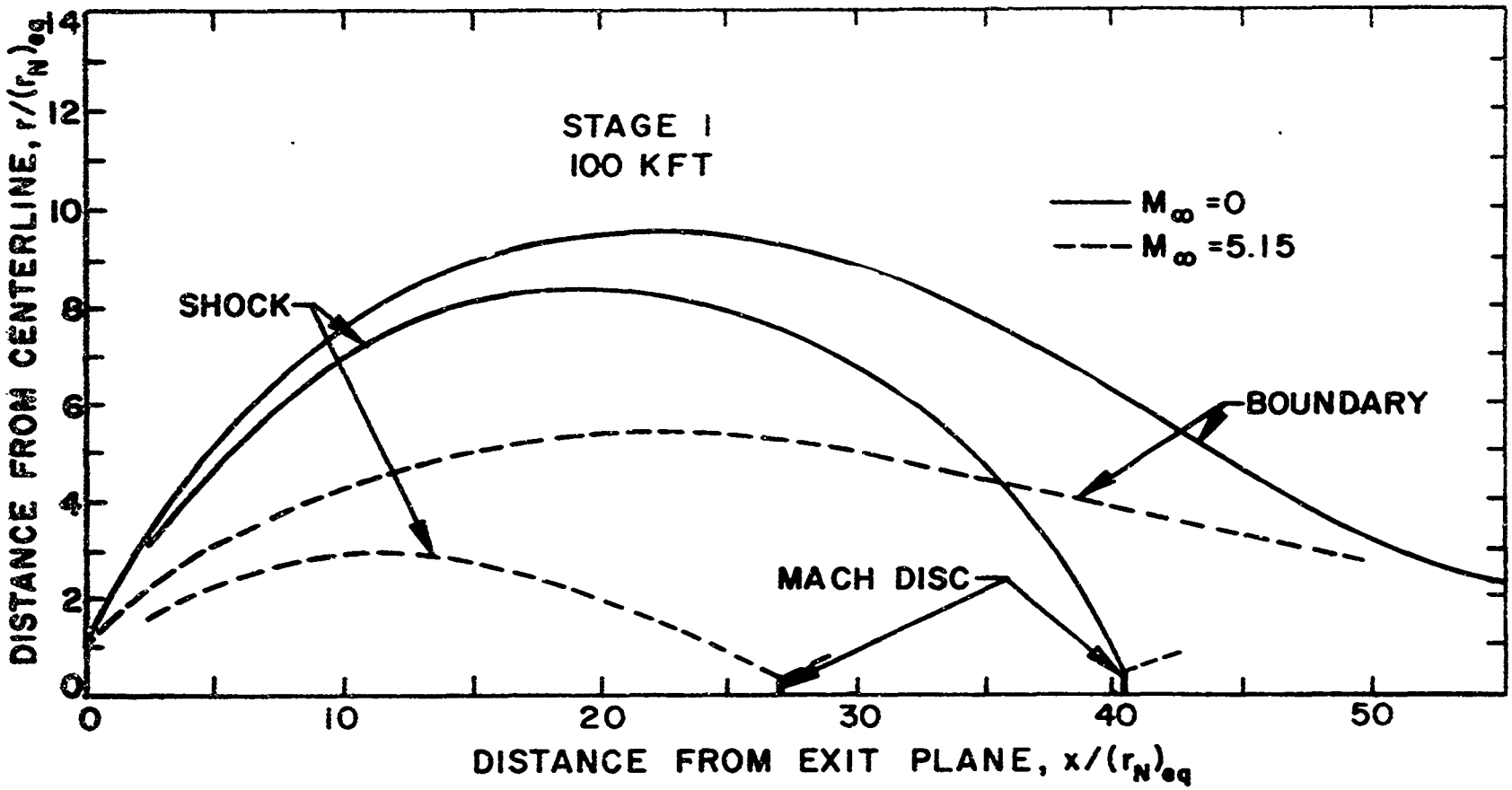

FIG. 34 INFLUENCE OF FREE STREAM MACH NUMBER ON PLUME BOUNDARIES AND SHOCK STRUCTURE

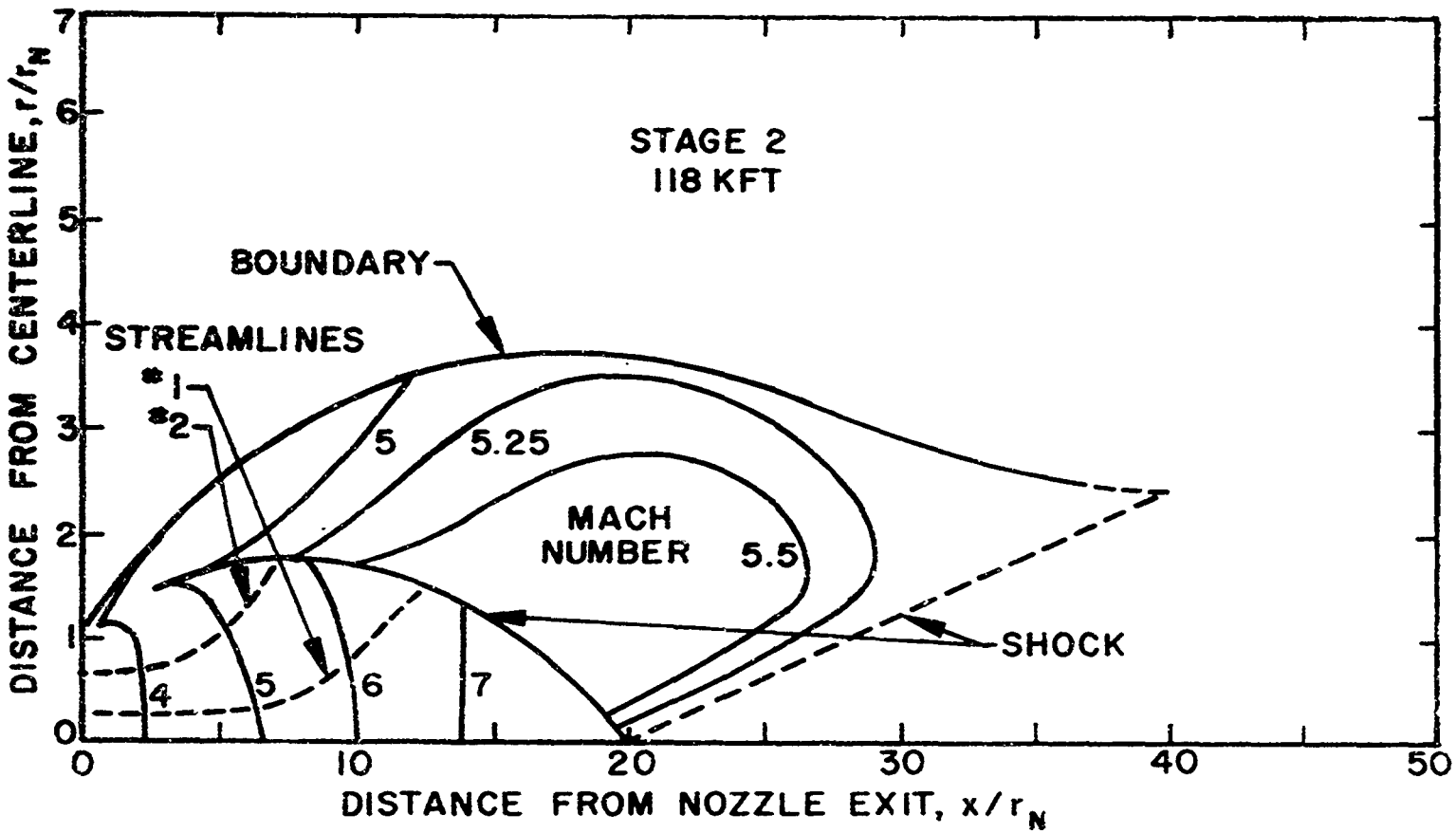

FIG. 35 PLUME BOUNDARIES, SHOCK STRUCTURE
AND CONSTANT MACH NUMBER CONTOURS
FOR STAGE 2 PLUME (118 kft)

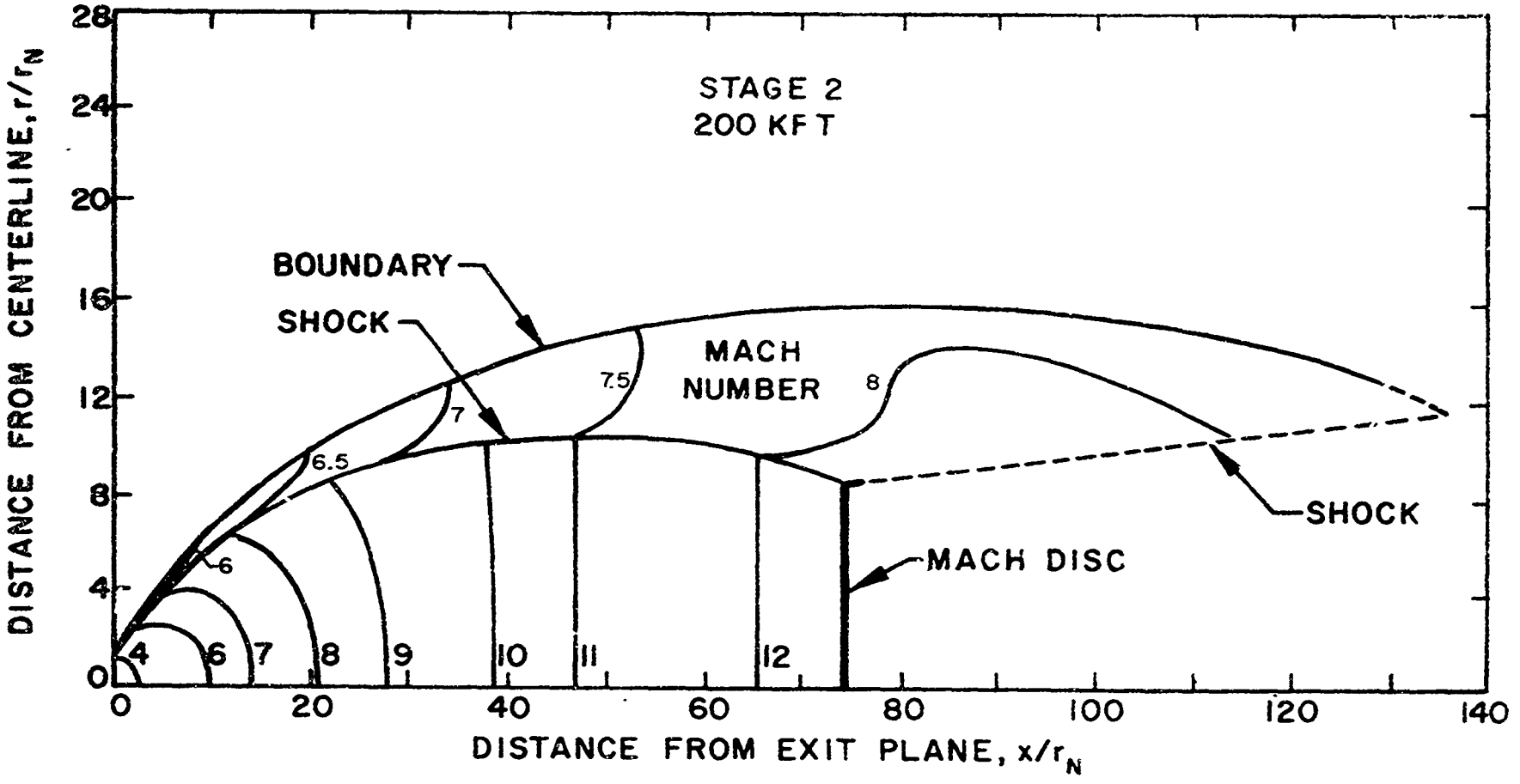

FIG. 36 PLUME BOUNDARIES, SHOCK STRUCTURE
AND CONSTANT MACH NUMBER CONTOURS
FOR STAGE 2 PLUME (200 kft)

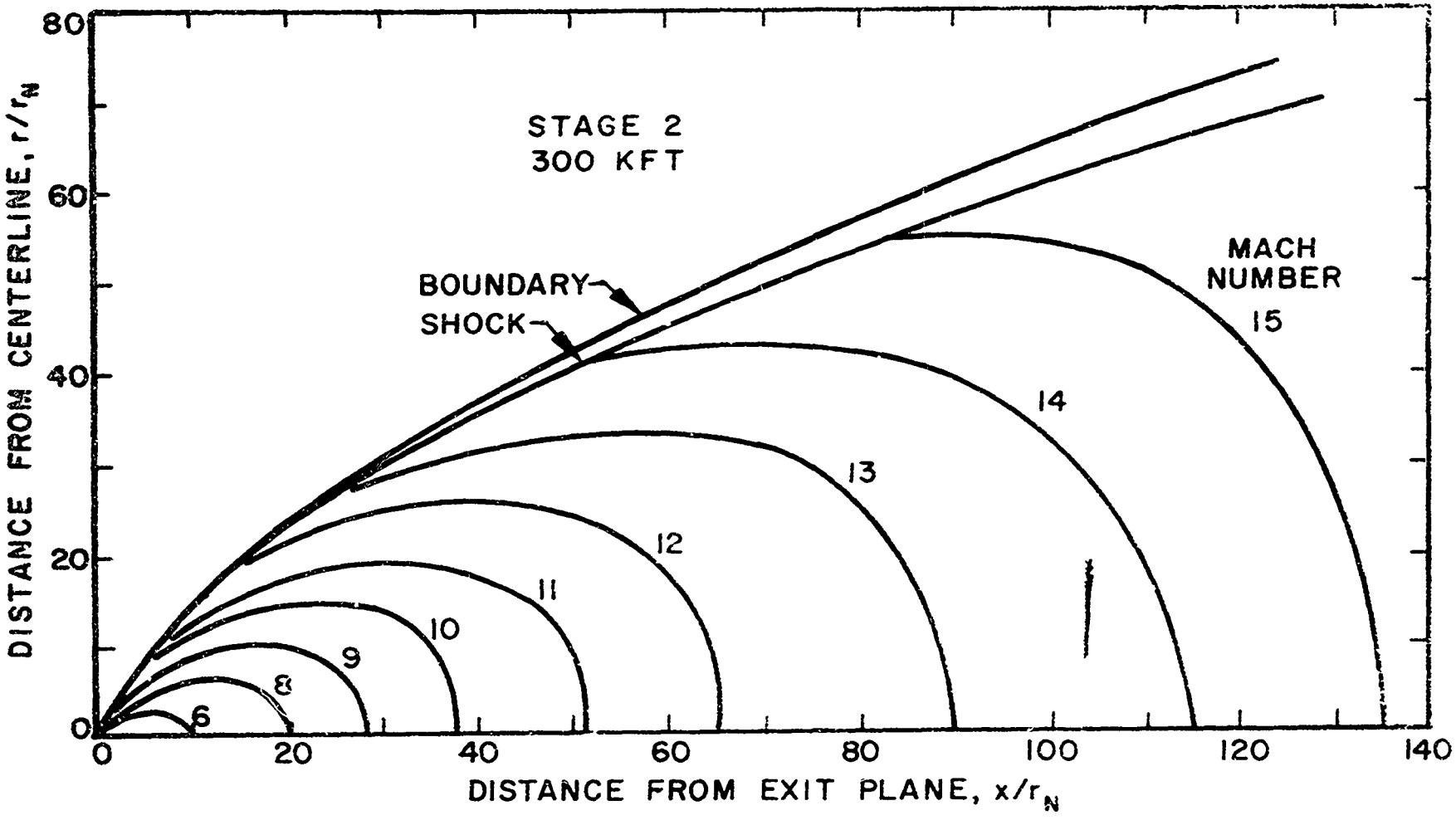

FIG. 37 PLUME BOUNDARIES, SHOCK STRUCTURE
AND CONSTANT MACH NUMBER CONTOURS
FOR STAGE 2 PLUME (300 kft)

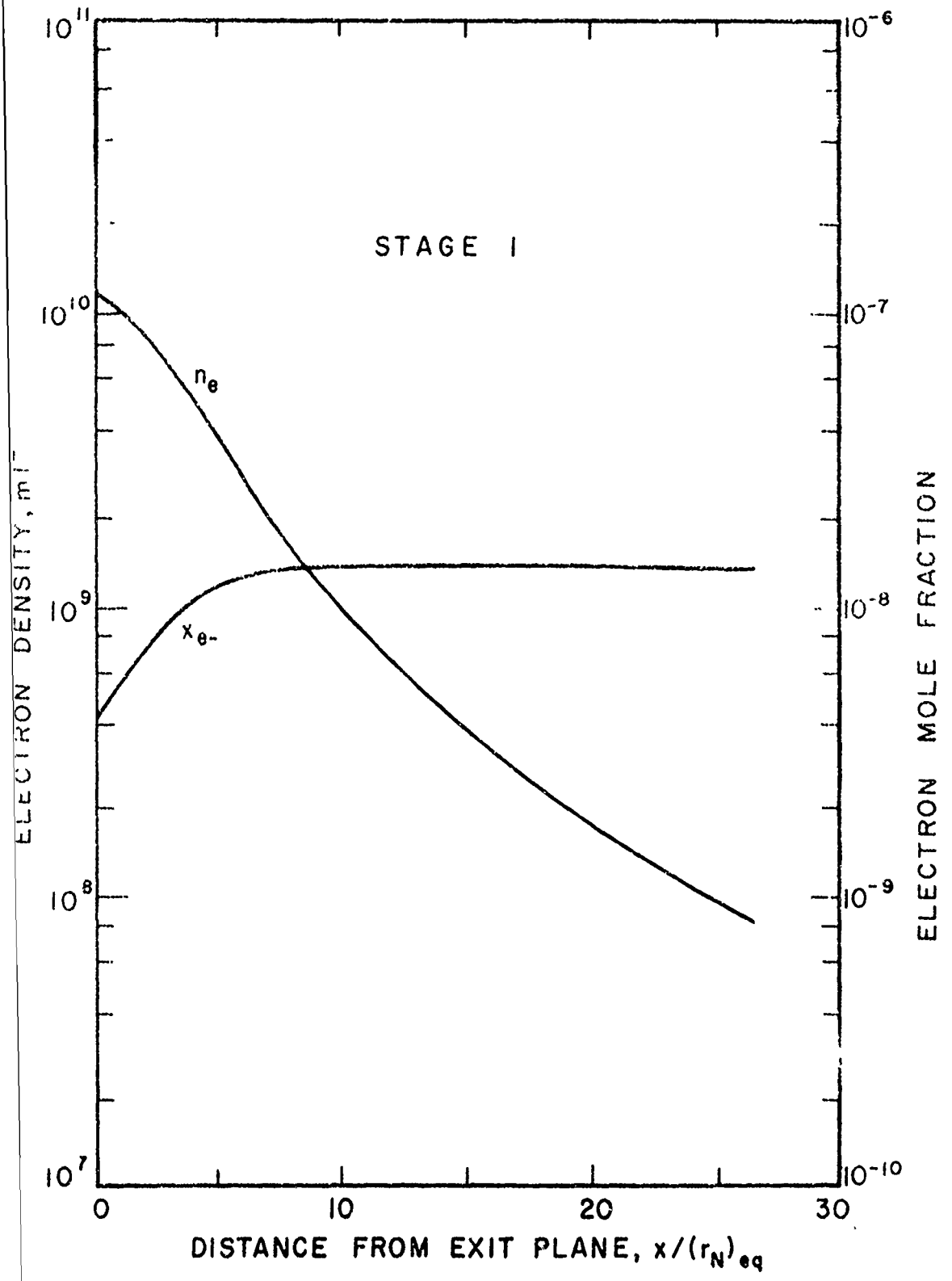

FIG. 38 ELECTRON DENSITY AND ELECTRON MOLE FRACTION DISTRIBUTIONS ALONG CENTERLINE OF STAGE I PLUME

$k_{22}/100$

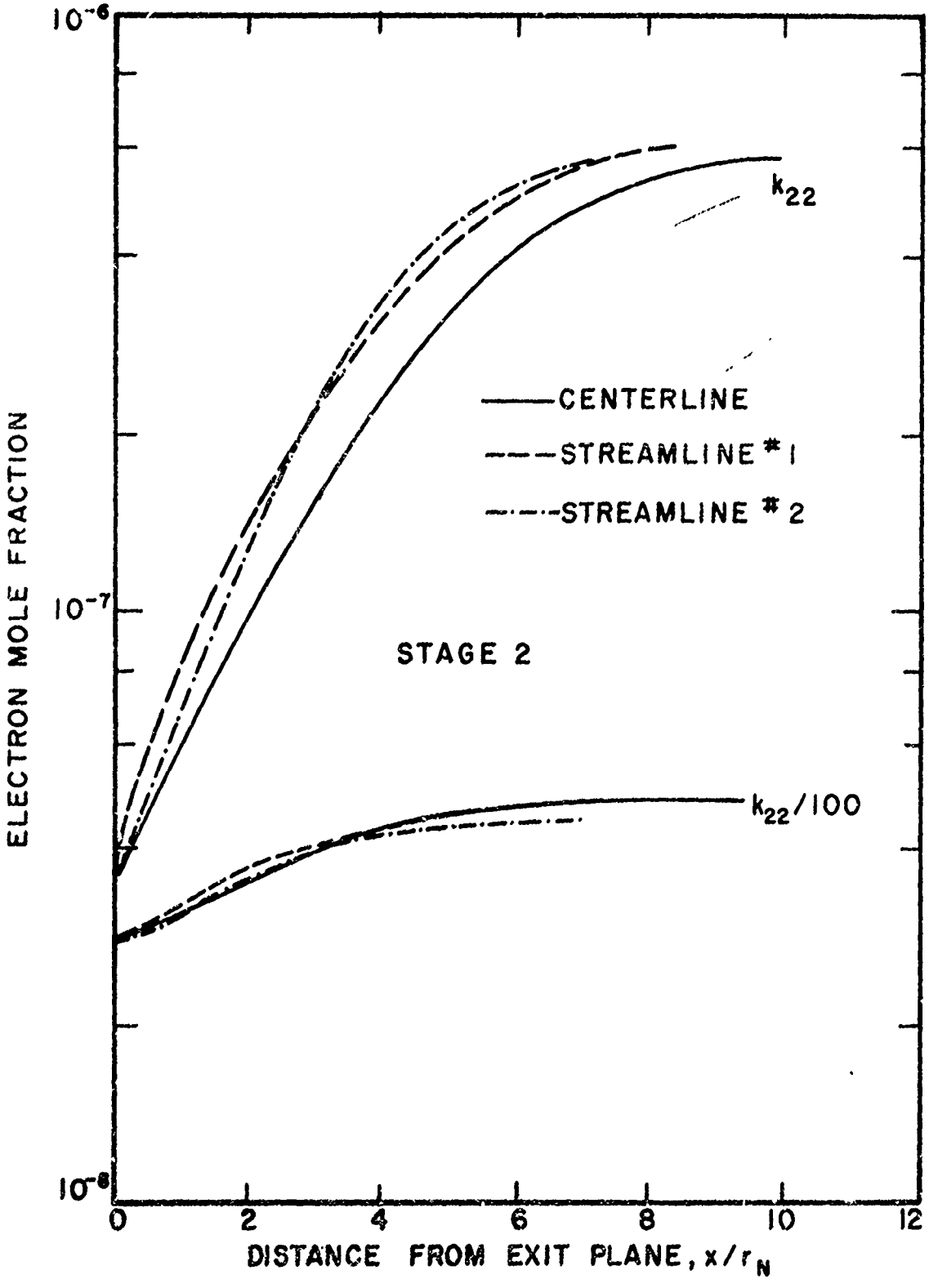

FIG. 39 ELECTRON MOLE FRACTION DISTRIBUTIONS IN STAGE 2 PLUME

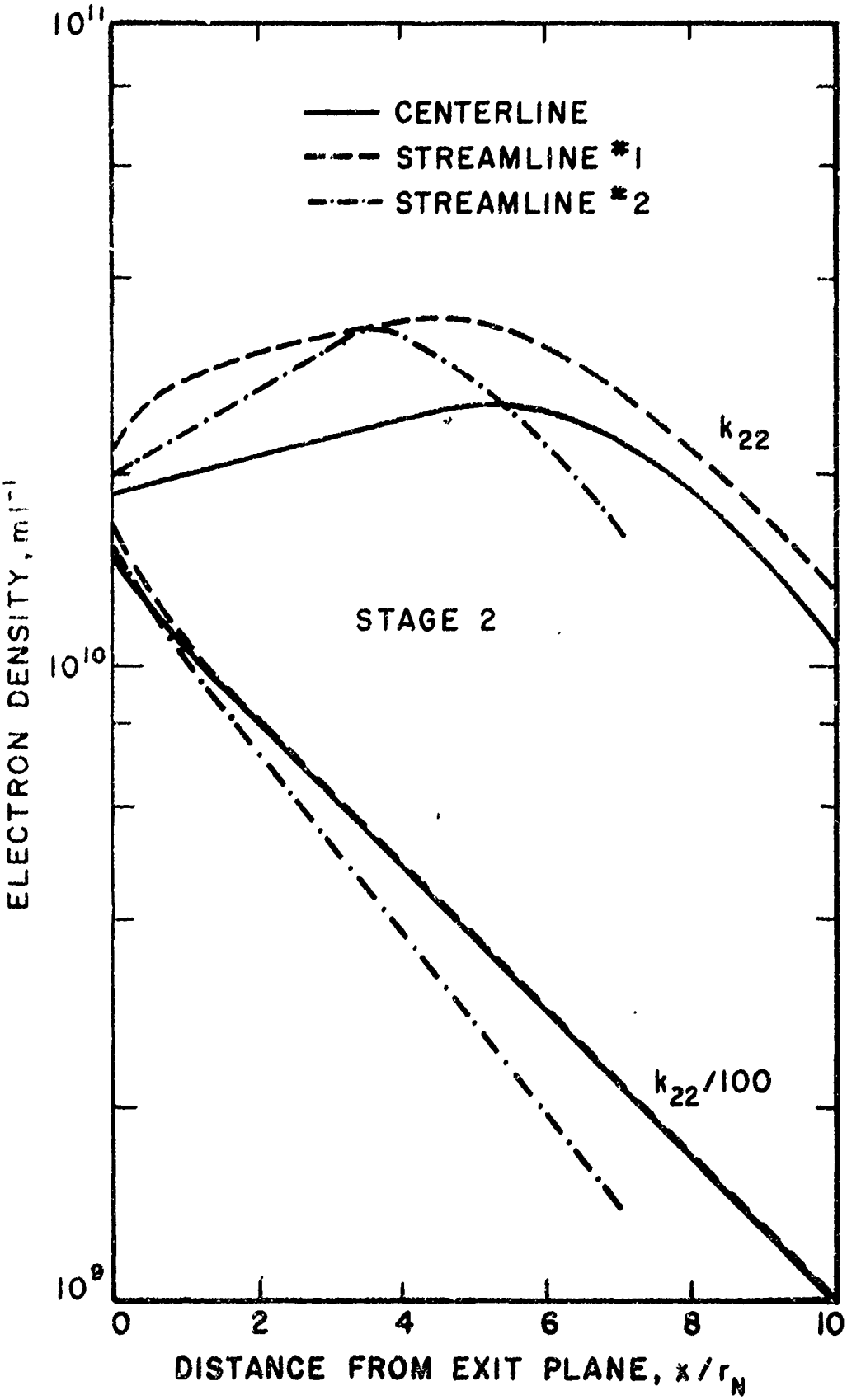

FIG. 40 ELECTRON DENSITY DISTRIBUTIONS IN STAGE 2 PLUME

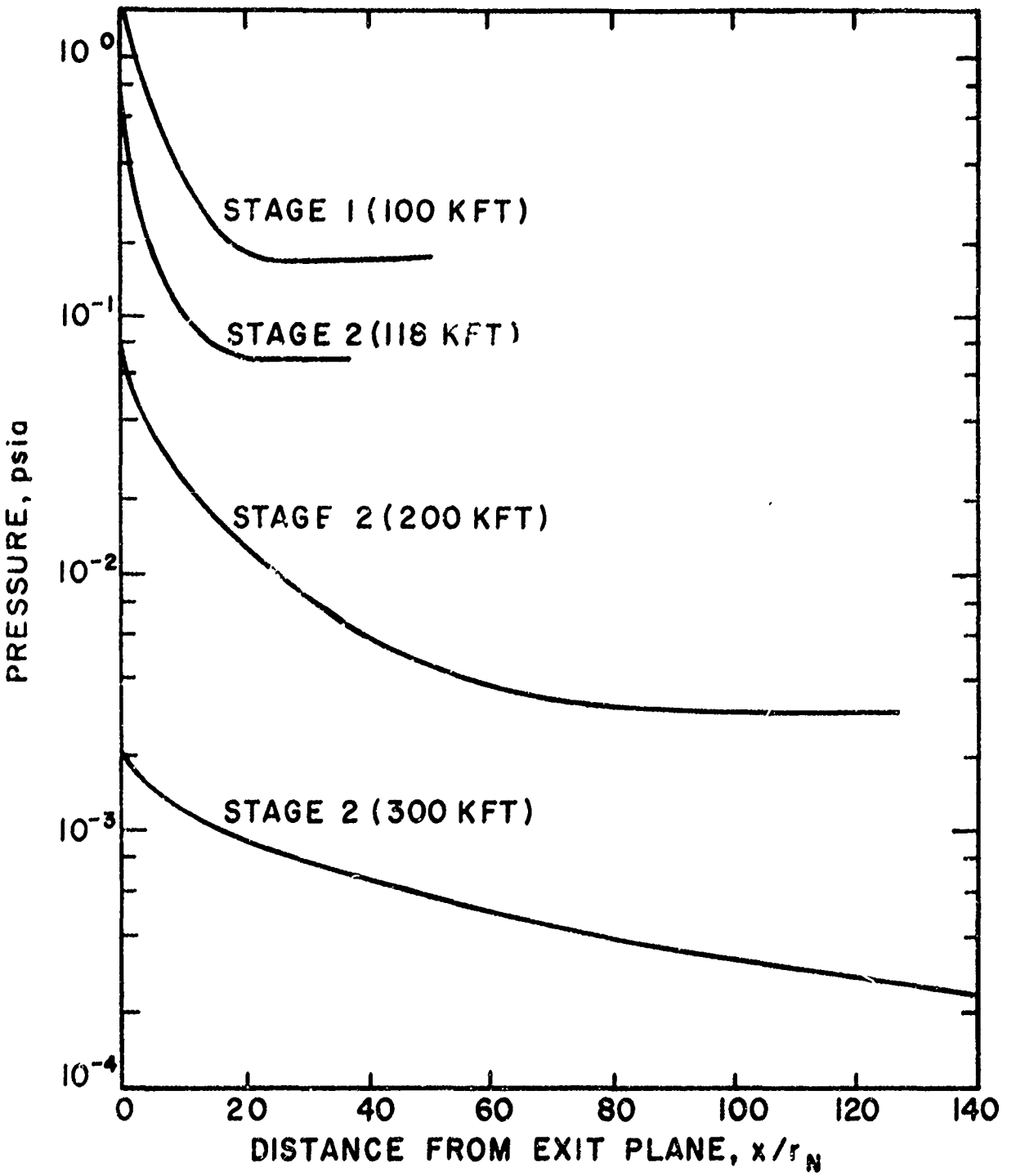

FIG. 41 PRESSURE DISTRIBUTIONS ALONG PLUME BOUNDARIES

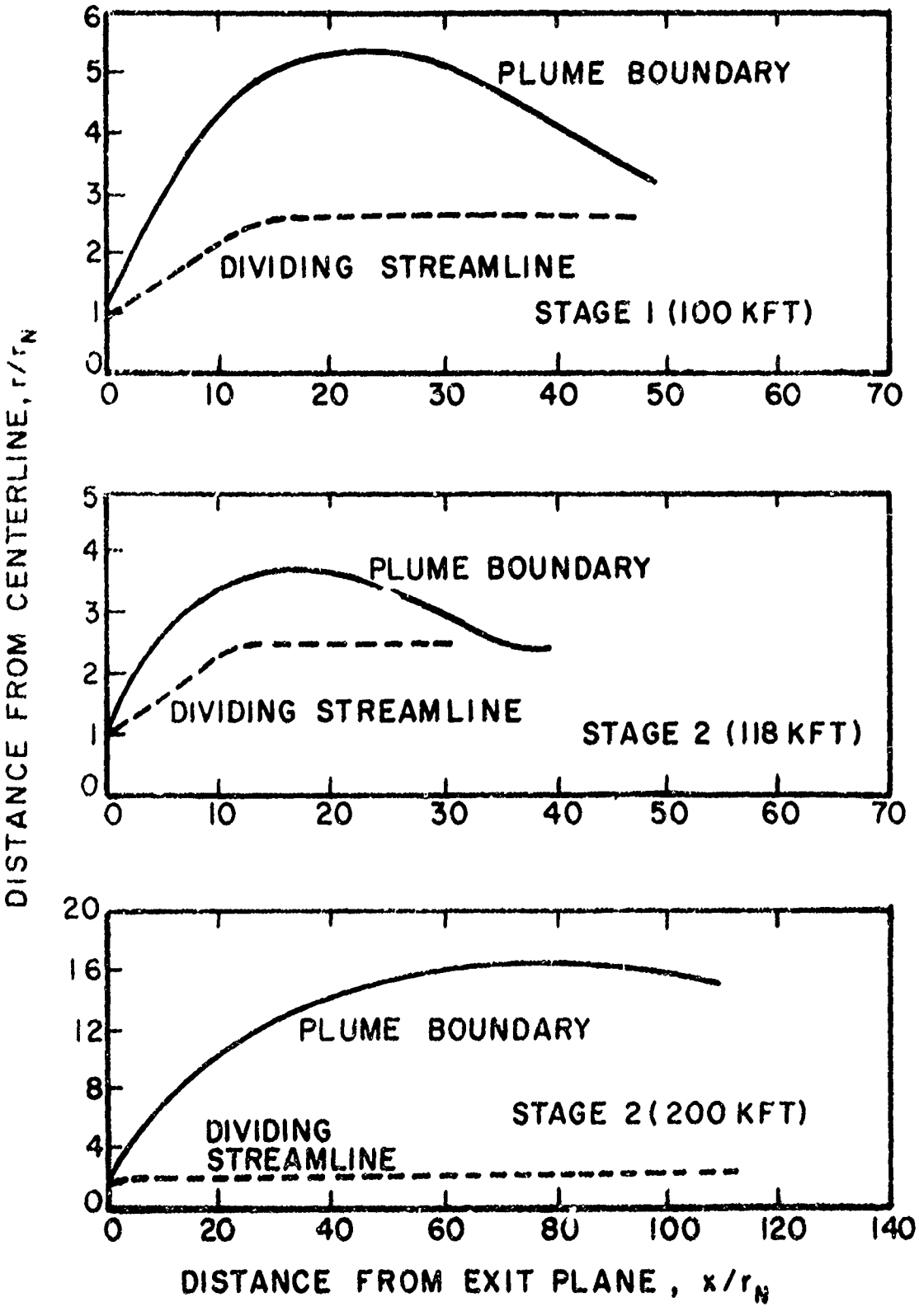

FIG. 42 DIVIDING STREAMLINE LOCATIONS

Computed from Mixing with Nonequilibrium Chemistry program

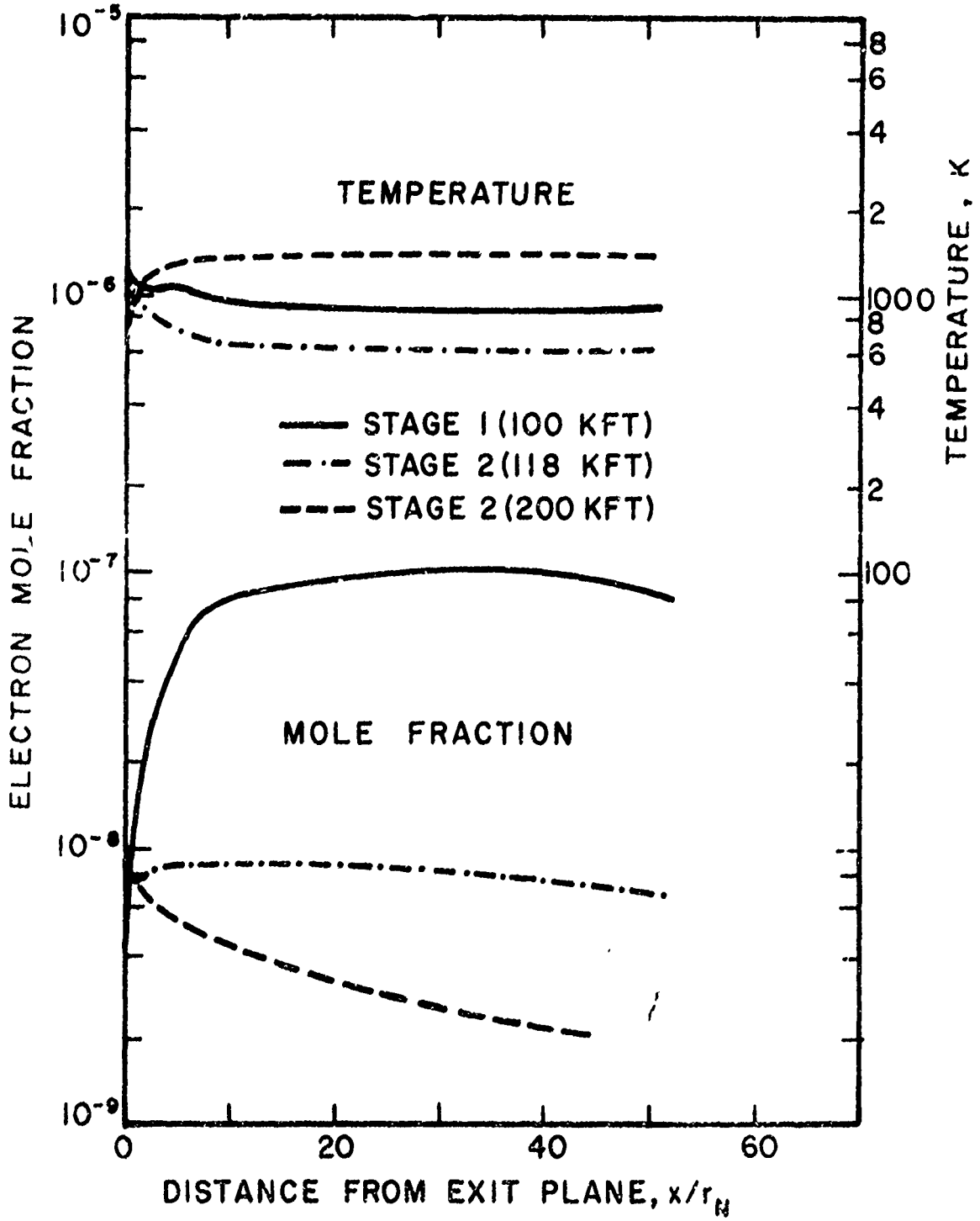

FIG. 13 TEMPERATURE AND ELECTRON MOLE FRACTION DISTRIBUTIONS ALONG DIVIDING STREAMLINES

$k_{22}/100$

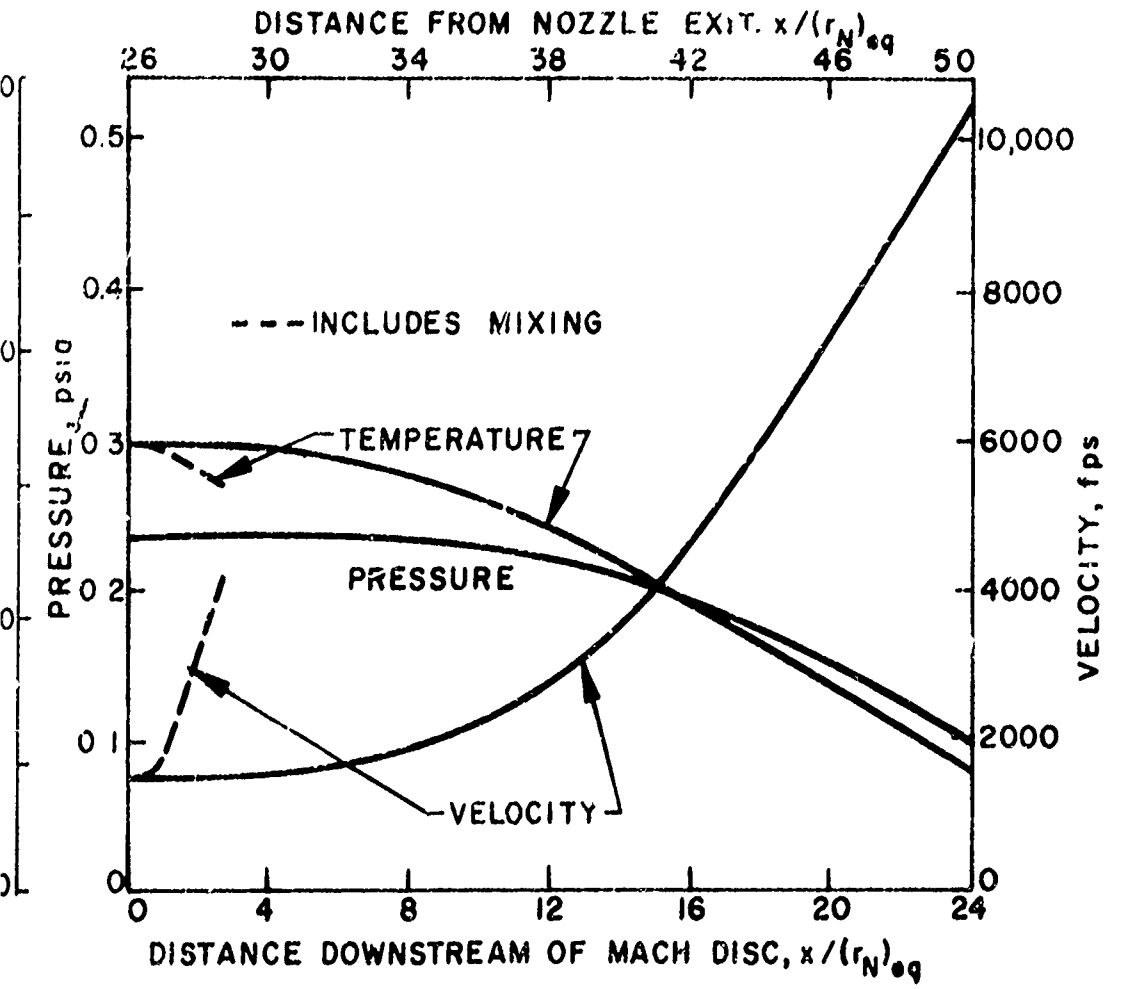

FIG. 14 ESTIMATED PROPERTY DISTRIBUTIONS DOWNSTREAM OF MACH DISC - STAGE I PLUME

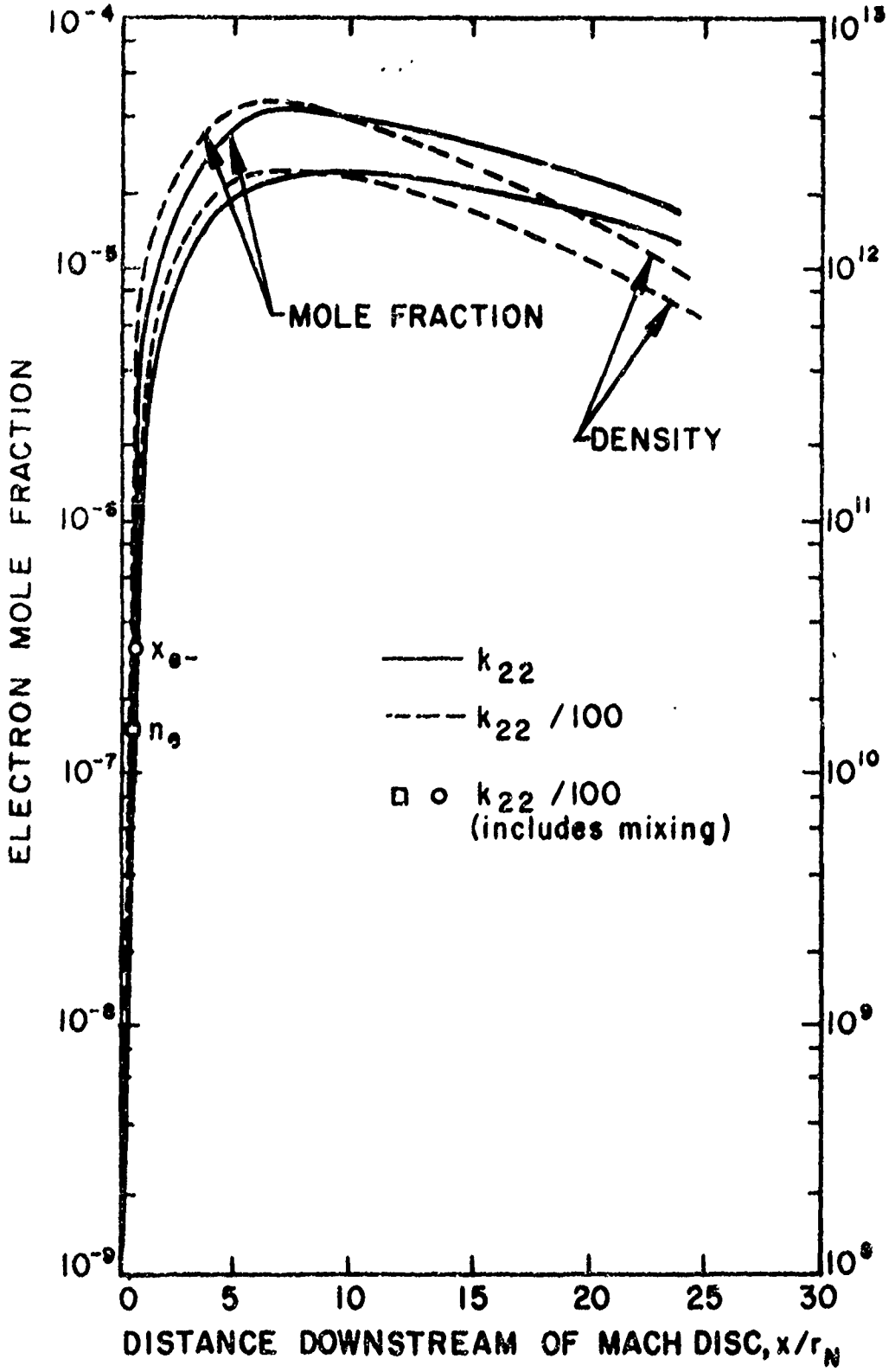

FIG. 45 ELECTRON MOLE FRACTION DISTRIBUTIONS DOWNSTREAM OF MACH DISC - STAGE 1 PLUME

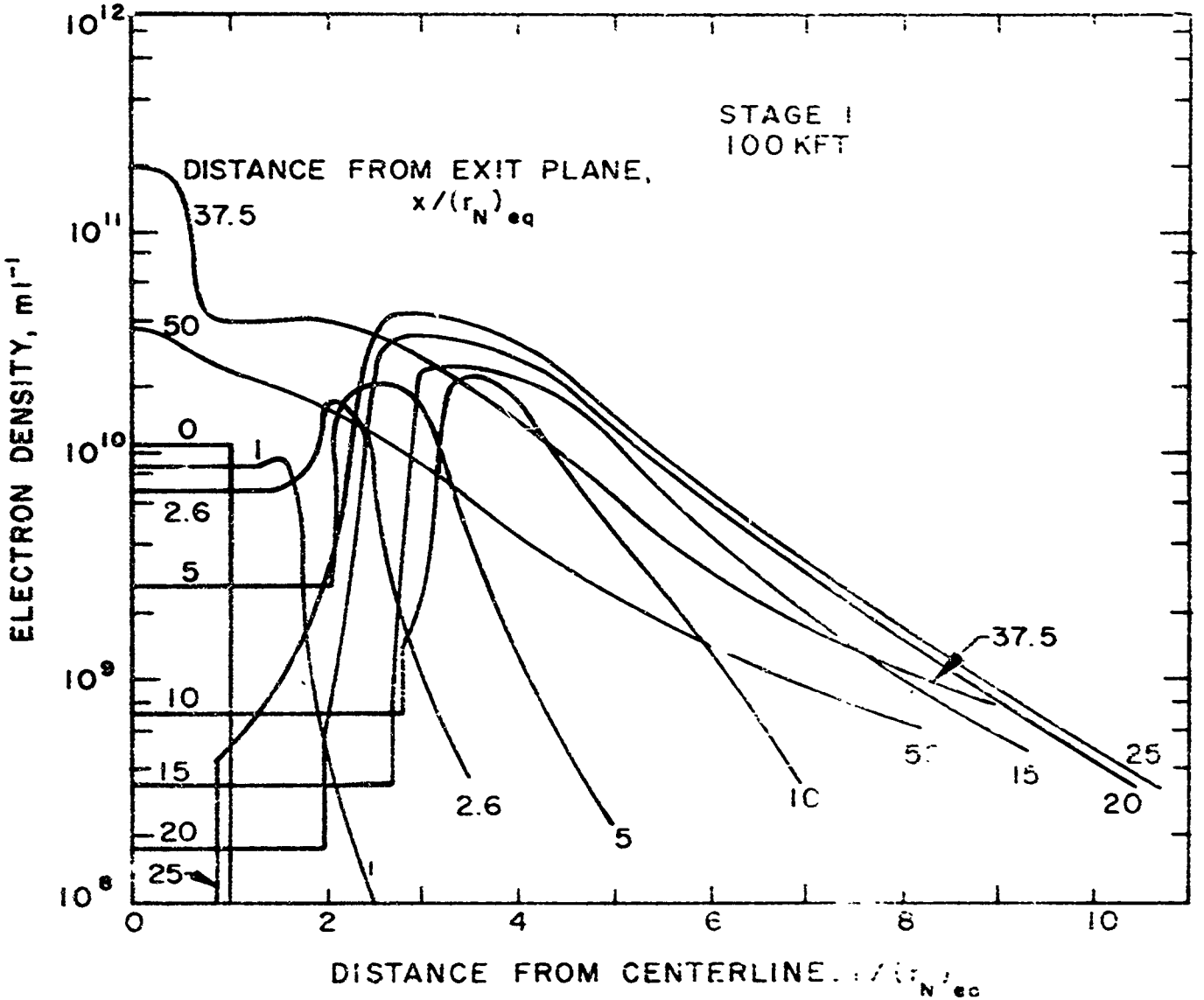

FIG. 4c ELECTRON DENSITY PROFILES IN STAGE I PLUME 100 KF

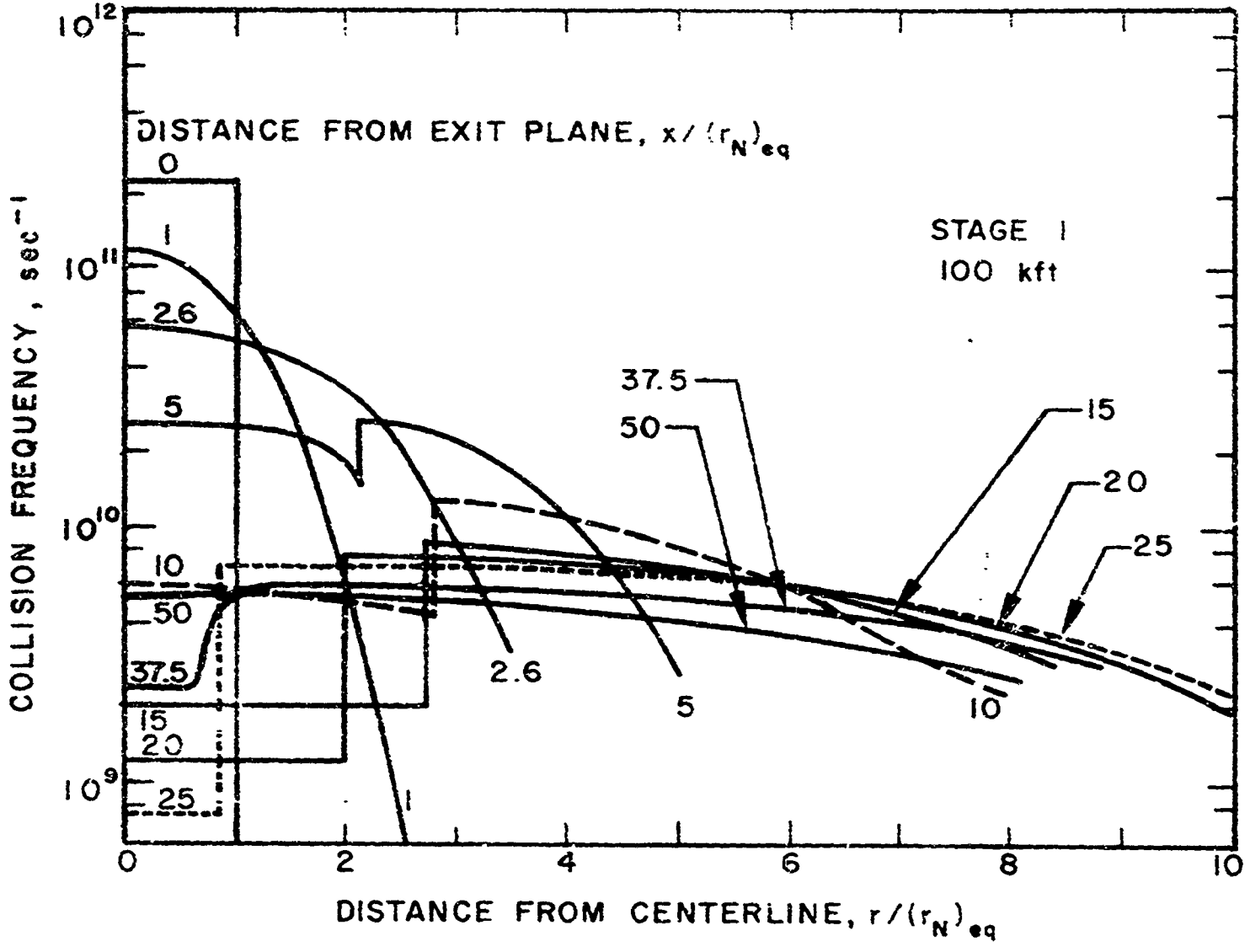

FIG. 47 COLLISION FREQUENCY PROFILES IN STAGE I PLUME [illegible]

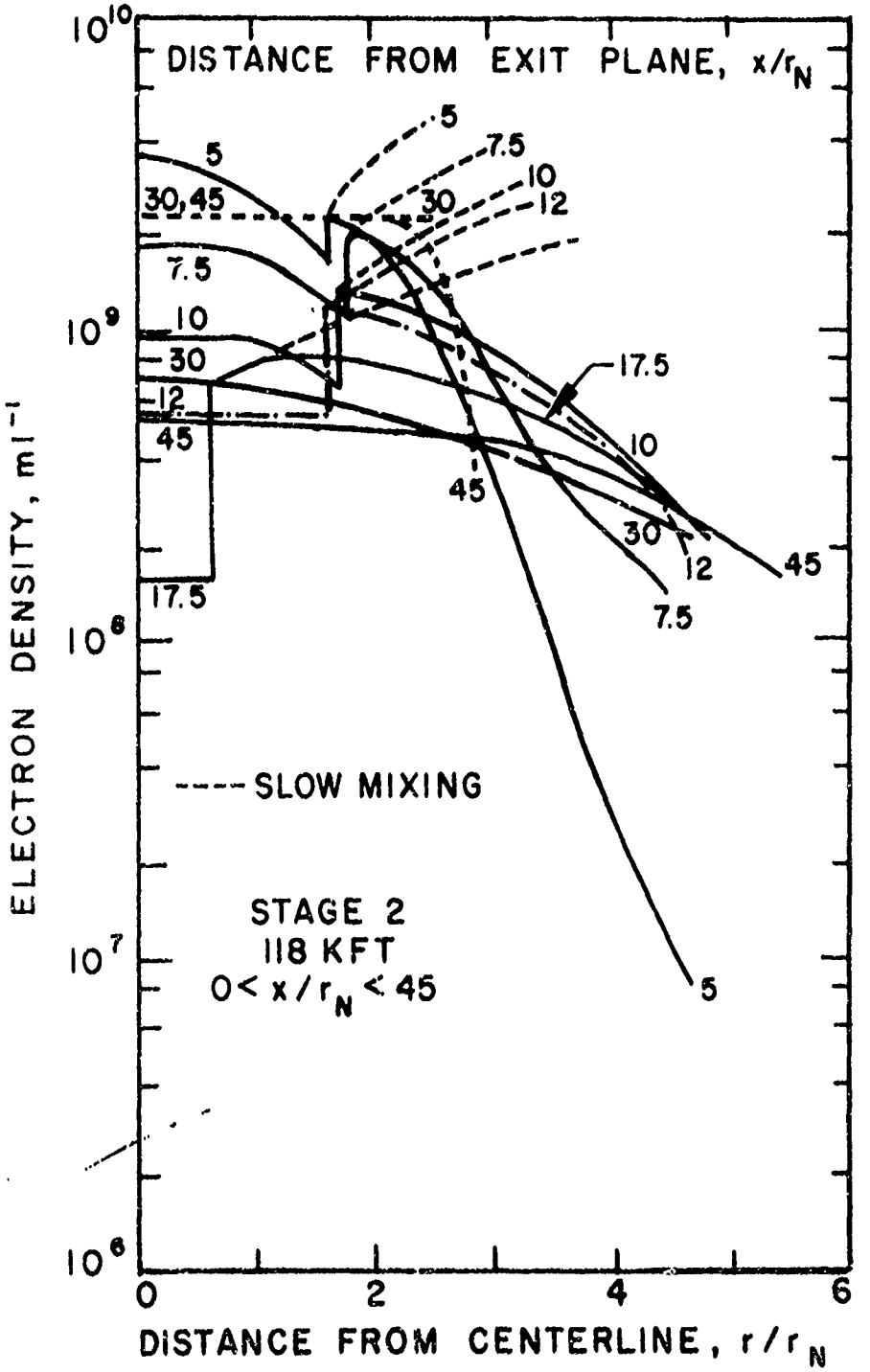

FIG. 48a ELECTRON DENSITY PROFILES
IN STAGE 2 PLUME (118 kft)

$0 < x/r_N < 45$

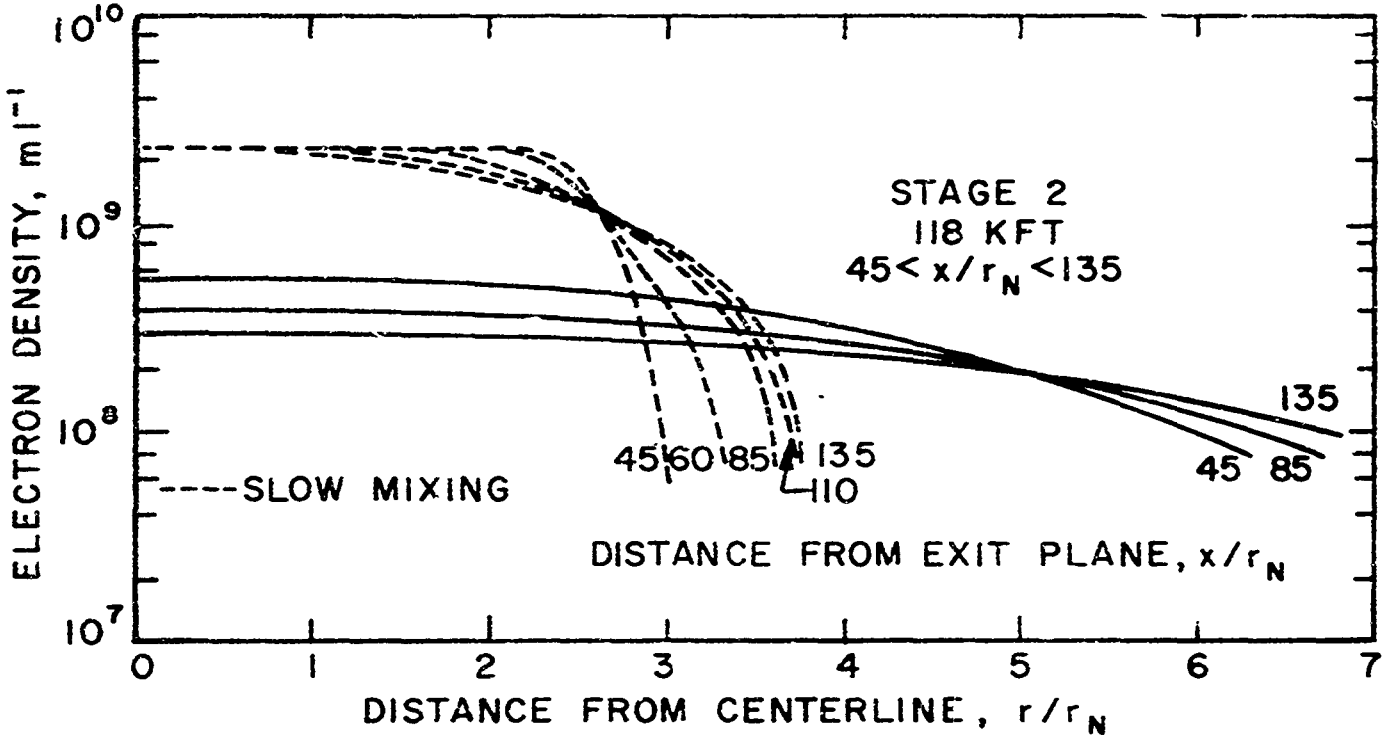

FIG. 48b ELECTRON DENSITY PROFILES
IN STAGE 2 PLUME 118 KFT

$45 < x/r_N < 135$

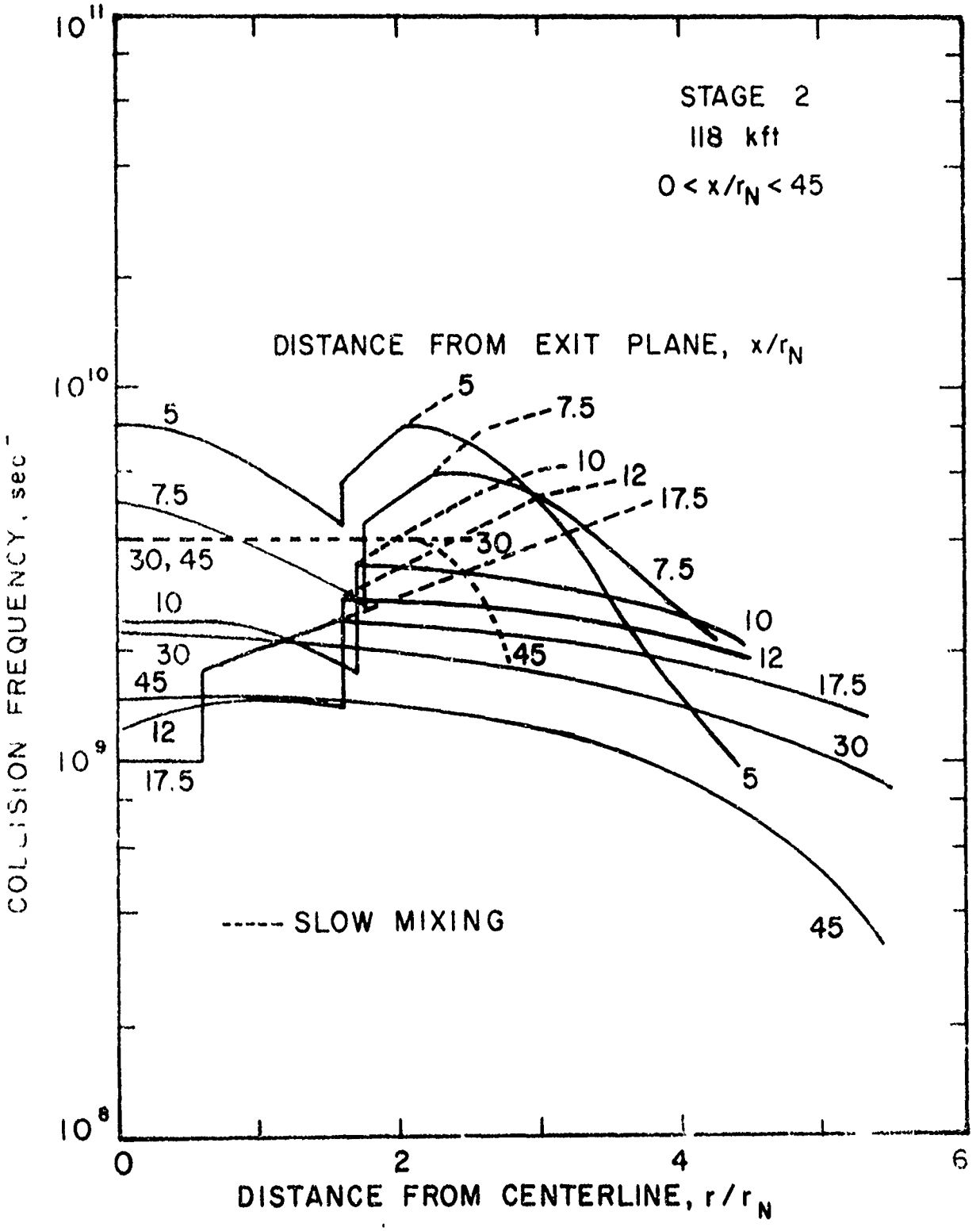

FIG. 49a COLLISION FREQUENCY PROFILES
IN STAGE 2 PLUME (118 kft)

$0 < x/r_N < 45$

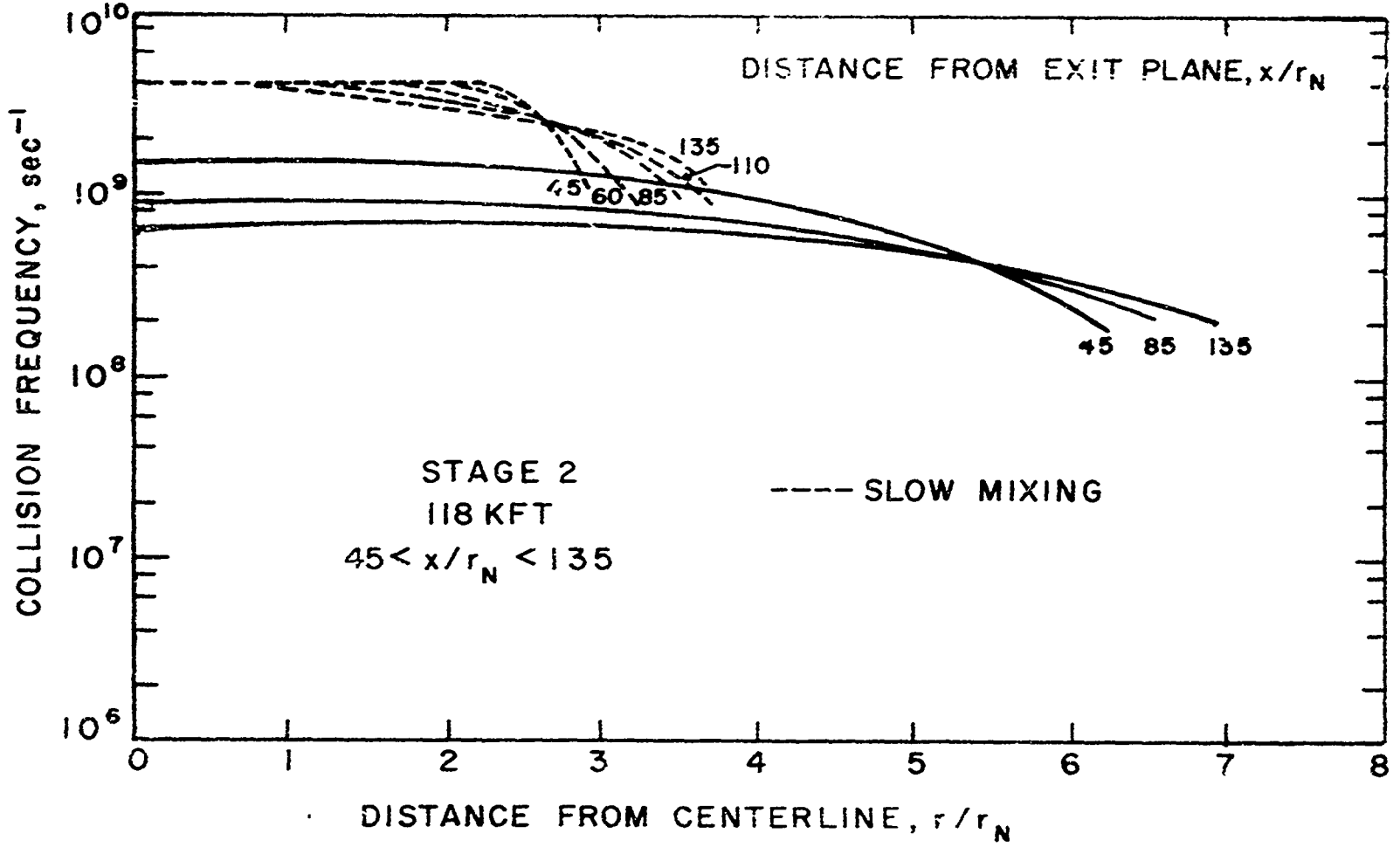

FIG. 49b COLLISION FREQUENCY PROFILES
IN STAGE 2 PLUME (118 kft)

$45 < x/r_N < 135$

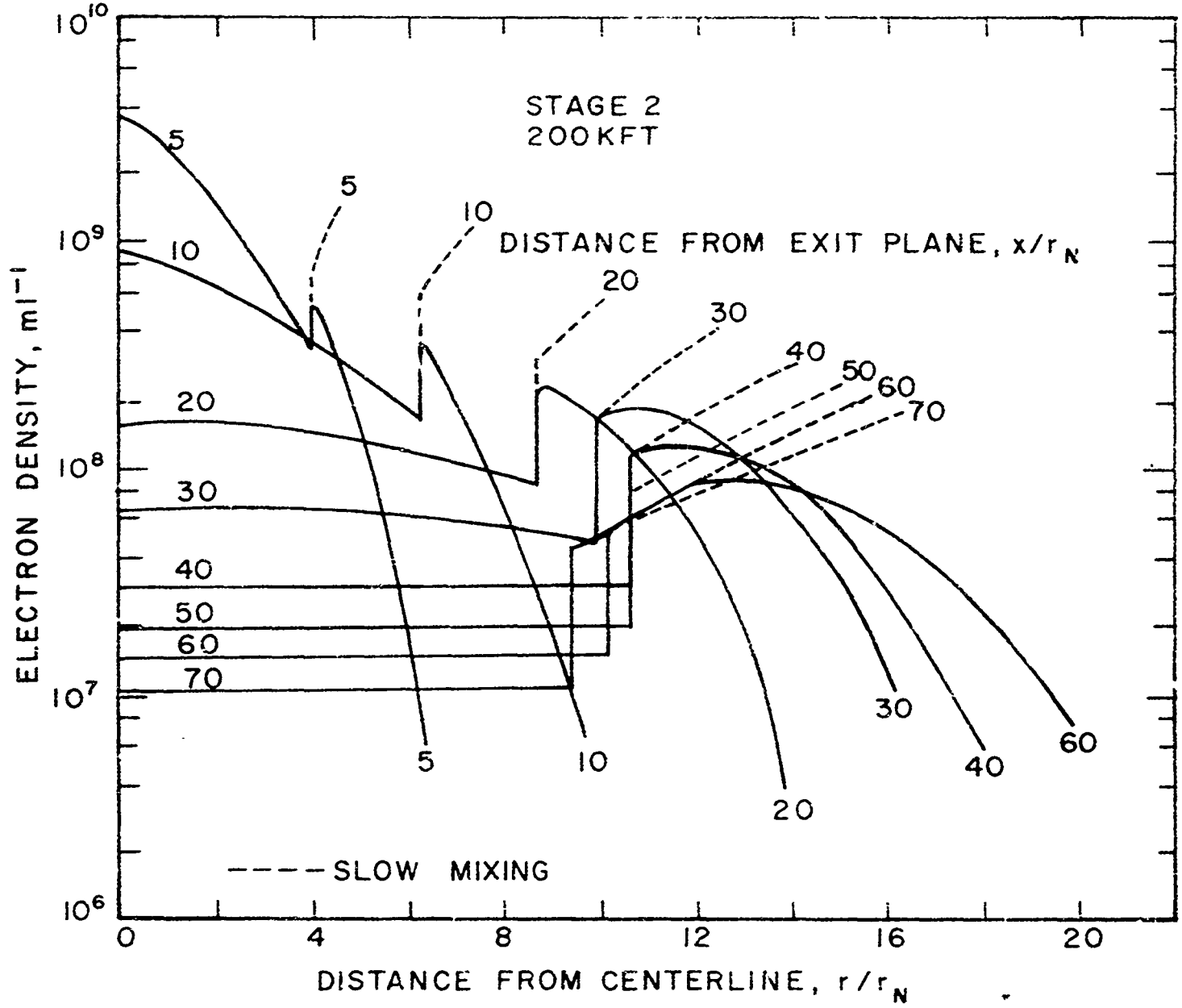

FIG. 7 ELECTRON DENSITY PROFILES [illegible]

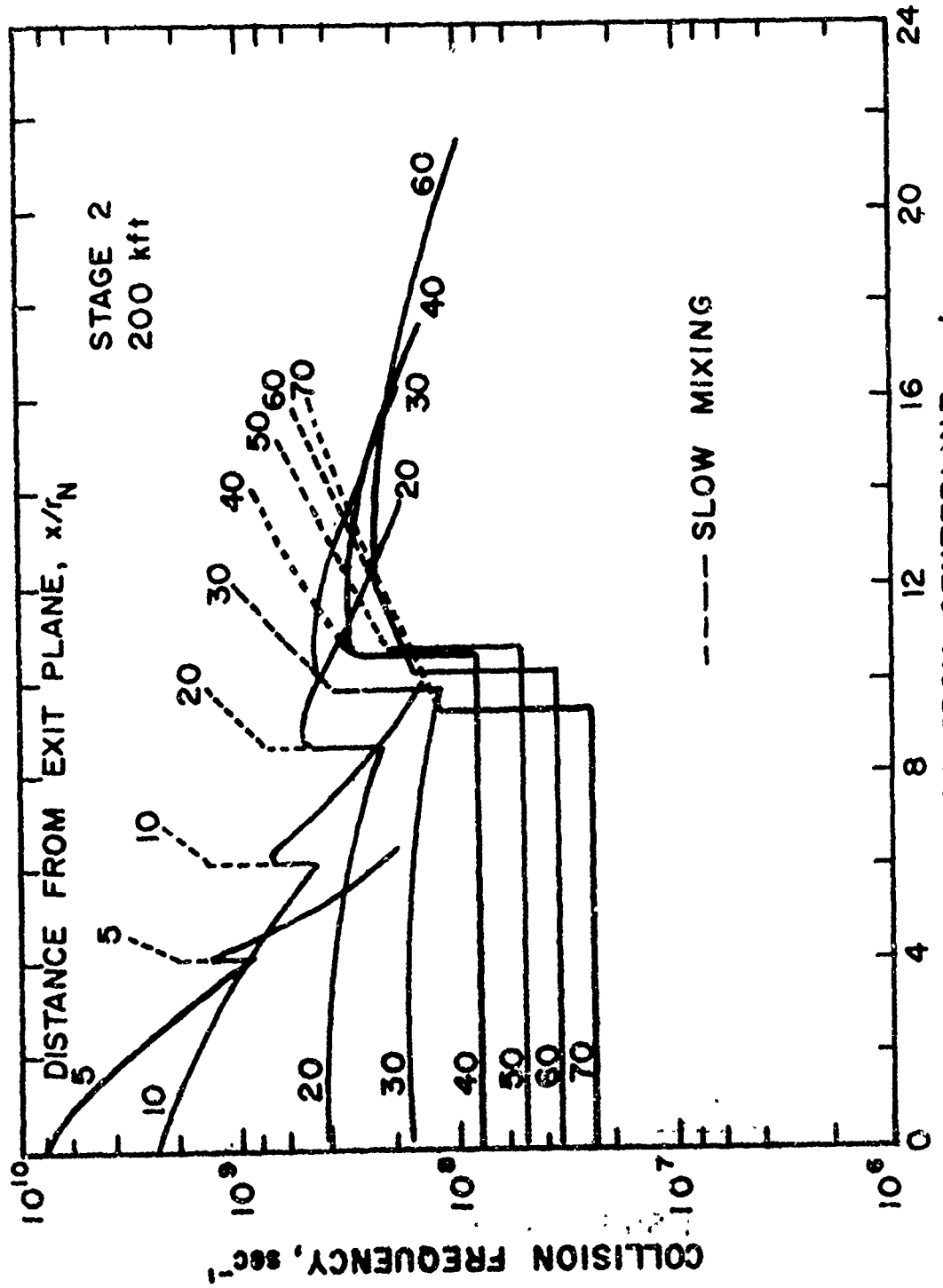

FIG. 51 COLLISION FREQUENCY PROFILES IN STAGE 2 PLUME (200 kft)

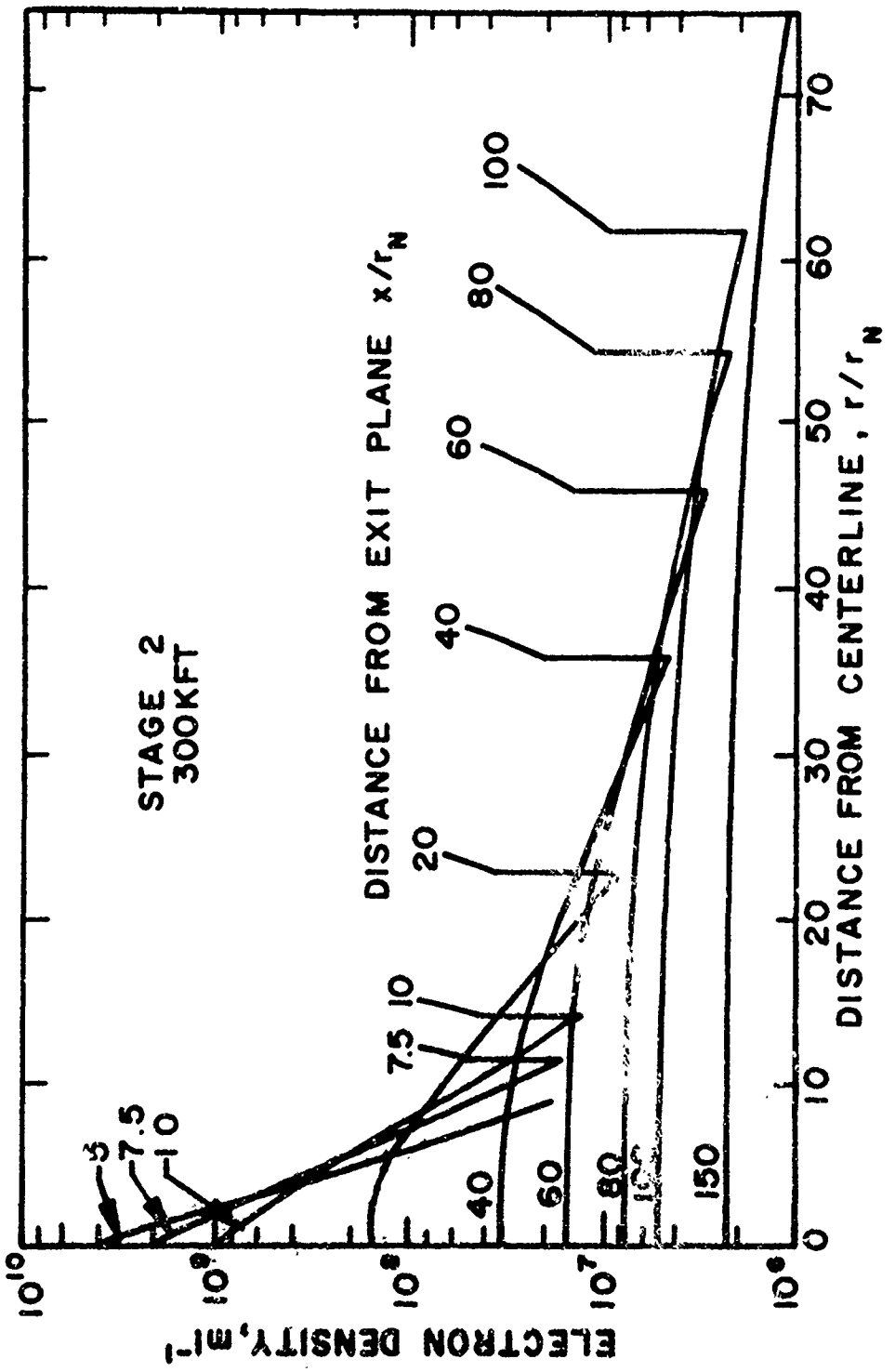

FIG. 52 ELECTRON DENSITY PROFILES IN STAGE 2 PLUME (300 kft)

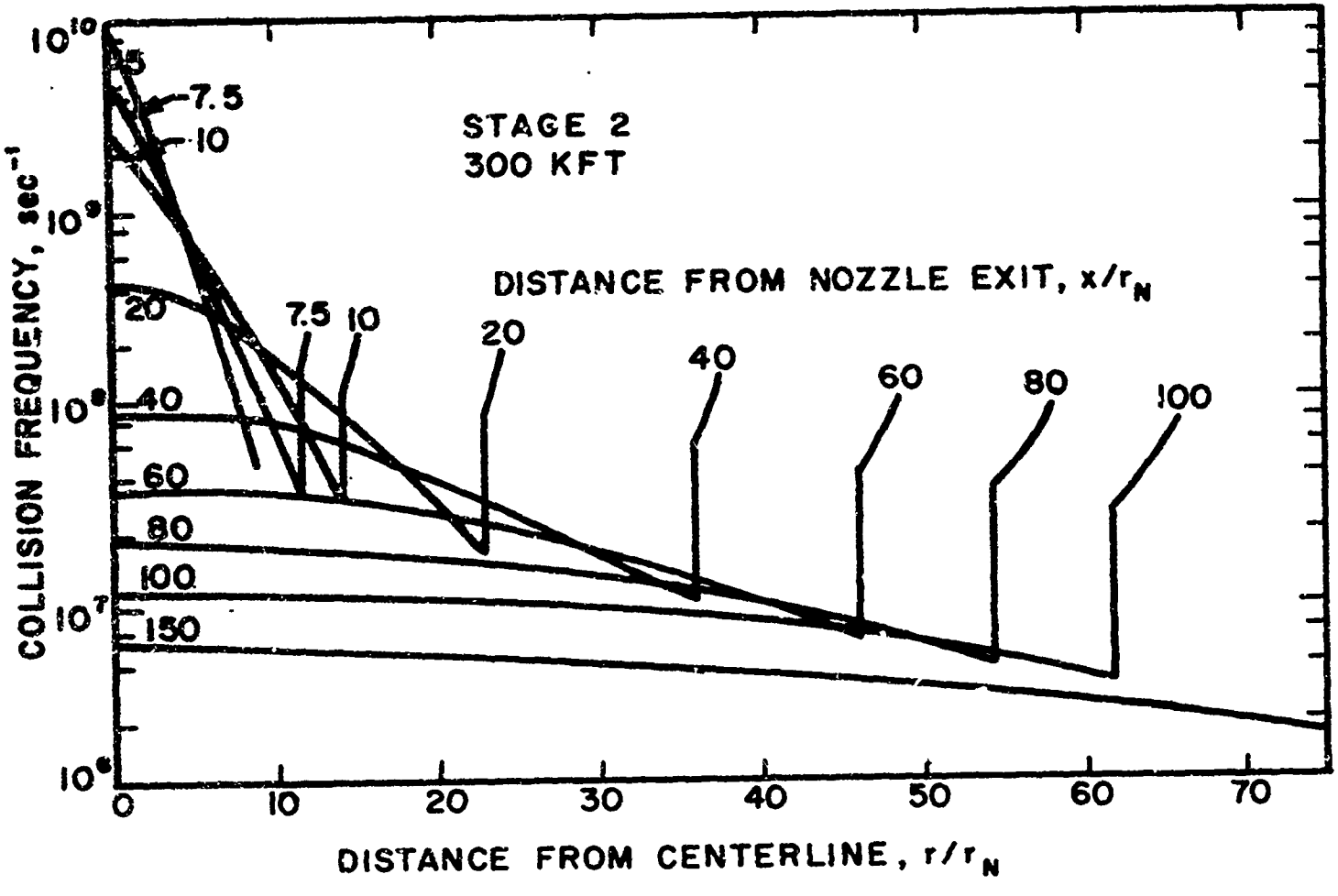

FIG. 53 COLLISION FREQUENCY PROFILES IN STAGE 2 PLUME (300 kft)

APPENDIX A

NOZZLE FLOW CALCULATIONS

Possible approaches to computing flow properties and composition in the Minuteman first and second stage nozzles and their limitations are listed below in order of increasing accuracy.

(1) One-Dimensional Gas/Particle and Thermochemical Equilibrium Neglecting both particle thermal and velocity lags and non-equilibrium chemistry effects during the nozzle expansion makes the subsequent calculations of plume electron densities meaningless.

(2) One-Dimensional, Two-Phase Flow - Equilibrium or Frozen Chemistry - Neglecting the 2-dimensional nature of the flow is likely to result in serious errors in nozzle exit plume properties. Assuming frozen electron mole fractions in the nozzle will drastically overestimate exit plane electron densities; assuming equilibrium flow will drastically underestimate exit plane electron densities.

(3) Two-Dimensional, Two-Phase Flow - Nonequilibrium Chemistry Along Streamlines - In this approach the two phase nature of the flow is accounted for together with the two-dimensional effects. The influence of nonequilibrium chemistry on the streamline locations, pressure, and gas and particle temperature and velocity is neglected (a reasonably good assumption). The above properties are input to a nonequilibrium calculation of neutral and charged species concentrations along streamlines.

(4) Two-Dimensional, Two-Phase Flow Coupled with Nonequilibrium Chemistry - A program which incorporates the influence of nonequilibrium chemistry on pressure and gas and particle temperature, and velocity yields an "exact" solution to this problem.

After consulting with those research laboratories* likely to have program (4) we concluded that none was available for use in this study. We therefore chose analysis (3) to make the Minuteman nozzle calculations.

---

* Including United Aircraft, Lockheed-Huntsville, Grumman, Purdue University

UNCLASSIFIED

Security Classification

DOCUMENT CONTROL DATA - R & D

(Security classification of title, body of abstract and indexing annotation must be entered when the overall report is classified)

1 ORIGINATING ACTIVITY (Corporate author) AeroChem Research Laboratories, Inc. P.O. Box 12, Princeton, New Jersey 08540	2a. REPORT SECURITY CLASSIFICATION UNCLASSIFIED 2b. GROUP

3 REPORT TITLE

Prediction of Minuteman Exhaust Plume Electrical Properties

4 DESCRIPTIVE NOTES (Type of report and inclusive dates)

Interim Report

5 AUTHOR(S) (First name, middle initial, last name)

Pergament, H.S. and Mikatarian, R.R.

6 REPORT DATE July 1973	7a. TOTAL NO. OF PAGES xi plus 89	7b. NO OF REFS 33
8a CONTRACT OR GRANT NO F04611-71-C-0064 b PROJECT NO d.	9a. ORIGINATOR'S REPORT NUMBER(S) AFRPL-TR-72-129 9b. OTHER REPORT NO(S) (Any other numbers that may be assigned this report) AeroChem TP-281	

10 DISTRIBUTION STATEMENT Distribution limited to U.S. Government agencies only: Test and Evaluation; 30 Oct 72. Other requests for this document must be referred to AFRPL/STINFO/DOZ, Edwards, CA 93523

11 SUPPLEMENTARY NOTES	12 SPONSORING MILITARY ACTIVITY AF Rocket Propulsion Laboratory Director of Science and Technology AFSC, USAF, Edwards AFB, CA

13 ABSTRACT

Results of a comprehensive investigation of Minuteman exhaust plume electrical properties are presented. Electron density and electron-neutral collision frequency profiles are given for the Stage 1 plume at 100 kft and the Stage 2 plume at 118, 200 and 300 kft. This work is motivated by the need to determine plume electrical conductivities, input data to an evaluation of EMP/exhaust plume interactions. The calculations are described in detail and include analyses of: (i) two-phase nozzle flow via the method of characteristics, (ii) nonequilibrium chemistry along nozzle and plume streamlines, (iii) inviscid plume properties via the method of characteristics, (iv) turbulent mixing / nonequilibrium chemistry along curved plume boundaries, and (v) nonequilibrium chemistry behind the Mach disc. The results include: gas and particle properties and chemical kinetic distributions of all neutral and charged species concentrations in the nozzle: inviscid boundaries, shock structure, Mach number contours and electron densities in the plume.

FORM FOR [illegible]

UNCLASSIFIED

UNCLASSIFIED

Security Classification

KEY WORDS	LINK A		LINK B		LINK C	
	ROLE	WT	ROLE	WT	ROLE	WT
Minuteman						
Rocket Nozzle Flows						
Rocket Exhaust Plumes						
Plume Electrical Properties						